1-2005

Fabrication of electronic devices using high volume printing techniques

Yu Xia

Fabrication of Electronic Devices Using High Volume Printing Techniques

Yu Xia

Materials Science and Engineering

Rochester Institute of Technology

Fabrication of Electronic Devices Using High Volume Printing Techniques

A Thesis

Presented to

The Graduate Faculty of Rochester Institute of Technology

In partial fulfillment of the requirements for the degree of

Master of Science in Materials Science and Engineering

Yu Xia

April 2005

Fabrication of Electronic Devices Using High Volume Printing Techniques

Yu Xia

Approved:

Bruce E. Kahn

Dr. Bruce Kahn (Advisor)
Department of Imaging &Photographic Technology
And
Center for Materials Science and Engineering

Accepted:

Dr. K.S.V. Santhanam (Director)
Center for Materials Science and Engineering

Copyright Release Form

Fabrication of Electronic Devices Using High Volume Printing Techniques

I, Yu Xia, hereby grant permission to the Wallace Memorial Library of the Rochester Institute of Technology, to reproduce my thesis in whole or in part. Any reproduction will not be for commercial use or profit.

Date: 05/20/05

Signature: Yu Xia

Acknowledgement

My parents, Jianxiong Xia and Yueping Huang, my fiancée, Lan Miao, and my friends for their support which gives me the power to conquer every challenge in my two years' master program at RIT.

My advisor, Dr. Bruce Kahn, for his introduction of printing electronics, his ideas, patience and direction in research, and his considerate help in everywhere.

My committee member, Dr. K.S.V. Santhanam, for his guidance during the summer project and his helpful discussions on the printed gas sensor.

My committee member, Dr. Thomas Smith, for his encouragement and guidance.

Franz Sigg for the lithography and flexography plate design.

Daniel M. Clark for providing the printing equipment and the great suggestions about the process.

Eastman Kodak company for their generous funding for the lithography project.

William J. Grande and Gary A. Fino for their collaboration in the MicroPen project.

Parelec, Precisia and H.C. Starck companies for their generous donation of the conductive materials used in this work.

Les Green, Steve Scott, Keith Steadman, and Mike Rodenhouse of Reflexite Precision Technology Center, and Steve Kobak of Zygo Corporation for their assistance with optical Profilometry.

Dr. Surendra K. Gupta in the mechanical Engineering Department at RIT for allowing us to use the AFM.

Anupama Karwa, Stephen Paquette, Carl Smith, Iris Sprow, Markijan Lylak, B. David Damant, Jenna Venturini, Jamie Lewis, Hui Liu, Pamela Martinez, Lindsay Sargeant for their involvement in this work.

Publications
(Refereed Journals)

Yu Xia, Anupama Karwa, Franz Sigg, Daniel M. Clark, and Bruce E. Kahn, "All Printed Polyaniline Gas Sensor", in preparation.

Anupama Karwa, Yu Xia, Dan Clark, Franz Sigg, Bruce Kahn, "A Printing Process Capability Study: Conductive Inks Printed with Offset Lithography", submitted to Journal of Graphic Technology.

Presentations/Posters

Yu Xia, Carl G. Smith, Anupama Karwa, and Bruce E. Kahn, "Printed Chemical Sensors", presentation, *American Chemical Society National Meeting, PMSE 159, Mar. 2005, San Diego, CA,*

Yu Xia, Bruce E. Kahn, Gary A. Fino, and William J. Grande, "Patterning organic materials using a micropen", presentation, *American Chemical Society National Meeting, PMSE 162, Mar. 2005, San Diego, CA,*

Yu Xia, Anupama Karwa, Franz Sigg, Daniel M. Clark, and Bruce E. Kahn, "Organic Devices Printed with High Volume Printing Processes", presentation, *IDTechEx Printed Electronics 2004, Dec. 7, 2004, New Orleans, LA*

Yu Xia, Anupama Karwa, Franz Sigg, Daniel M. Clark, and Bruce E. Kahn, "Fabrication and Testing of Printed Organic Electronic Devices made using High Volume Printing Processes", poster, *Material Research Society Fall Meeting, A5.28, Nov. 30, 2004, Boston, MA*

Anupama Karwa, Yu Xia, Franz Sigg, Daniel M. Clark, and Bruce E. Kahn, "Printable Electronics: Patterning of Conductive Materials for Novel Applications", poster, *Material Research Society Fall Meeting, A5.29, Nov. 30, 2004, Boston, MA*

Yu Xia, Anupama Karwa, Franz Sigg, Daniel M. Clark, and Bruce E. Kahn, "Fabrication and Calibration of All-Printed Gas Sensor", presentation, *American Chemical Society Northeast Regional Meeting, 239, Nov. 2, 2004, Rochester, NY*

Yu Xia, Anupama Karwa, Franz Sigg, Daniel M. Clark, and Bruce E. Kahn, "Fabrication and Calibration of All-Printed Gas Sensor", poster, *American Chemical Society Northeast Regional Meeting, 334, Nov. 2, 2004, Rochester, NY*

Anupama Karwa, Yu Xia, Franz Sigg, Daniel M. Clark, and Bruce E. Kahn, "Formulation of Conductive Flexo Inks Using Electrically Functional Polymers", poster, *American Chemical Society Northeast Regional Meeting, 335, Nov. 2, 2004, Rochester, NY*

Stephen Paquette, Yu Xia, K.S.V. Santhanam, "Template-Free Synthesis of Polyaniline Nanostructures By Electrochemical Polymerization", poster, *American Chemical Society Northeast Regional Meeting, 51, 330, Nov. 2, 2004, Rochester, NY*

Yu Xia, Anupama Karwa, Rajiv Sangoi, Franz Sigg, Carl G. Smith, Daniel M. Clark, William W. Pope, Timothy J. Richardson, and Bruce E. Kahn, "Using High Volume Printing Techniques to Pattern Materials for Low Cost Device Fabrication", presentation, *IMAPS/TAGA 3rd Advanced Technology Workshop on Printing an Intelligent Future, 3.18, Sep. 29 2004, Annapolis, MD*

Yu Xia, Anupama Karwa, Rajiv Sangoi, Franz Sigg, Carl G. Smith, Daniel M. Clark, William W. Pope, Timothy J. Richardson, and Bruce E. Kahn, "Patterning Conductive Materials Using High Volume Printing Processes", poster, *6th International Symposium on Functional π Electron Systems, DP. 64, June 17, 2004, Ithaca, NY*

Rajiv Sangoi, Carl G. Smith, Anupama Karwa, Yu Xia, Franz Sigg, Daniel M. Clark, William W. Pope, Timothy J. Richardson, and Bruce E. Kahn, "Printing Conductive Materials using High Volume Printing Processes", poster, *Organic Thin Film Electronics: Materials, Devices, and Applications, American Chemical Society ProSpectives Conference Series. Jan. 26 2004, Miami, FL*

Table of Contents

Abstract I

Acknowledgement II

Publication III

Presentation III

1. Printing Electronics 1

2. Printing Technologies and Applications 7

2.1 Flexography Printing 7

2.2 Offset Lithography Printing 10

2.3 Gravure Printing 13

2.4 Pad Printing 14

2.5 Screen Printing 15

2.6 Inkjet Printing 17

2.7 Thermal Transfer Printing 19

2.8 MicroPen Printing 21

2.9 Soft-lithography 21

2.10 Summary 25

3. Lithography Printed Conductive Patterns — Printing Capability Study 27

3.1 Introduction 27

3.2 Experimental 29

3.3 Test Target ····· 31

3.4 Line and Space Width ····· 33

3.5 Line Thickness ····· 37

3.6 Conductivity ····· 39

3.7 Conclusion ····· 42

4. Polymerization of Polyaniline ····· 44

4.1 Electrochemical Synthesis of Polyaniline ····· 44

4.2 Interfical Polymerization of Polyaniline ····· 49

5. All-printed Humidity and Gas Vapor Sensor ····· 52

5.1 Introduction ····· 52

5.2 Conductivity Dependence (General Sensing Mechanism) of PANI ····· 56

5.3 Experimental ····· 61

5.4 Humidity Sensing ····· 65

5.5 Acid and Base Sensing ····· 71

5.6 Volatile Organic Compounds ····· 74

5.7 Natural Gas Sensor ····· 77

5.8 Fish Preservation Sensor ····· 78

5.9 Polyaniline Degradation ····· 80

5.10 Conclusion ····· 83

6. Pattern Electronic Devices Using Micropen ····· 85

6.1 MicroPen Direct Writing System ····· 85

6.2 PEDOT:PSS Conductive Lines ····· 86

6.3 Organic Thin Film Transistor and Polythiophene ····· 90

6.4 Fabricating Thin Film Transistor Using Micropen ····· 95

6.5 Conclusion ····· 100

7. Further Research ····· 101

References ····· 103

List of Figures

1.1 High Mobility Organic Semiconductor Materials ····· 2

2.1 Flexographic Printing Process ····· 8

2.2 Commercially Printed RFID Tag Made in RIT and Typical RFID Antenna ···· 8

2.3 Optical Microscopy and Optical Profilometry Image of the Antenna Corner ·· 9

2.4 Lithographic Printing Process ····· 11

2.5 Lithographic Printed Transistor ····· 11

2.6 Chemical Structure of PEDOT:PSS ····· 12

2.7 Gravure Printing Process, Plate and Image ····· 13

2.8 Pad Printing Process ····· 14

2.9 Screen Printing Process ····· 15

2.10 Inkjet Printing ····· 17

2.11 Inkjet Printed Transistor ····· 17

2.12 Inkjet Printed Bi-Stable Active Matrix Display ····· 18

2.13 Surface Roughness in Inkjet Printing ····· 19

2.14 Thermal Transfer Process used in Conductive Polymer Printing ····· 20

2.15 MicroPen Printing ····· 21

2.16 Micro Contact Printing ····· 22

2.17 Active Matrix Backplane Circuit ····· 23

2.18 E-Ink Display ····· 23

2.19 Nanoscale Transfer Printing ····· 24

3.1 Test Pattern ····· 32

3.2 Optical Micrographs of Printed Lines with Different Widths ····· 33

3.3 Optical Micrographs of Printed Lines with Number of Impressions ····· 34

3.4 Actual Line Width Increase vs. Nominal Line Width and Number of Impressions ····· 35

3.5 Absolute Line Width Increase vs. Nominal Line Width and Number of Impressions ····· 35

3.6 Optical Micrographs of 42 μm Three Impression Printed Patterns ····· 36

3.7 Profilometry vs. Number of Impressions ····· 38

3.8 Line Thickness vs. Nominal Line Width and Number of Impressions ····· 38

3.9 Line Thickness and Sheet Resistance Increase with Number of Impressions 38

3.10 Line Resistance vs. Nominal Line Width and Number of Impressions ····· 40

3.11 Line Conductance vs. Nominal Line Width and Number of Impressions ····· 40

3.12 Resistance of a Sample ····· 41

4.1 Reaction Steps in the Electrochemical Polymerization of Aniline ····· 45

4.2 Nanotube Polymerization Voltammograms Using Different Mole Ratios of Aniline to Dopant in H_3PO_4 (aniline/dopant) ····· 47

4.3 Optical Microscopy Image of Polyaniline ····· 49

4.4 Interfacial Polymerization of Aniline in a Water/Chloroform System ····· 51

4.5 Polyaniline Powders Obtained after Filtration ····· 51

5.1 Sketch of Fabrication Process ····· 61

5.2 Spectra of printed polyaniline ····· 63

5.3 Sketch of Sensor Testing Equipment ····· 64

5.4 Humidity Response on Coated Paper ····· 66

5.5 Performance Comparison of the Sensor with/without HCl Treatment ····· 67

5.6 Humidity Response on Plastic Film ····· 68

5.7 Humidity Cycling Response ····· 68

5.8 Sensor Response Comparison ····· 69

5.9 Performance Comparison of Single and Double Layer Printed ····· 70

5.10 Sensor Response to Acid and Base ····· 72

5.11 Sensor's Response to Ammonia Injection ····· 73

5.12 Sensor's Response to Volatile Organic Compounds Flow ····· 74

5.13 Sensor's Response to Volatile Organic Compounds Injection ····· 75

5.14 Sensor Response to Natural Gas ····· 77

5.15 Bad Fish Detecting ····· 79

5.16 Photo Image of the Sensor before fish testing and after fish testing ····· 80

5.17 Protonation and Redox Reaction Between Various Forms of Polyaniline ····· 81

5.18 Diffuse Reflectance Fourier-Transform Infrared Spectra of Polyaniline Sensor ····· 82

5.19 UV/Visable Spectra of Polyaniline Sensor 83

6.1 Conductive Line Testing Plate 86

6.2 AFM Image of the Conductive Line 87

6.3 Roughnesses of Line and Substrate 87

6.4 Profilometry Image of the Conductive Line 88

6.5 Profilometry Image of the Parallel Lines and Gaps 89

6.6 Device Cross Section of OTFTs 90

6.7 Characteristic Curves of an OTFT Based on F8T2 92

6.8 Regioregular Isomers of Poly(3-substituted thiophene)s 93

6.9 Molecular structure of and 3D packing of PQT molecules 94

6.10 Thin Film Transistor Fabrication 96

6.11 Optical Microscopy Images of TFTs with Different Channel Lengthes 96

6.12 Optical Profilometry Image of TFT 97

6.13 Output Family Curves of the OTFT Fabricated by Micropen 98

6.14 I_{ds}-V_{gs} curve at Vds = -10V 99

6.15 Output Family Curves after annealing 100

List of Tables

1.1 Comparison of Device Fabrication Process 4

2.1 Printing Process Comparison 26

3.1 Line Width and % Increase of the Size 35

3.2 Space Width and % Decrease of the Size 36

3.3 Line Thickness 37

3.4 Resistance and Sheet Resistance of the Lines 40

3.5 Change of Resistance with Curing Conditions 42

4.1 Peak Currents Obtained For Different Dopant Concentrations in Polyaniline Nanotube Synthesis in H_3PO_4 48

5.1 Volatile Organic Compounds Sensitivity and Detection Limitation 76

6.1 Performance Characteristics of the MicroPen 85

6.2 Roughness Analysis Data 87

List of Formulas

5.1 Doping-Dedoping Reaction of PANI 52

5.2 PANI's Resistance Change with Ammonia Concentration 53

5.3 Definition of Percentage Sensitivity 66

6.1 Standard "Linear Regime" Equation for TFT 98

Chapter One: Printing Electronics

For the past forty years conventional microelectronic devices have been spectacularly successful in supporting the development of the world. The inorganic silicon and gallium arsenide semiconductors, silicon dioxide insulators, and materials such as aluminum and copper have been the backbone of the semiconductor industry. The number of functional units on a single chip double every 18 months according to the Moore's law [1]. However, up till now, the silicon based semiconductor devices still suffer a number of limitations. For instance, the industry process is complicated and toxic, the cost is high and the production period is generally longer than a month. Moreover, flat and rigid wafers are required as substrates and the functional devices cannot be made over very large areas. Last but not least, with modern feature size decreasing to lower than 0.1 μm, the tunneling between the conductive lines becomes a critical problem.

Alternatively, there is increasing interest in organic electronic materials. The intriguing discovery of electrical conduction in organic solids can be traced to the report on the dark conductivity and photoconductivity of anthracene crystals [2,3] in 1906. Later on, the synthesis of tetracyanoquinodimethane (TCNQ) and its derivatives provided the first true organic metal with high electrical conductivity and activation energy [4,5]. Electroluminescence was found as the first organic solid state electrical effect in anthracene in 1960s [6,7]. Meanwhile the foundations of our current knowledge of electronic excitations, energy transport, and photochemistry were all laid [8]. In 1977,

Alan Heeger, Hideki Shirakawa, Alan MacDiarmid and their coworkers synthesized conjugated polymer polyacetylene, whose conductivity can transfer from insulator, semiconductor to conductor by adding trace amounts of donor or acceptor into the material [9]. Nowadays, a series of organic semiconductors with good electrical, electrochemical and photoelectrical properties have been prepared. Figure 1.1 shows several materials developed recently (symbol μ is the carrier mobility, an important characteristic of semiconductor materials). These materials are much cheaper than high purity inorganic crystal, (Si, Ge, GaAs, etc) while their properties are comparable, and they are able to be processed at low temperatures, over large areas and on materials such as plastic or paper. Based on these materials, a wide range of technological applications including thin film transistors (TFTs), organic light-emitting diodes (OLEDs), photovoltaic cells and solid state memories have already been fabricated.

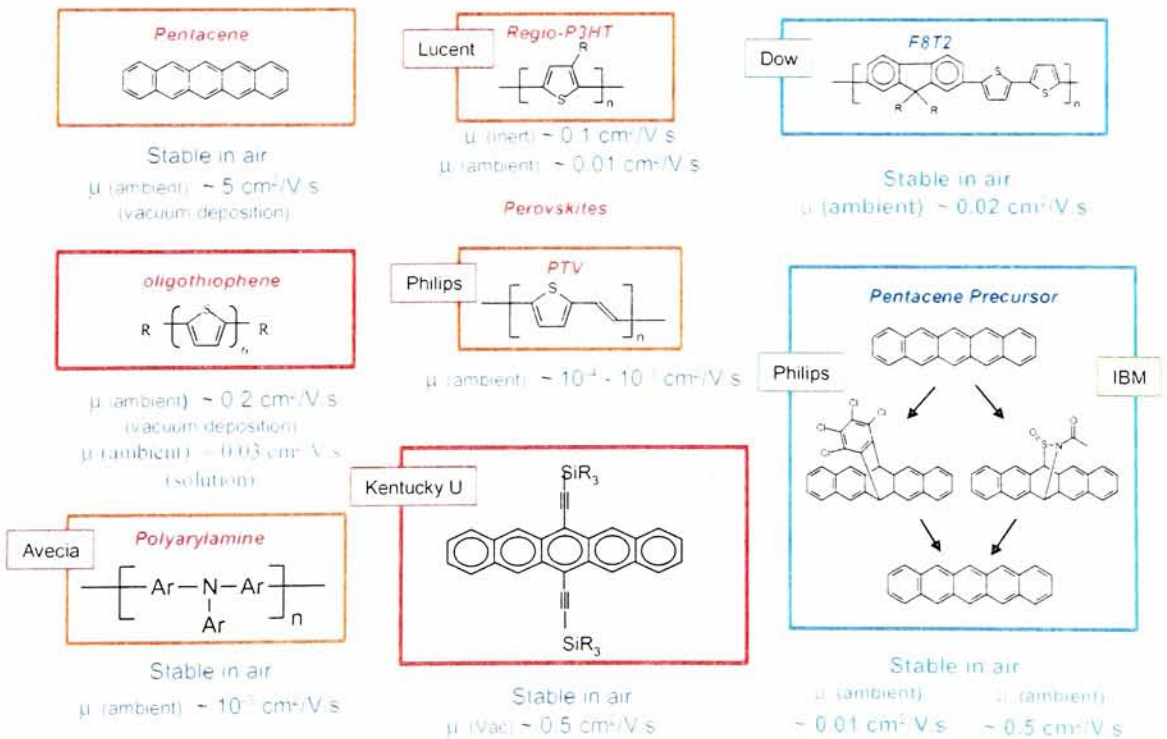

Figure 1.1 High Mobility Organic Semiconductor Materials (attribute to Beng Ong from Xerox Co.)

The research in this area is promising to change our life in the next several decades.

One of the major challenges in this field is how to transfer the "cheap" functional materials into "cheap" devices. Conventional fabrication methods used in organic thin film devices is physical or chemical vapor deposition (PVD/CVD) and spin coating. Vapor deposition requires a vacuum environment and high temperature, which is a time consuming process and not suitable for low glass transformation temperature (T_g) polymers. Spin coating is generally used over small area and have low throughput. Moreover, most of the materials are wasted in both of the processes. Compare to those, various printing techniques provide a continuous process at atmospheric pressure and room temperature with far greater production speed, lower cost, and less manufacturing complexity. Although there remains much fundamental research to achieve this goal, the advantages of exploring such a transition will provide a much wider array of applications. Devices made by different printing techniques like inkjet, gravure, screen, microcontact printing, etc. have already been reported which show acceptable performance [10-13].

A certain ink is used to make materials that may be printed. The ink can be either a suspension or solution of the functional materials, combined with solvent and other additives like resin, surface tension modifiers (surfactants), etc., to adjust the viscosity and its adhesion to substrates. During fabrication, the ink must be deposited to form a desired pattern determined by the printing processes, then it must be solidified to create

a permanent example of that pattern. The use of available printing processes and properly designed inks allows very rapid patterning in ambient conditions. Sometimes post treatment like UV light and heat are used to accelerate the drying process. Complicated device structures can be reached by printing different functional material layers on top of each other. It is a typical bottom-up fabricating process.

	Conventional Silicon Process	Printed Electronics
Process	Batch	Continuous
Production Speed	**Slow**	**Potentailly Fast**
Procedure	Complex, Toxic	Simple, Harmless
Cost	**Moderate**	**Low to Moderate**
Capital Cost	Extremely High	Low to Moderate
Materials	**Well Defined**	**Developmental**
Substrate	Rigid Silicon	Various, Flexible
Max. Functional Area	**Wafer Size**	**Large, Depends on Equipment**
Environmental	Acceptable	Friendly

Table 1.1. Comparison of Device Fabrication Process

Table 1.1 compares the differences between conventional integrated circuit manufacture and those using printed processes. Printing electronics has its own advantages, however, the bulk properties of the printed particles and/or polymers cannot yet duplicate these semiconductor industry products. Generally, during printing the structure crystallization or molecular ordering is hard to realize. It might result in a relatively rough interface which traps the electrons, and the structure also may contain numerous gaps through which carriers cannot go through. All of these will influence the charge transfer properties of the materials and impair the devices performance. Also, the traditional printing methods are not initially designed for fine device fabrication purposes. Feature sizes can only be reached on the order of ~10 μm and the

thickness of the film is difficult to adjust, which also limit its application. Further study still needs to be done in printing quality, ink formulation, and device fabrication.

The possibility of using high volume offset lithographic and flexographic printing methods to fabricate single and multiple layer electronic devices are investigated in this thesis. The printed device performance and applications are discussed as well. Attempt to use modification methods to print fine feature size solid state devices is also demonstrated here. The outline of this thesis is as follows:

In chapter two, different kinds of printing technologies are introduced according to their working mechanism and print capability. Their advantages and disadvantages are discussed and compared. Recent applications in printing electronics are discussed as well.

In chapter three, offset lithographic printing technology was studied by printing conductive lines using silver particle ink. The lines were printed with different line width, gap distance and difference number of impressions. The resolution, thickness and conductivity of the conductive lines were measured and compared. The post-treatment was discussed as well.

In chapter four, two polymerization methods was studied to synthesis the polyaniline nanostructures. Polyaniline was then formulated into the ink and printed as functional

material in the humidity and gas vapor sensor demonstrated in the next chapter.

In chapter five, an all-printed polyaniline sensor was fabricated using flexographic printing. The sensor can be used for humidity and volatile organic compound (VOCs) sensing. Its sensitivity was tested and compared with commercial sensors. Several applications such as natural gas leakage detection, fish preservation sensing, etc. have been studied.

In chapter six, MicroPen is demonstrated as special patterning equipment which has the capability to draw parallel conductive lines with good shape and small gap distance. Surface morphology of the organic conductive lines has been studied by AFM and optical profilometry. By drawing this on a highly doped silicon wafer with silicon dioxide surface, and filling the channel using air stable regioregular poly(3,3''-dialkylquaterthiophene) (PQT), a thin film transistor prototype was fabricated.

In chapter seven, further research in the field of printing electronics is discussed.

Chapter Two: Printing Technologies and Applications

Printing is one of the oldest and most important inventions in human history. It is developed by Chinese around 1400 years ago and from then on, information can be recorded, duplicated, and transmitted much easier. Recently printing has been offered a brand new application: electronic device fabrication. By patterning functional inks onto the substrates layer by layer, devices can be built more directly and continuously than what is used in the traditional silicon based semiconductor industry. Several technologies which have the potential to be used for printing electronics are reviewed in this chapter and some device applications are demonstrated as well.

2.1 Flexographic Printing

Flexography, offset lithography and gravure printing are three most commonly used high volume printing technologies. Flexography got its name because of the use of a flexible plate to transfer the image. The image pattern is raised on the plate like a rubber stamp. The plates were originally made of rubber, but recently people use photopolymers to increase the resolution and lifetime. Figure 2.1 shows the working mechanism of the flexographic printing process. The plate is attached to a plate cylinder so that it can print in a rotary fashion. The anilox roller has small cells or wells all over its surface, which can carry a precise volume of ink inside. The rest of the ink is wiped off by the doctor blade so there will be controlled amount of the ink transferred uniformly onto the flexographic plate. Only the raised (image) part on the

plate receives the ink, and the pattern is transferred to the substrate by the pressure of the impression cylinder. The thickness of the film can be adjusted by the rotation speed and the pressure applied to the substrate.

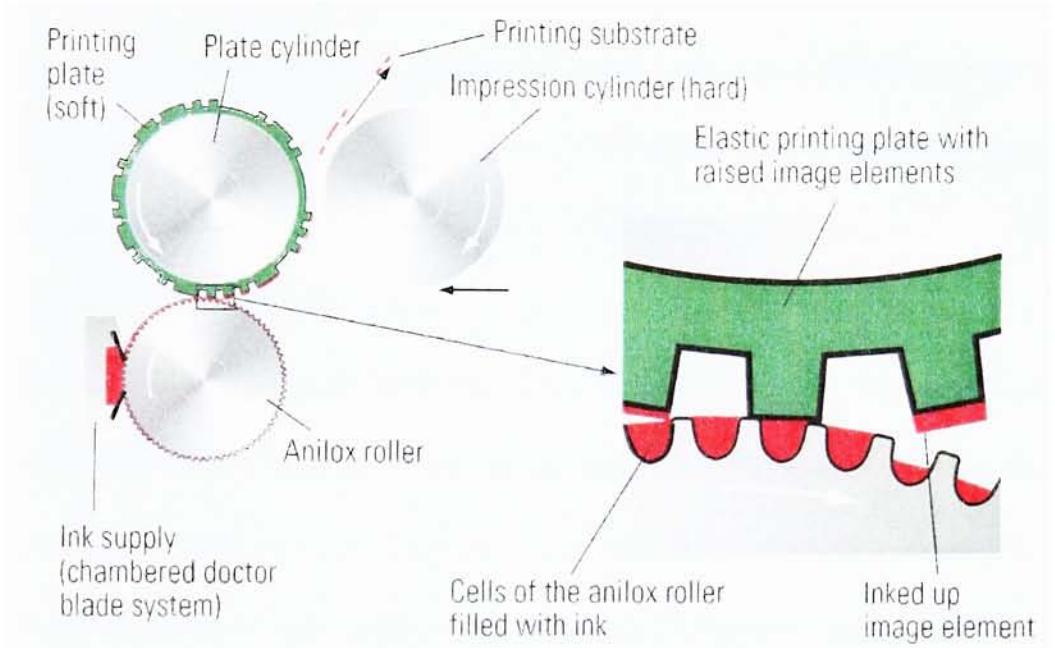

Figure 2.1 Flexographic Printing Process [14]

Flexography is a typical high volume printing technology with speeds possible up to 1500 feet per minute (fpm). It is suitable for printing functional layers having large area and relatively high thickness (up to 10 μm). Using this technique, radio frequency

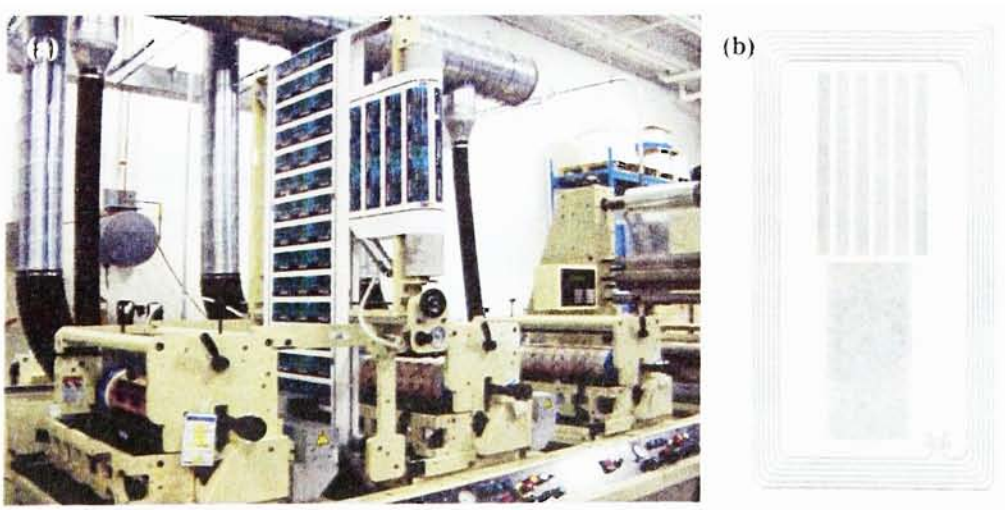

Figure 2.2 (a) Commercially Printed RFID Tag Made in RIT (b) Typical RFID Antenna

identification (RFID) antennas have been printed in our lab [15], as shown in figure 2.2. An RFID tag is a device that allows communication between different objects using magnetic fields. It generally comprises an antenna to capture and transfer the magnetic signal and a microchip containing data. The coil structure shown in figure 2.2b is a typical antenna pattern. To print the antenna we used a conductive ink containing silver particles, which was provided by Parlec Inc. The printed feature showed a sheet resistance < 0.1Ω/□.

Other than conductive metal particles, conductive semiconductor oligomers and polymers can also be formulated into ink as suspensions or solutions. In our lab polyaniline ink has been made and printed by flexography to fabricate a sensor. The work will be discussed specifically in chapter 4. The flexographic ink generally has low viscosity (0.05-0.5 Pa·s) [14] and sometimes it is difficult to dry quickly after printing. Curing processes using heating in an oven or ultraviolet treatment can be helpful. The heating temperature should be controlled not to melt or decompose the materials, especially when a organic ink is used.

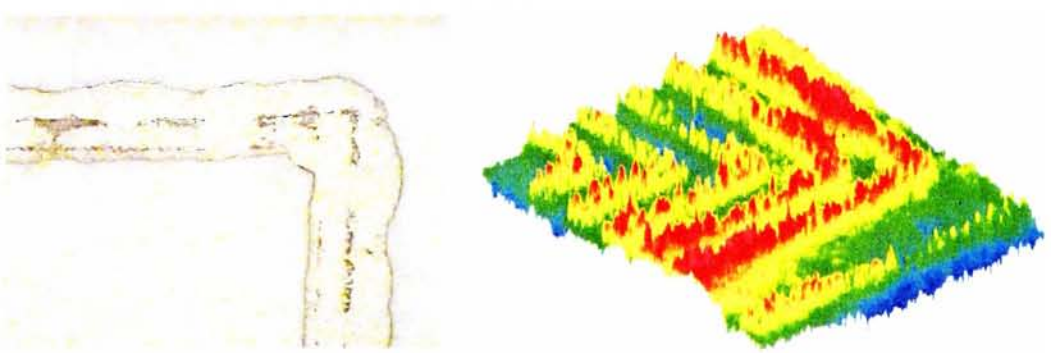

Figure 2.3 (a) Optical Microscopy (b) Optical Profilometry Image of the Antenna Corner

The flexographic printing plate is relatively cheap and easy to make. However, its

rubber-like texture tends to be distorted under pressure. It will affect the edge sharpness and surface uniformity, which can cause serious problems in device fabrication. Also, the influence from impression, substrate smoothness and plate wear makes it hard to control the actual size of the feature over time. Figure 2.3 shows the optical microscope and profilometry images of our printed antenna. As can be seen, the edges and the surface are rough. It is most suitable for printing devices whose feature size is larger than 100 μm.

Another process we used in our device fabrication is called rotary letterpress, which is very similar to flexography printing. The plate used is made by the same materials, and the printing process can also be controlled by rotation speed and the pressure from the impression cylinder. The only difference is it doesn't have an anilox roller. Every time before printing the plate needs to be inked separately. It's useful for small volume experiments and can be used to simulate the print quality of flexography.

2.2 Offset Lithographic Printing

Lithography is a common and important procedure in silicon industry, but it actually got the name from the lithographic plate manufacturing process in printing. The printing plate is generally made of aluminum and pre-coated with a thin layer of photopolymer. When the plate is covered with a mask and placed under UV light, reaction will take place in the photopolymer where exposed to light and change its solubility. So after developing (which removes non-exposed photopolymer), two

different surfaces will exist on the plate, just similar to the process to make the functional layers on the wafer in microelectronic clean room.

The surfaces on the plate have different surface energies, which is the key mechanism of lithography printing. As can be seen from figure 2.4, the pattern area on the plate is oleophilic and during printing it will accept the ink applied from ink rollers. While the non-image part on the plate is hydrophilic so the fountain solution will adhere to it and keep the ink away. Then the ink is transferred to the substrate as a pattern through an offset blanket cylinder.

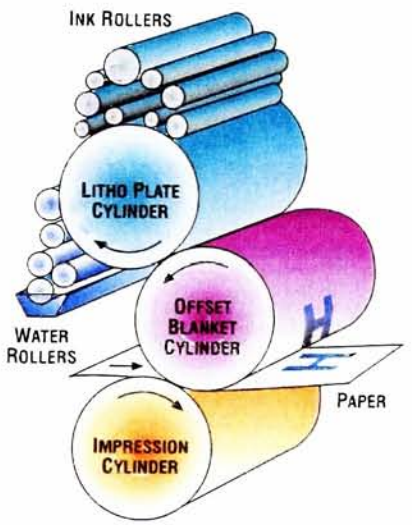

Figure 2.4 Lithographic Printing Process

Figure 2.5 Lithographic Printed Transistor

The image part on the lithographic plate is almost the same height as the other area, so the plate will not be distorted during printing. The offset blanket is also hard to reform, which assures offset lithography has big advantage in resolution compared to other high volume printing process like flexography and gravure. The printed edge can be very straight with feature size limitations lower than 50 μm and layer thickness around

1 μm. These properties make offset lithography possible for fabricating relatively fine feature devices.

Figure 2.5 shows a thin film transistor (TFT) whose source and drain electrodes were printed by lithography [15]. A thin film transistor is a kind of device in which the carrier can pass through the semiconductor material between the source and drain electrodes and the flow rate is controlled by the gate voltage through the dielectric layer in between of the semiconductor layer and the gate electrode. It is used for signal control and can work as fundamental units in active matrix display and logic circuitry. Generally TFTs need a short channel length (the distance between the source and drain) to decrease the response time and current draw of the devices. In the investigation demonstrated in figure 2.5, conductive polymer PEDOT:PSS (chemical structures shown in figure 2.6) was printed as interdigitated source and drain electrodes, semiconductor polymer poly(3-hexylthiophene) (P3HT, chemical structure can be found in figure 1.1) was spin coated on top. The channel length they printed is 120 μm, with carrier mobility 3 x 10^{-4} $cm^2/V \cdot s$. It's a good start although the device suffered a serious problem in on-off current ratio ($I_{on}/I_{off} = 2$).

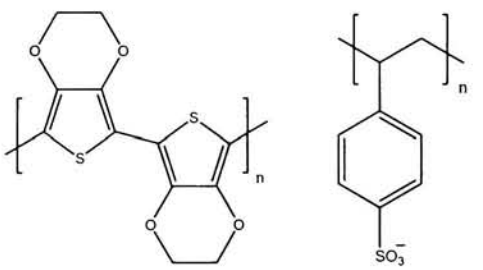

poly(3,4-ethylenedioxythiophene) poly-(styrenesulfonate)

Figure 2.6 Chemical Structure of PEDOT:PSS

To fit the requirement of the process, the lithography ink needs to be made highly

viscosous (40-100 Pa·s) with sheer thinning properties. However, it is hard to formulate different functional polymer inks like that without additives. And the thickness of the printed layer is hard to adjust. Therefore, most of the lithography research is focused on printing conductive lines and electrodes. Supported by Eastman Kodak, we have also studied the lithography printed conductive lines with variable number of impressions to change the thickness. The smallest feature we have achieved is 42 μm. This work will be discussed in Chapter 3.

2.3 Gravure Printing

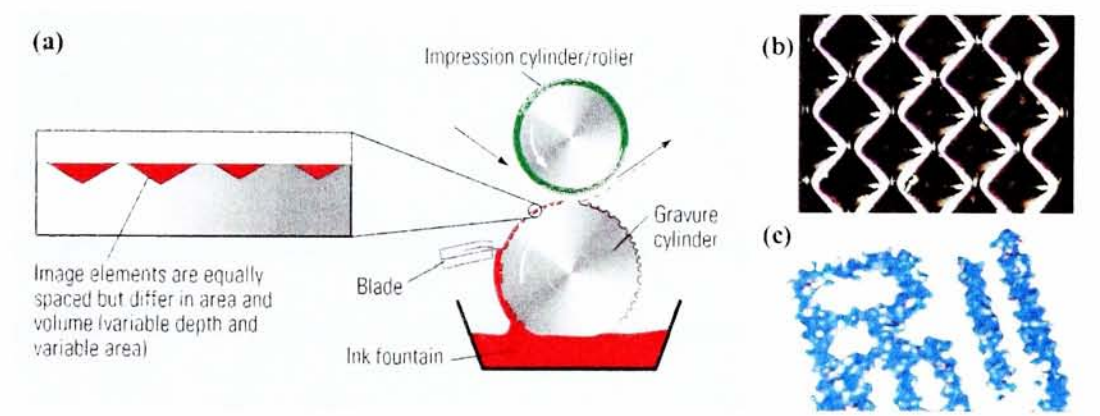

Figure 2.7 (a) Gravure Printing Process (b) Plate (c) Image [14]

Gravure is the fastest printing process whose press speed can be up to 3000 fpm [14]. Its equipment is relatively simple, an ink fountain, an engraved cylinder, a sharp doctor blade and a rubber covered impression roll, as can been seen in figure 2.7. On the surface of the cylinder a lot of small cells can be found which form the image. During printing, the ink on the cylinder is wiped away by the doctor blade, except that remaining in the cells. Then they can be directly transferred to the substrate in between of the gravure and impression cylinder.

Gravure is also a possible method for printing electronic devices. It has a typical film thickness up to 10 μm and line resolution around 50 μm [14]. Many fluids with different viscosities can be used as ink. However, during the process the ink is first printed by separate cells and then merged together, so that the images may not be continuous everywhere, which may lead to electronic discontinuities in small feature devices like thin film transistors. It is difficult to achieve a very straight pattern edge and very fine features as well. So gravure printing is more suitable to print patterns over relative large areas.

2.4 Pad Printing

Pad printing uses a cliché plate which is very similar to a gravure plate. The printing process is sketched in figure 2.8. First the recessed area on the plate is filled with ink

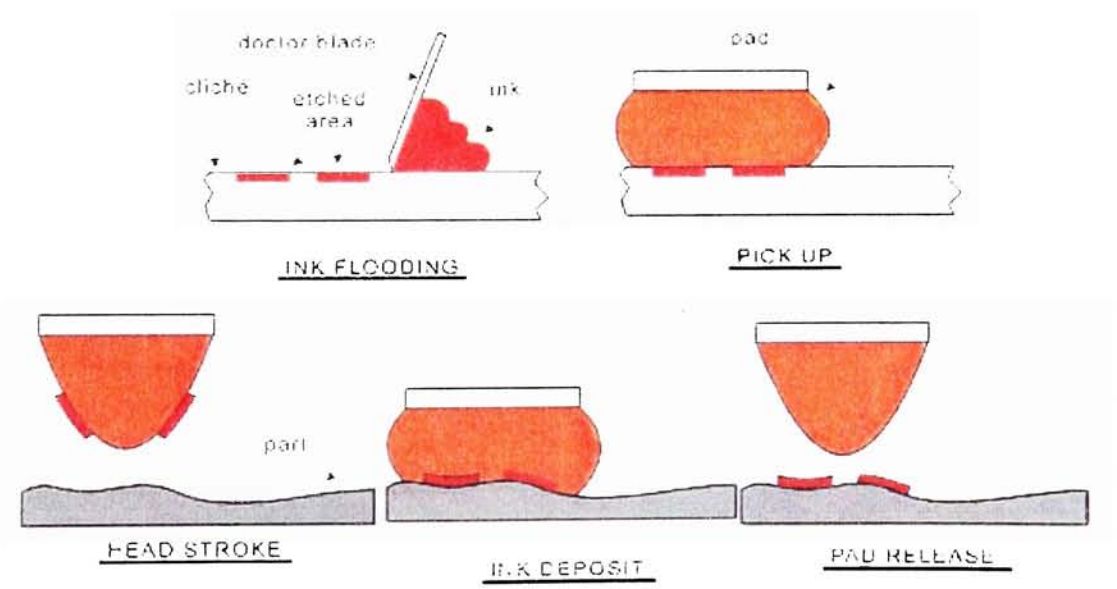

Figure 2.8 Pad Printing Process [16]

by passing a doctor blade across the plate surface. Then a pliable pad is used to pick up

the ink out of the cliché plate and transfer it to the substrate, according to the adhesion strength of the ink to the different surfaces as well as the thermodynamic process of solvent evaporation.

The apparent advantage of pad printing is it can make images on relatively rough surfaces. And in some sense it solves the resolution and discontinuity problems in gravure printing. By using the pad rather than transfer the ink in the engraved cells directly to the substrate, the surface and edge of the ink unit can be quite smooth. Moreover, instead of using very small dimension gravure cell, the etched area in the cliché plate can be relatively large so the image can be transferred as a unit. A passive display device patterned on a flexible paper substrate by pad printing has recently been demonstrated [17]. However, the low throughput and cost of plate may limit its application.

2.5 Screen Printing

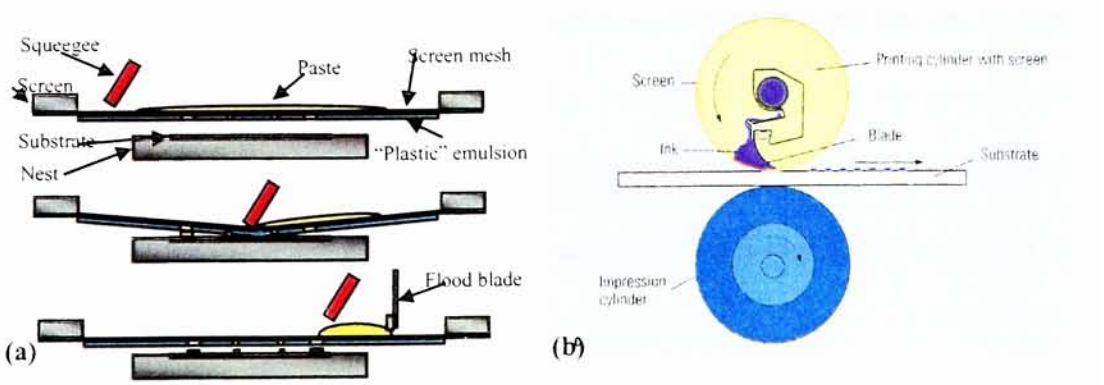

Figure 2.9 Screen Printing Process [14] (a) Working Mechanism (b) Overview

Screen printing is able to print ink films from sub micrometer to hundreds of

micrometers thick, which makes it possible to have a wide range of applications. It has already been used under clean room conditions to attach and fabricate microelectronic components and interconnects during assembly process. Many researchers also use this technique to make conductive electrodes for thin film devices [18,19].

Figure 2.9(a) shows the equipment and the principle of screen printing. The ink is deposited on the upper surface of the screen, which is held slightly above the substrate. The structure of the image to be printed is pre-patterned on the screen. During the process, a squeegee blade is used to force the screen near the substrate and push the ink through the screen forming the image. For high volume printing a rotary screen cylinder can be applied, as shown in figure 2.9(b).

Screen printing can print thick ink films with great precision, which most of other processes cannot achieve. But its suitability for printing thin layers is relatively low. High viscosity shear thinning ink is needed so that the ink can stay on the screen without shearing while transfer smoothly through the screen by the passage of the squeegee. It is hard to formulate such ink using soluble organic semiconductor materials without additives. As a result, screen printing is mainly used in making large conductive areas.

2.6 Inkjet Printing

Inkjet is a non-impact printing process, which means that the printing is controlled by

an electronic device and the image on the computer can be directly printed onto the substrate without any traditional printing media like a plate or screen. It offers the process a great flexibility and because of that, inkjet printing has been widely used in our daily life. Figure 2.10 is a cross section sketch of Drop-on-Demand (DoD) inkjet system. The ink chamber has a nozzle at one side and a piezo-electric crystal (PZT) at the other end. When it is moved to the printing position, an electric pulse is applied to the PZT which make it expand and contract. The pressure wave created in this process will eject ink droplets through the nozzle onto the substrate. Instead of PZT, another very similar process called bubble jet printing places a vapor bubble inside the chamber whose volume is controlled by a microheater. The moving of the print head and the oscillation of the ink is precisely controlled by a computer so very high resolution can be achieved by inkjet printing.

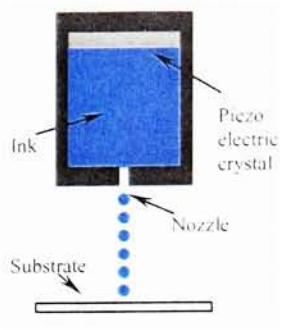

Figure 2.10 Inkjet Printing

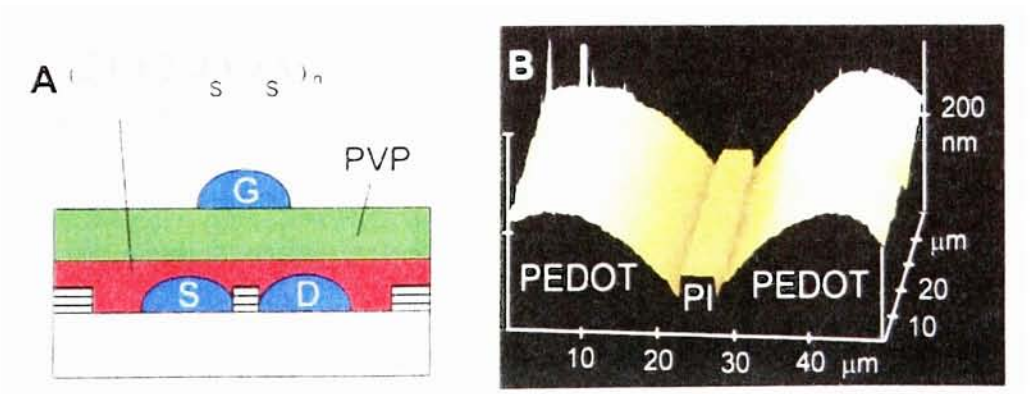

Figure 2.11 Inkjet Printed Transistor [10] (a) Cross Section (b) Source and Drain Image

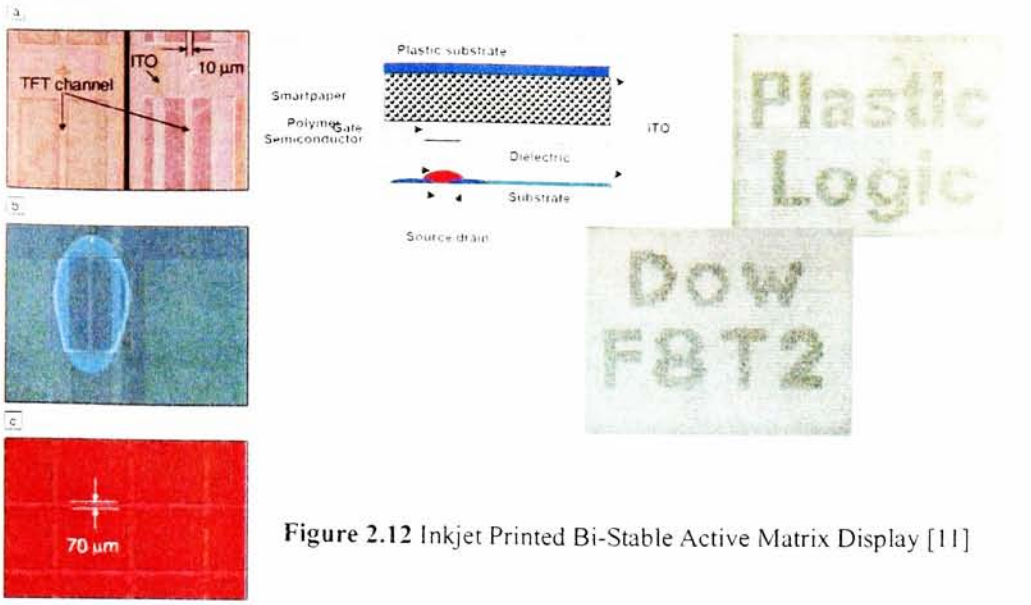

Figure 2.12 Inkjet Printed Bi-Stable Active Matrix Display [11]

Given the high resolution, a lot of research has been done on inkjet printing electronics. Figure 2.11 shows a transistor printed by inkjet. It is the first all organic transistor which was made by printing technology. Its source and drain were printed using PEDOT:PSS and the distance between them (channel length) is less than 10 µm, as can be seen from the AFM image of the electrodes. F8T2 (Poly(9,9-dioctylfluorene-co-bithiophene) alternating copolymer) and PVP were used as semiconductor and dielectric layer, respectively. These devices were used to control a bi-stable active matrix display, which is shown in figure 2.12. In this device, each display unit (pixel) was controlled by a thin film transistor. The smart paper deposited on top of the TFT can switch its color according to the bias voltage which is controlled by the on/off state of the transistor. The monochrome image can be programmed and switched like a display. Color displays are expected in the near future if people can assemble OLEDs and filters with these transistors.

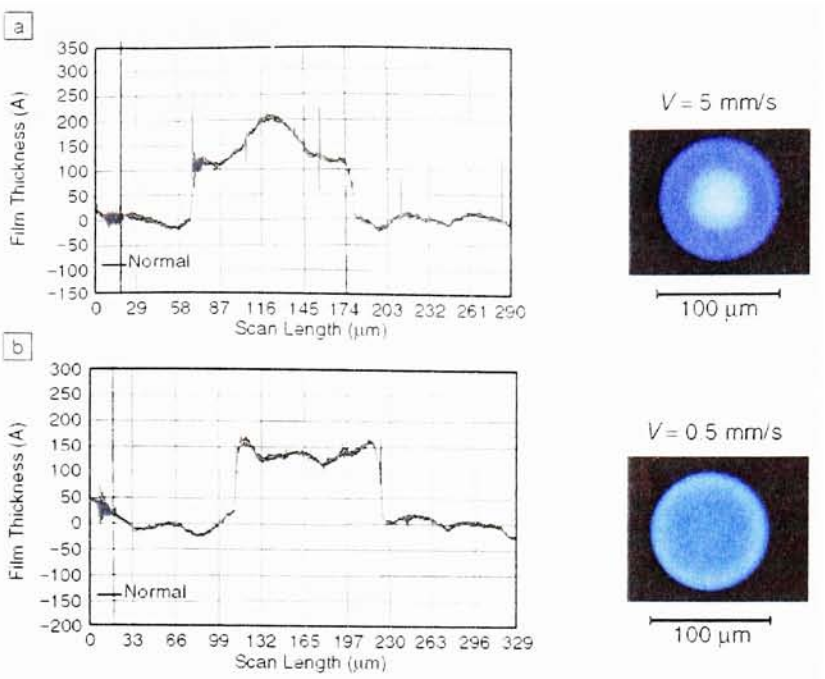

Figure 2.13 Surface Roughness in Inkjet Printing (a) Higher Center(b) Higher Edge [20]

Besides high resolution, inkjet printing has other advantages. A large variety of materials can be used, the printing process is non-contact and clean (do not need to clean up accessory printing equipments like plate, screen, doctor blade, etc), and there is almost no waste of ink. However, the throughput of inkjet is relatively low, and the printed surface may not be quite uniform. Figure 2.13 shows the "coffee stain" phenomenon caused by uneven evaporation of solvent. Moreover, since in inkjet, images are always printed dot by dot, large uniform areas and long continuous lines are hard to achieve. Further work needs to be done for the commercial application of inkjet printing.

2.7 Thermal Transfer

Thermal transfer (also called laser transfer, laser ablation, laser forward transfer, etc) is another popular printing process for producing high quality images. It was first used

for printing electronics by DuPont Co. [21] As can be seen from figure 2.14, an ink sheet comprising a transparent substrate (plastic), a light sensitive layer and a pre-coated functional layer is placed upside down under the laser emitter. During printing the sheet can be placed either adjacent to the substrate or separated slightly. At the printing location, a high energy laser transfers the pre-coated material to the substrates. The energy of the beam and the surface energy of the material are selected properly so the image can stick onto the substrate tightly.

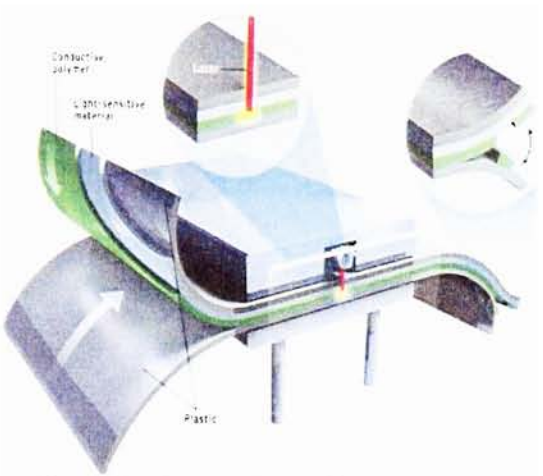

Figure 2.14 Thermal Transfer Process used in Conductive Polymer Printing (DuPont Co.)

One of the unique advantages of thermal transfer is that it is a completely dry process. All the printing processes described above need liquid ink, which means the functional materials must be combined with some solvent, or other additives to meet the required viscosity and other requirements. After drying there can be some contaminates remaining in the ink, which will influence the properties of the functional materials. Moreover, most of the complicated electronic devices can only fabricated by multi-layer printing. This cannot be achieved if the ink contains a solvent which will dissolve materials in previous layer(s). This technique can also achieve relatively high resolution (5-10 μm), which makes thermal transfer a very promising device fabrication technique.

2.8 MicroPen Printing

MicroPen direct writing system is a unique fabrication tool that deposits materials under high pressure through a fine conical capillary tip. The writing process is similar to a ball pen except its movement is controlled by the computer in micrometer precision. It can be considered an easy and high flexible printing process. The equipment, shown in figure 2.15, is made by Ohmcraft Inc. and primarily used to print resistors. A study by the author in collaboration with this company found that this method is able to print conductive and semiconductive materials having good resolution and sharp edges. This will be discussed further in chapter 5.

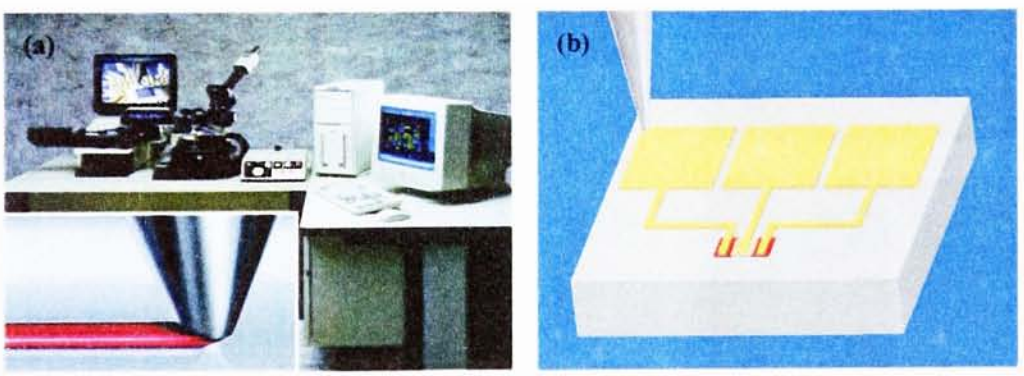

Figure 2.15 MicroPen Printing (a) Equipment (b) MicroPen Printed Electrodes

2.9 Soft-lithography

Soft-lithography describes a group of contact printing techniques used extensively for organic thin film devices fabrication. These techniques include contact printing, transfer molding, near field lithography, and other related techniques [22-25]. Soft lithography can produce features smaller than 0.1 μm, which is much less than the

resolution of the traditional printing processes (>10 μm) as discussed in the past several sections. Meanwhile, its field size is not restricted to the wafer size, and its throughput can be greatly improved relative to the silicon process, particularly when using reel-to-reel patterning configuration similar to flexographic printing. Two typical soft lithography processes (micro contact printing and nanoscale transfer printing) will be discussed here.

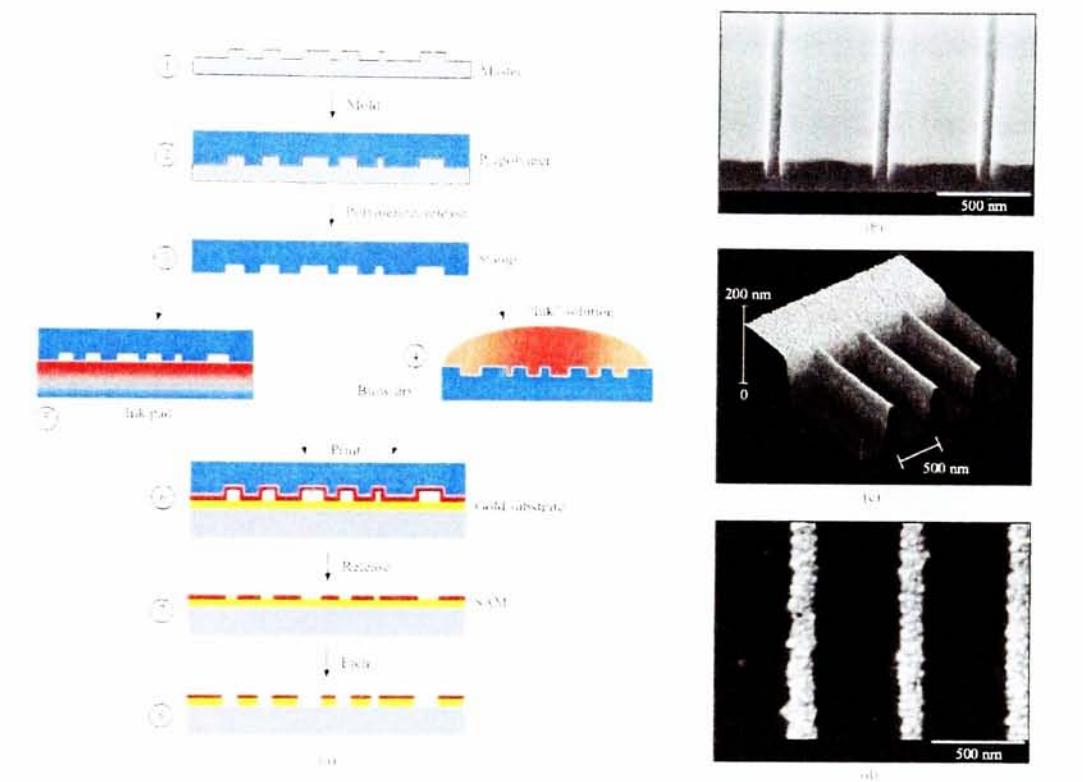

Figure 2.16 Micro Contact Printing [30] (a) Process Sketch (b)~(d) Stamp Images

In micro contact printing (μ-CP), the master is generally patterned using e-beam or photolithography and the process is carefully controlled to produce the critical size, uniform etch thickness and smooth etched surface. Then a stamp is molded from a template (master) having the features of the pattern in relief. The stamp is always made of polydimethylsiloxane (PDMS), which has a low surface energy and is able to

transfer different materials (metals [26], polymers [27] and even proteins [28]) to a variety of substrates. Before printing, the functional layer is pre-coated on the stamp or substrate. By bringing the stamp into conformal contact with the substrate, the ink from raised regions of the stamp is transferred. Frequently, alkane thiols are used to form self-assembled monolayer (SAMs) on the surface of gold layers [29]. Since the monolayer has a low surface energy and prevents further chemical attachment, it will protect the underneath layer during the etching process, while the part not covered by SAM will be etched away and a patterned material having fine feature sizes can be fabricated. A sketch of the whole process can be found in figure 2.16.

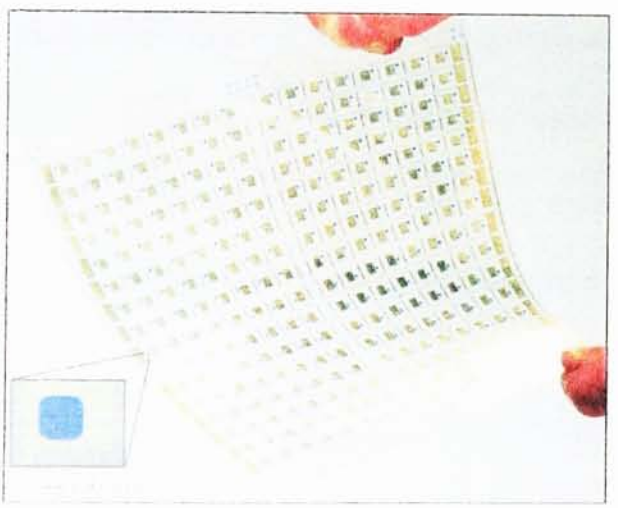

Figure 2.17 Active Matrix Backplane Circuit [31]

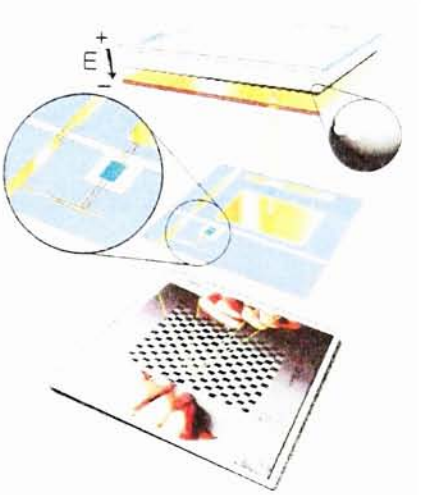

Figure 2.18 E-Ink Display [32]

Some of the applications of micro contact printing achieved by John Rogers' group are shown in figures 2.17 and 2.18. As can been seen, a large area active matrix display has been printed on plastic (PET). The display is black and white, 16×16 pixel array, over a 5×5 inch area. Each pixel is composed of a printed polymer thin film transistor and an electrophoretic display. The display consists of a sandwich of two electrode layers outside of a layer of micro-capsules which have two colors of pigment particles inside.

The color (pigment particles) shown in the visible side of the capsules is controlled and switched by the bias voltage applied on the electrode [33], which is determined by the on/off state of the transistor. The mechanism is similar to the inkjet printed display demonstrated in the last section, but μ-CP is expected to achieve much higher resolution in batch production.

The use of PDMS restricts the resolution of micro contact printing, which suffers limitations of surface diffusion, edge disorder and post-printing etching. To improve these properties, a technique called nanoscale transfer printing (nPT) was recently developed[34]. Figure 2.19(a) shows a scheme of the printing process using a silicon wafer substrate. The wafer is pretreated to generate surface hydroxyl (-OH) groups on the native SiO_2 layer, then a SAM layer is generated with thiol group oriented upward by the introduction of 3-mercaptopropyltrimethoxysilane (MPTMS). Upon contact

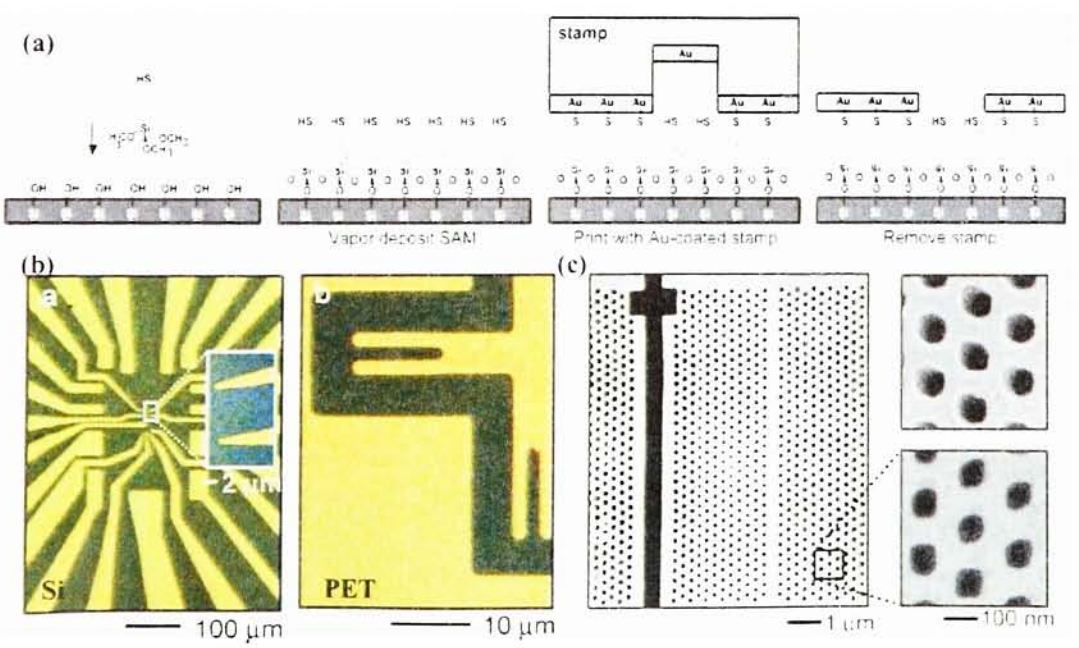

Figure 2.19 Nanoscale Transfer Printing [34] (a) Printing Process (b) Gold Electrode Printed on Silicon Wafer and PET (c) Ultra-high Feature Size Pattern and Coated Stamp (Top Right)

with the gold deposited on the stamp, sulfur-gold bonds will be formed which show good adhesion. Using this method, no etching is needed. Figure 2.19(b) shows some printed samples on silicon wafer and plastic, respectively. To increase the resolution, a GaAs stamp is used to replace the PDMS stamps. Using a similar process [34], ultra-fine patterns can be achieved which are shown in figure 2.19(c).

2.9 Summary

The possibility of bringing thin film electronic devices into batch production makes printing electronics an important research topic. With the advantages of low cost, large area and flexible substrates, these techniques may become good complements to the silicon based integrated circuit. Table 2.1 summaries the properties of different printing technologies. The ones written in green are advantages, while red indicates disadvantages. Clearly, no single technique is perfect for every aspect of consideration. For different patterning requirements the proper methods should be chosen. Several printed devices have been fabricated and tested which will be demonstrated in the following chapters.

	Relief					No Relief			
	Raised			Lowered					
	Flexography	Letterpress	Soft Lithography	Gravure	Pad	Offset Lithography	Screen	Ink-Jet	Thermal/Ablation
Lat. Res. (µm)	75	75	0.03	75	20	10-50	30	20-50	5
Ink thickness (µm)	3-8	~3	Monolayer	2-5	4-6	< 2.5	100	~ 0.1	< 1
Ink viscosity (mPas)	50-500	50,000-150,000		50-200	> 50	20,000-100,000	500-50,000	< 20	N/A
Throughput (m^2/sec.)	10	1		60	0.1	20	< 10	0.01	0.002
Resolution	Low		Best	Dots		Good		Dots	
Production volume	High		Low	High	Low	High	Low	Low	Low
Ease/$ of making plates	Easy	Easy	Hard	$	$	Easy	Moderate	N/A	N/A
Amount of material			Small		Small		Small	Small	
Substrate requirements				Smooth	Wide Variety				
Ink viscosity	Low		Low	Low	High	High, Sheer thining	High	Low	N/A
Additives needed			None			Worst		Good	Good
Thin ink layer			Extremely			Thin		Extremely	Yes
Thick ink layer	Thick		No		Yes		Thickest	Yes	No
Particulates	Yes	Yes	No	Yes	Yes	Yes	Yes	Yes	
Soluble polymers	Yes	Yes	Yes	Yes	No	With additives	Yes	Yes	Yes
Need for ink leveling	Anilox			Yes			Yes	Overlap	
Material versatility	Good		Good					Good	
Other issues		Less common Ink metering				(Water)		Ink spreading Coffee stain Solvent compatibility Satellites	Dry Heat

Table 2.1 Printing Process Comparison [35]

Chapter Three: Lithography Printed Conductive Patterns — Printing Capability Study

The process capabilities of lithographic printing for producing electrically conductive patterns were investigated in this study. Test patterns were designed specifically for this purpose. Commercially available conductive lithographic ink loaded with silver metal flakes was used to print the targets. The printed test patterns were characterized by profilometry, optical microscopy, and electrical measurements. A number of parameters were examined, including physical parameters (line width, line thickness, space between lines) and electrical parameters (electrical conductivity, sheet resistance, longest electrically continuous path length, shorts between adjacent conductors, etc.) as a function of the printing conditions (number of impressions, registration, post treatment, substrate).

3.1 Introduction

Printing technologies have received much interest recently for their ability to pattern a variety of different types of functional materials. Direct printing of electronic features may eliminate complex procedures employed in traditional electronics manufacturing, leading to low cost devices. One of the largest current market opportunities is using printing to produce antennas for RFID tags. The demand for RFID tags may grow to billions or trillions of tags per year in the near future. Announcements by Wal-Mart and the U.S Department of Defense of their desire to implement RFID technology on a

large scale are largely responsible for much of this demand. In addition to the large market for RFID, other products such as displays, thin film transistors, photovoltaics, and sensors may benefit from the unique advantages offered by using printing as a manufacturing technology.

The majority of the work in this area has involved ink-jet and screen-printing technologies. However, screen and ink-jet printing are relatively slow which limits their volume and use in manufacturing [11][36]. One of the major high volume printing processes currently in use is offset lithography. Printing of conductive inks to fabricate circuits [37,38], sensors [39], microwave integrated circuits (MIC) [40], radio frequency circulator components on a wide range of flexible materials [41] etc. have been reported using this technology. However, most of the systematic studies on lithography focused on how to make a stable printing plate with high resolution [42-45]. Apparently, there are a lot of factors that will influence the printing quality. A patent from Akihiro et al. [43] claimed an X-ray lithography plate with submicron feature size, but the general resolution reported is still in the scale of ten microns [14]. A patent by Akihisa Nakajima [46] reported using an organic solvent and surfactant to accomplish "waterless" lithography, which eventually increased the quality of the pattern. But the influence on print quality of the printing process itself, including printing directions, dispersion of the ink, post-curing conditions, etc. remains unclear. For printed electronics, the ability to adjust the thickness of the patterns, the conductivity and continuity of the pattern are all very important issues, which haven't

been reported elsewhere. In the current investigation we assessed the process capabilities of the offset lithographic printing process by printing conductive lines having different line width, space width and line thickness, and measuring their structural and electrical properties. Interdigitated test patterns [38] were designed specifically for this purpose. Commercially available conductive lithographic ink loaded with silver metal flakes was used to print the targets.

Some of the parameters examined include:

- Line width and spacing: minimum, maximum and tolerance
- Multiple impressions: effect on conductivity, line thickness, resolution and alignment.
- Post treatments: curing and time interval.

We characterized the test targets using electrical and physical means in order to establish limits of what can be expected/obtained using this process and equipment.

3.2 Experimental

The test targets were designed and programmed in PostScript. The PostScript code includes parameters to change the line widths and gaps to obtain the various targets in both the vertical and the horizontal orientations. The internal logic of PostScript adapts to the output device and gives the required resolution. The resolution used was 2400dpi. The test targets were written to Kodak Recording 2000 negative film at a resolution of 2400 dpi using an AGFA SelectSet 5000 Imagesetter. The film was developed using

RA 2000 developer and Kodak RA 3000 fixer in a Dupont Easy Compact 95 Rapid Access Film Processor.

Enco aluminium plates covered with a UV sensitive photoresist polymer were used. These plates have a ridged/grained texture that helps to hold water on the non image areas during the printing process. These plates were exposed for 1.5 minutes in a 25 psi vacuum using a Nu-arc Ft32V3UP ultra-plus flip flop platemaker. They were developed using Enco ND-143 Negative aqueous developer, and finished using New Century Press Room Product-Plate Cleaner, Preserver and Finisher.

An Itek 960 Offset Duplicator press was used with R10 Conductive Ink Formula 2 (Precisia), and Anchor # 7039 ISO 99 fountain solution. The ink viscosity was determined to be 100 Pa.s at 10 rpm using a Brookfield viscometer. The equipment and rollers were cleaned after printing using Varn Wash V-120 and LBC Special General Purpose Cleaner from Danka Industries. The substrate used was Sapp Lustro Coloss 100# text paper. Different numbers of impressions were obtained by feeding printed (and dried) patterns back into the duplicator.

Each sample was evaluated in both the horizontal (pattern lines perpendicular to the direction of printing) and the vertical (pattern lines parallel to the direction of printing) directions. The line widths used in the test patterns were 42, 84 and 126 μm. To obtain

two and three impression samples, single impression samples were dried after printing and some of them were fed into the duplicator again to receive a second impression. Following this second impression, the samples were dried again, and some of them fed into the duplicator for a third time.

The actual line widths were obtained using an Olympus BX60 optical microscope at 120X magnification and ImagePro (Media Cybernetics) image evaluation software. Line thickness (height) measurement was carried out using a Tencor P2 profilometer, using the following conditions: 1000 μm scan length, 50 μm/sec scan speed, 40 sec scan time, 50 Hz sampling rate, 1.00 μm horizontal (lateral) resolution, 300 μm/25 Å vertical range resolution. Electrical conductivity was tested using a Fluke 73 Multimeter.

3.3 Test Target

The design of the interdigitated test pattern is shown in figure 3.1. Six patterns with line widths of 42μm, 84μm and 126μm, respectively and in vertical or horizontal orientations with respect to the printing direction were incorporated in one test form. In every pattern there are two continuous parallel lines whose terminals are marked as 1 and 2, respectively as shown in the figure. The widths of the lines as well as the space between them are the same and are written below each pattern in the target. In order to assess the contribution of printing direction (horizontal or vertical) on the electrical

results, the lines that run horizontally on this test pattern are thicker than the lines that run vertical. This gives the advantage that the conductivity is dominated by the lines running in the vertical direction. Furthermore, the thick horizontal lines also serve as convenient pads for measuring the conductivity at intermediate positions along the test pattern. Including the two extreme terminals there are a total of 26 electrodes for every line. By measuring adjacent electrodes along the same line, the resistance as well as the

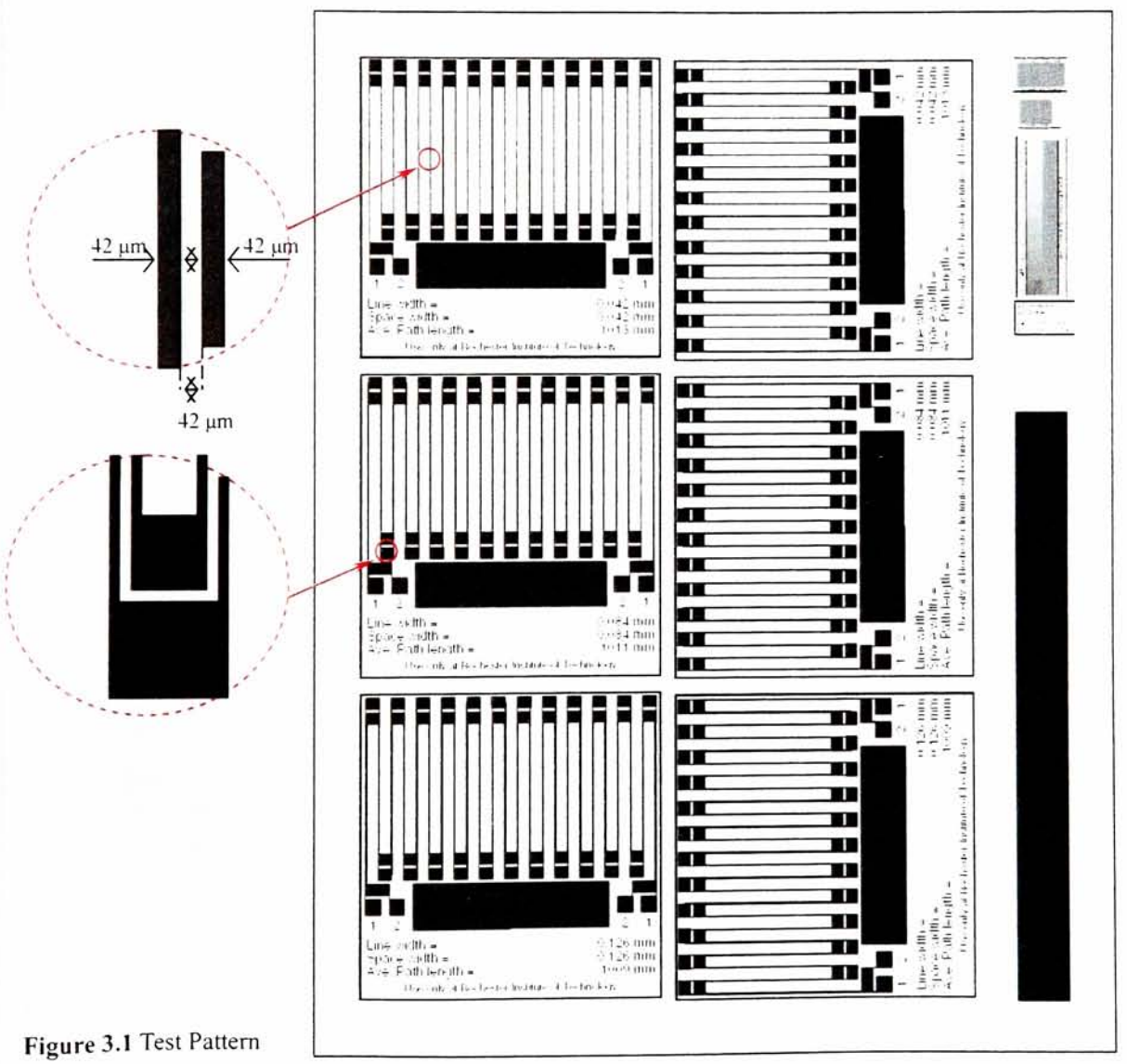

Figure 3.1 Test Pattern

sheet resistance can be tested for short lengths of the lines. Short circuits can be detected and located by testing the resistance between two adjacent electrodes in different lines.

3.4 Line and Space Width

Different line widths were printed having one, two and three impressions. Representative patterns with different line widths are shown in figure 3.2. Figure 3.3 shows lines printed with different number of impressions. As can be seen from these figures, the line edge is relative sharp and smooth (compare to flexographic image shown in figure 2.3). We can achieve the minimum line width (as well as space width) that we attempted of 42 μm while keeping the lines separate from each other.

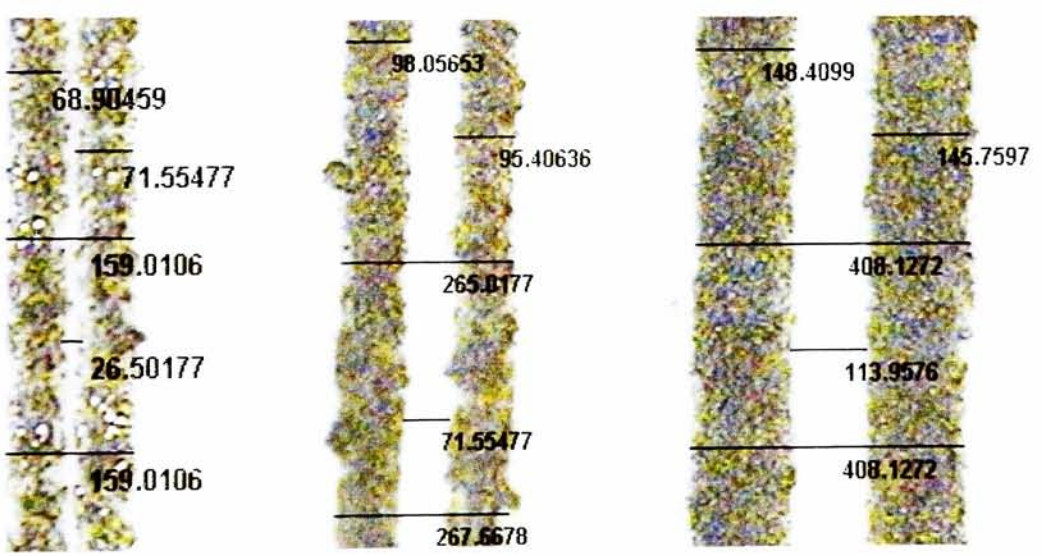

Figure 3.2 Optical Micrographs (120 X) of Printed Lines with Different Widths: the nominal line widths are (left to right) 42, 84, 126 μm, respectively.

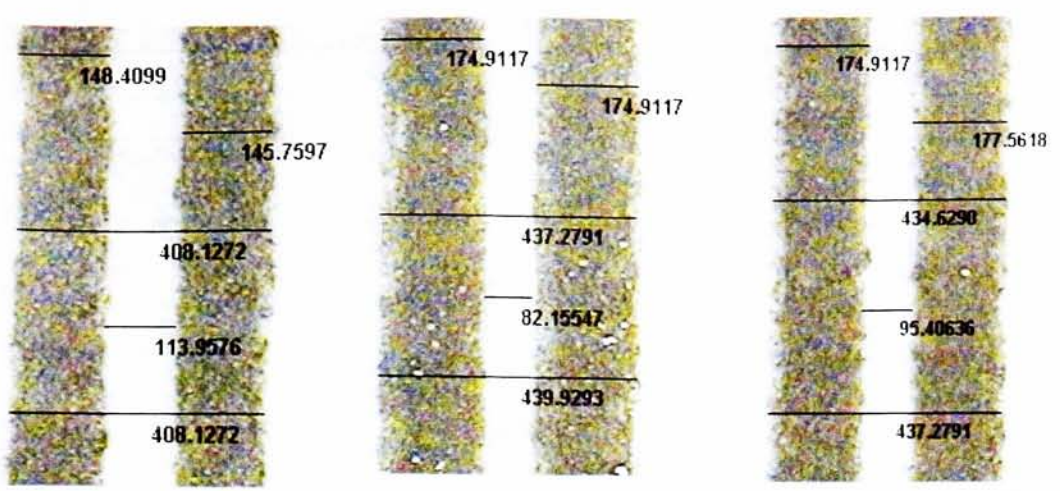

Figure 3.3 Different Number of Impressions: (left to right) one, two and three impressions for 128 μm line.

Table 3.1 shows the measured line widths as well as the percent increase from the designed (nominal) dimensions. It is due to the spreading of the ink during and after the printing. This information is shown graphically in figures 3.4 and 3.5. The table and figure show that the degree of increase is not proportional to the width of the pattern printed. Actually, the increase is relatively constant. According to the working mechanism of offset lithography printing discussed in chapter two, the non-image part on the plate is hydrophilic which keeps ink away. Moreover, the lithographic ink is viscous and printed layer is only around 1μm in thickness. So the smooth edge and the limited amount of excess-printing compared to flexographic printing was observed

Results Table		Line width					
		Vertical			Horizontal		
# of Impressions	Line width (μm)	Ave. Measured	Increase	% Increase	Ave. Measured	Increase	% Increase
1	42	69	27	64	83	41	98
	84	98	14	16	124	40	47
	126	147	21	17	167	41	33
2	42	70	28	67	78	36	85
	84	125	41	48	137	53	64
	126	175	49	39	169	43	34
3	42	72	30	70			
	84	135	51	61			
	126	176	50	40			

Table 3.1 Line Width and % Increase of the Size

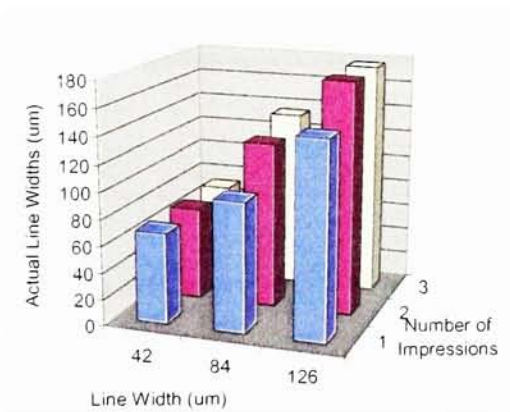

Figure 3.4 Actual Line Width Increase vs. Nominal Line Width and Number of Impressions

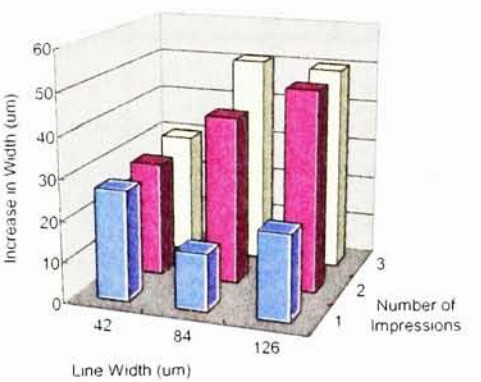

Figure 3.5 Absolute Line Width Increase vs. Nominal Line Width and Number of Impressions

An important factor that influences the line width is the printing direction. The horizontal sample is perpendicular to the direction of printing and to the direction of release of the substrate. This direction shows a larger line width increase than the vertical lines. We observed that in the horizontal direction, the registration between

two layers was worse than in the vertical direction. This can be seen from figure 3.6 where the three impression image printed horizontally shows worse registration than the similar feature printed vertically. The

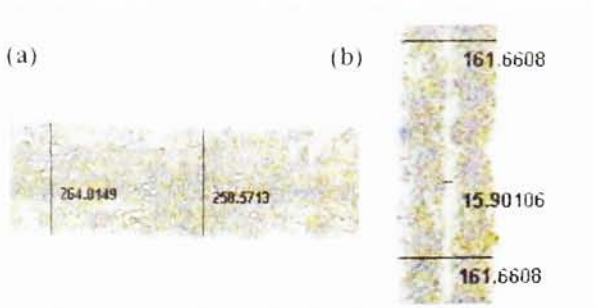

Figure 3.6 Optical Micrographs of 42μm Three Impression Printed Patterns **a)** Horizontal Direction (Poorly Aligned) **b)** Vertical Direction (Well Aligned)

corresponding space widths in relatively well aligned patterns and their decrease compared to the test target are shown in table 3.2.

Results Table		Space width					
		Vertical			Horizontal		
# of Impressions	Space width (μm)	Measured	Decrease	% Decrease	Measured	Decrease	% Decrease
1	42	24	27	64	27	41	98
	84	72	14	16	68	40	47
	126	147	21	17	167	41	33
2	42	70	28	67	78	36	85
	84	125	41	48	137	53	64
	126	175	49	39	169	43	34
3	42	72	30	70			
	84	135	51	61			
	126	176	50	40			

Table 3.2 Space Width and % Decrease of the Size

The major challenge in multilayer printing is the alignment accuracy of the subsequent layers of ink with the previous layers. As can be seen in the table and images, the best line resolution (minimum line width) was obtained for a single impression. The registration for the two and three impressions was not very good due to machine

limitations and this reduced the resolution. However, multiple layers improved the line thickness and hence the conductivity of the printed line. This factor also should be concerned when fabricating complicated multi-layer electronic devices.

3.5 Line Thickness

Table 3.3 shows the results of the line thickness for each of the samples. The stylus profilometry image of the line cross section is shown in figure 3.7. Although the surface of these printed layers is quite rough, it can be seen that the line thickness increases with the number of impressions. However, figure 3.8 and 3.9 shows that the line thickness increases by approximately 46% going from one to two impressions and by about 18% going from two to three impressions. This shows that multiple layers are not simply stacked on each other, and that the relative increase in height decreases with the number of impressions. This phenomenon can be explained several ways. First of all, the pressure between the blanket and impression cylinder increased as the substrate

		Thickness					
		Vertical (Average from five tests)			Horizontal		
# of Impressions	Line width (μm)	Line 1(μm)	Line 2	Average	Line 1(μm)	Line 2	Average
1	42	0.31	0.36	0.33	0.23	0.25	0.24
	84	0.66	0.69	0.67	0.20	0.55	0.38
	126	0.70	0.79	0.74	0.61	0.76	0.69
2	42	0.41	0.40	0.41	0.15	0.41	0.28
	84	0.97	1.02	1.00	1.08	0.44	0.76
	126	1.15	0.99	1.07	1.32	1.68	1.50
3	42	0.68	0.70	0.69			
	84	1.03	1.25	1.14			
	126	1.31	1.30	1.30			

Table 3.3 Line Thickness

(paper substrate plus original printed layer) became thicker, which resulted in a relatively thin layer. Also, the pattern might not be totally dried before a second layer printed on. Moreover, the substrate and silver ink are porous, which causes part of each new printed layer to penetrate through previous layers and decreasing the thickness of subsequent layers. Another phenomenon that can be seen is that the thickness increases with line width.

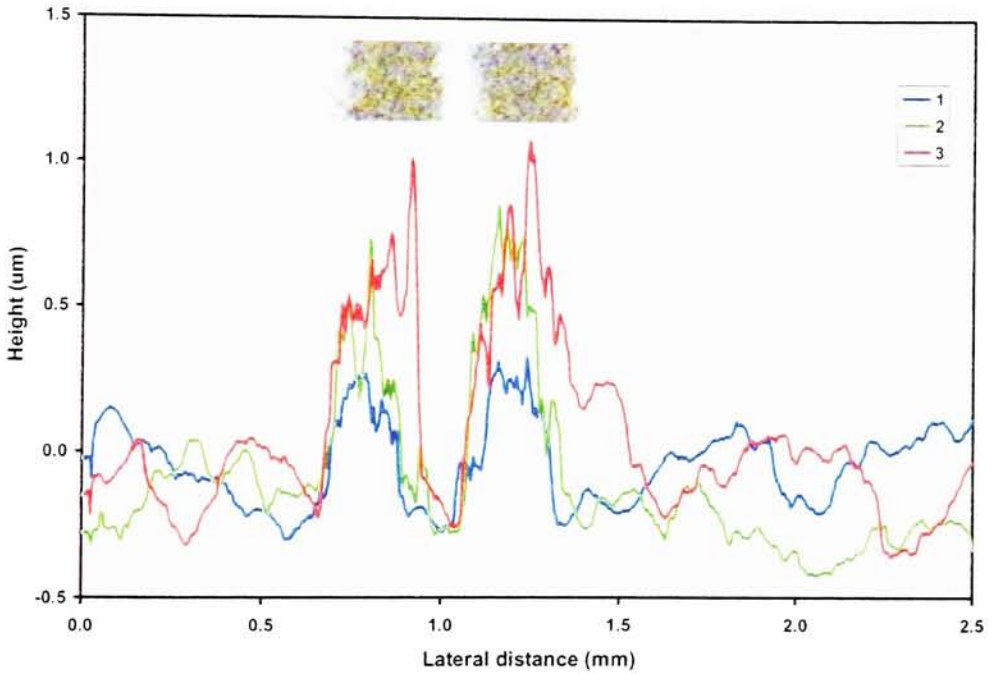

Figure 3.7 Profilometry vs. Number of Impressions

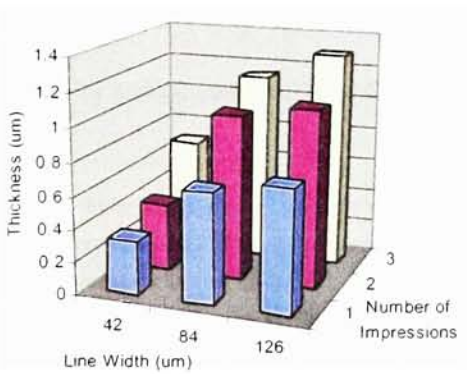

Figure 3.8 Line Thickness vs. Nominal Line Width and Number of Impressions

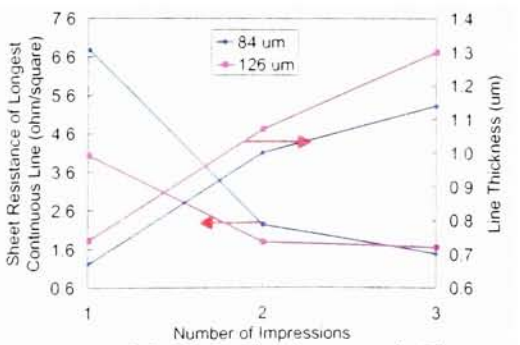

Figure 3.9 Line Thickness and Sheet Resistance Increase with Number of Impressions in 84 and 126 μm lines.

3.6 Conductivity

We tested the resistance of the lines (26 electrodes per line, two conductive lines per pattern, as shown in figure 3.1) and calculated the corresponding sheet resistance. The results are shown in table 3.4 and figures 3.9~3.11. The maximum continuous conductive length we obtained is about one meter (including pads). The lowest sheet resistivity along a distance of 551 mm is less than 1.5 ohm/□[1].

The sheet resistivity of the samples decreases (conductivity increases) with the number of impressions. As is shown in figure 3.9 there is a greater increase in conductivity (decrease in resistivity) going from one to two impressions than going from two to three impressions. This is because deposition of the second ink layer essentially fills up voids that are left in the first layer increasing the conductivity. Also, much of the first impression fills voids in the rough surface of the substrate (coated paper), and does not contribute as much to the conductivity as subsequent layers. This phenomenon is also exhibited in the results of the line thickness where the deposition of the second layer does not increase the thickness proportionally. The sheet resistance of the lines is essentially independent of the line widths. The continuous conductive length increases

[1] Ω/□: Essentially, the term □ takes into account the geometry of the trace that is measured. The resistance increases as the length of the line increases and decreases as the width of the line decreases. To take these geometrical factors into account, the measured resistance is divided by the length, and multiplied by the width. This is the same as dividing by the number of "squares" where square is the length divided by the width. As long as the same units are used for the length and width, they will cancel out. This unit compensates for the feature geometry in two dimensions.

from 42 μm to 126 μm feature size in each sample and also with the number of impressions.

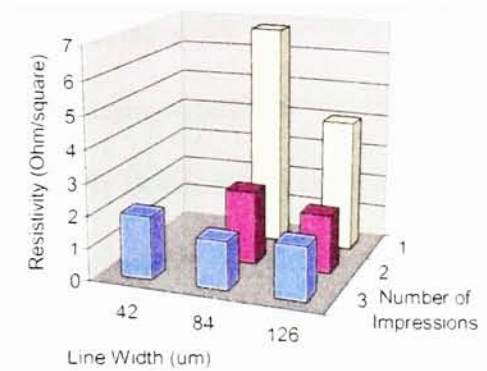

Figure 3.10 Line Resistance vs. Nominal Line Width and Number of Impressions

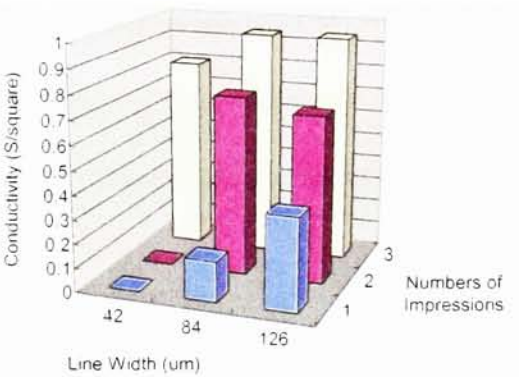

Figure 3.11 Line Conductance vs. Nominal Line Width and Number of Impressions

Results Table		Sheet Resistance (Using Actual Line Widths)							
		Vertical				Horizontal			
# of Impressions	Line width (μm)	minimum $R_{\square}$	average $R_{\square}$	standard deviation	longest continuous line(mm)/ $R_{\square}$	minimum $R_{\square}$	average $R_{\square}$	standard deviation	longest continuous line(mm)/ $R_{\square}$
1	42								
	84	5.98	7.04	0.82	77/6.79				
	126	2.59	4.36	0.99	192.5/4.03	4.58	8.20	4.05	77/5.58
2	42								
	84	1.34	2.62	0.50	500.5/2.23	2.11	2.91	0.36	934/2.89
	126	1.44	2.58	0.44	320/1.78	2.03	2.89	0.49	544/3.30
3	42	1.25	2.13	0.28	320/1.96				
	84	1.06	1.93	0.39	551/1.48				
	126	1.06	1.70	0.26	934/1.65				

Table 3.4 Resistance and Sheet Resistance of the Lines

For the ink that we used, the conductivity increased with time and heat treatment. Figure 3.12 shows the resistance of a sample (line width 84μm, horizontal printing, and two impressions) as a function of the curing conditions.

Table 3.5 gives the resistivity data for all the samples. This phenomenon is most likely due to drying of the ink (which may occur by a variety of mechanisms) which gives rise to improved packing of the silver particles with time. This causes a decrease in the resistivity (hence an increase in the conductivity). This process can be accelerated by high temperature treatment for a short time.

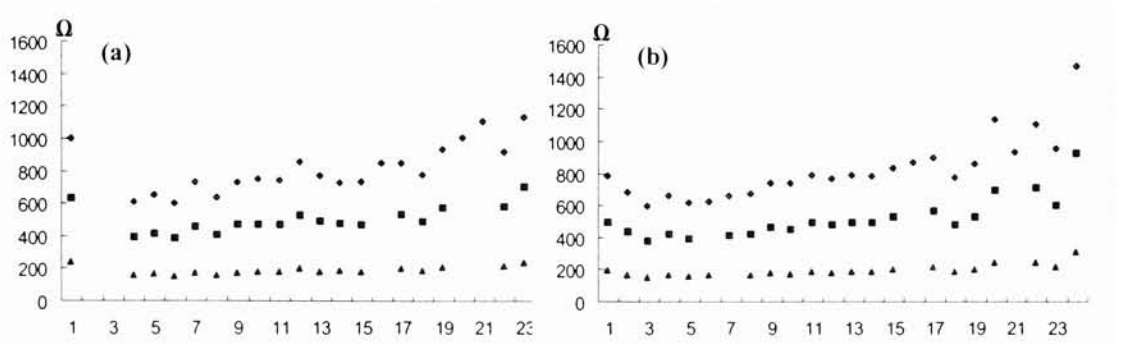

Fig 3.12 Resistance of a Sample (Line Width 84μm, Horizontal Printing, Two Impression) (a) and (b) are the two parallel lines, blue diamonds are the original data, pink squares were tested after two weeks put in room temperature and the green triangles were heated in 130^0C after 10 min and tested after sample cooled down to room temperature.

Line Parameters		84 um, double impression, horizontal	126 um, double impression, vertical	126 um, triple impression, vertical
Original	lowest R□	2.11	1.44	1.06
	average R□	2.91	2.58	1.70
	standard deviation	0.36	0.44	0.26
	longest continuous line(mm)/R□	934/2.89	320/1.78	934/1.65
After 2 Weeks	lowest R□	1.34	0.85	0.68
	average R□	1.85	1.52	1.10
	standard deviation	0.28	0.27	0.17
	longest continuous line(mm)/R□	462/1.61	320/1.07	934/1.07
130 °c 10 min.	lowest R□	0.54		
	average R□	0.69		
	standard deviation	0.07		
	longest continuous line(mm)/R□	462/0.62		

Table 3.5 Change of Resistance with Curing Conditions

3.7 Conclusions

A number of test targets for the conductivity studies were designed by changing factors like line width, space width, incorporation of the electrode pads in the test patterns and the path length. A suitable test form was then designed and a series of experiments were conducted using offset lithographic printing including changes in parameters such as printing direction, curing, substrate and line thickness.

We have successfully printed lines and spaces between lines from 42-126 μm. Electrical continuity was achieved for the 84 and 126 μm lines. The thickness of lines was found to lie in the range of 0.5 to 1.5 μm and increased with increase in number of impressions. Increasing the number of impressions improved the electrical

conductivity more than the thickness increased. We obtained a maximum continuous conductive length of longer than one meter (including pads) and sheet resistivity less than 1.5 ohm/□.

It was found that a post treatment of heat and time aided in increasing the conductivity. An average decrease of about 25% in sheet resistance was obtained due to the post treatments.

Chapter Four: Polymerization of Aniline

Conductive polymers have been studied for decades due to their optical, electrical, electrochemical properties, and the possibility of building devices based on these. Polyaniline is considered to be one of the most promising materials for industry. It has the advantage of commercial availability, environmental stablility [48], easy synthesis [49], and solubility [50-53]. Polyaniline is a well known material for sensing, and is used as functional layer for the all-printed sensor project, which will be discussed in detail in next chapter. A summer project advised by Dr. K.S.V. Santhanam on template free electrochemical synthesis of polyaniline nanostructure is demonstrated, another polymerization routine (interfacial polymerization) was also adopted to synthesize the polyaniline nanofiber, which was then formulated into ink to print. Nanofibers apparently increase the contact area between polyaniline and the environment, which enhances its performance as a sensor.

4.1 Electrochemical Synthesis of Polyaniline

The classical chemical synthesis of polyaniline was reported by MacDiarmid et. al. by using aniline, an oxidant and a strong mineral acid dopant [49]. The oxidation force can also be done electrochemically. Strongly acidic solution is required because aniline is only soluble in water under acidic conditions. Figure 4.1 is the scheme of the steps in electrochemical polymerization of aniline [54]. A^- is the counterion introduced from the acid.

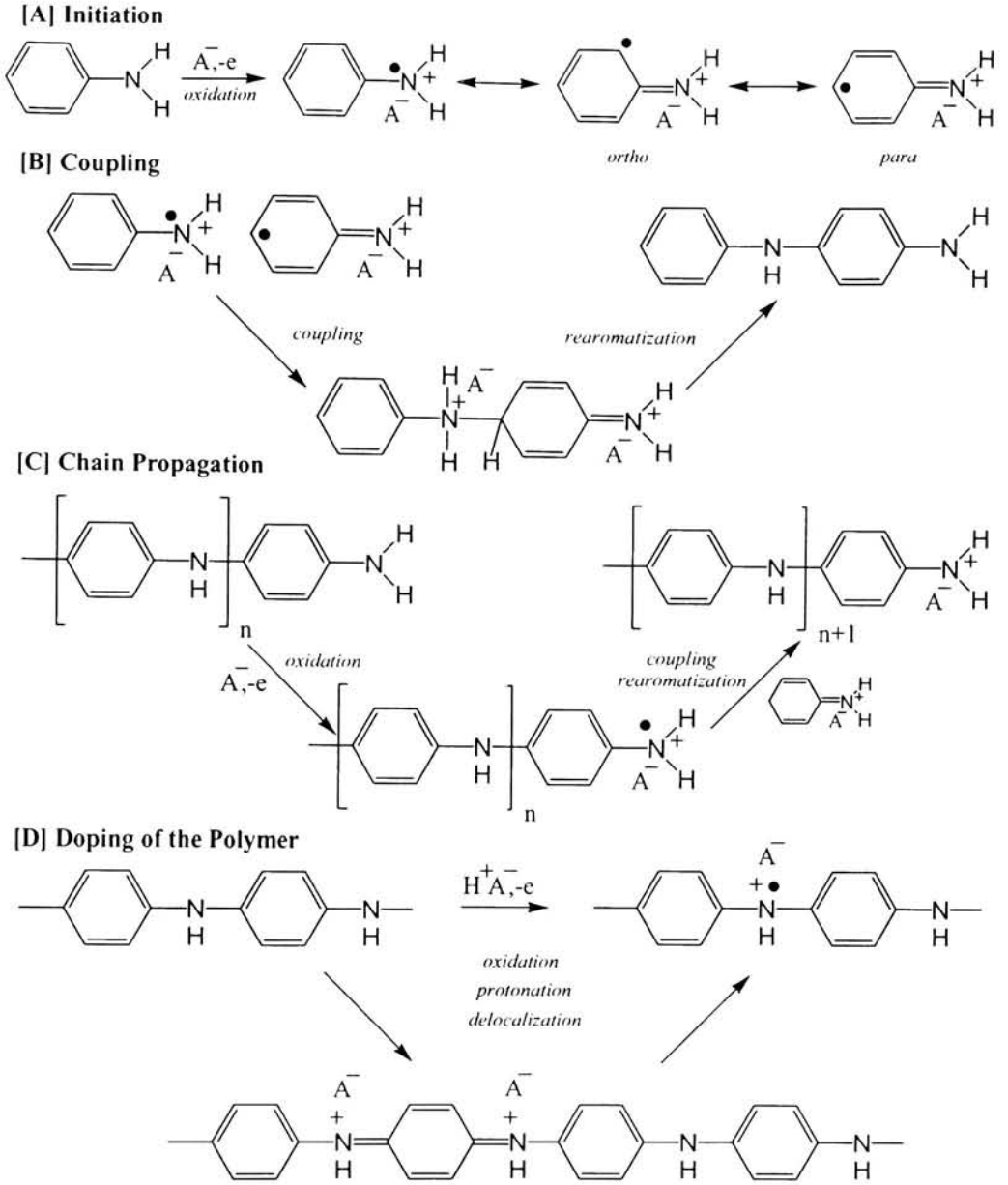

Figure 4.1 Reaction Steps in the Electrochemical Polymerization of Aniline [96]

Later, a series of methods have been used to synthesize nanostructured polyaniline (nanorods, wires, fibers) [55-58]. The nanostructure apparently increases the contact area between polyaniline and the environment, which enhances its performance as a sensor. In our work, a new template-free electrochemical polyaniline nanotube synthesis method has been used. In this method micellar aggregates are formed which

adopt a tubular mesostructure. It allows for varied aspect ratio (length/diameter) of the tubes based on the use of different reaction conditions. In order to achieve this, we have to carry out the electrochemical-oxidation of aniline in an emulsified medium which has characteristic channels formed by self-assembly of micellar aggregates.

Aniline monomer was distilled at 180°C prior to oxidation. The dopant/surfactant used for polymerization was 2-naphthalene sulfonic acid (β-NSA) which was used as received. Acidic mediums were prepared from concentrated HCl, H_2SO_4, and H_3PO_4 also used as received. Electrochemical template-free synthesis of polyaniline nanotubes was carried out in 0.1 N acidic medium containing various concentrations of beta-naphthalene sulfonic acid ranging from 0.1-0.4 M. The concentration of distilled aniline was kept constant for all reactions at 0.1 M. Nanotubes were formed on the platinum (Pt) plate working electrode by electrolytic oxidation of aniline. All reactions were carried out at 0-4°C with stirring. Reactions products which used surfactant were compared to those without surfactant in parallel experiments for all reactions.

Cyclic voltammetry (CV) curves, used in both synthesis and evaluation of polyaniline nanotubes, were recorded using a Gamry Instruments CV system. Sweep rates used were from 5-30 mV/s. Potentiostatic deposition of polyaniline nanotubes was carried out using a potential range which varied by medium but, ranged from 0.8-1.0 Volts vs. SCE.

The CV curves in Figure 4.2 show the polymerization of aniline to form polyaniline nanotubes using 1:1, 1:2, and 1:4 aniline/dopant ratios in H_3PO_4 medium. The figures show that in phosphoric acid, the surfactant allows for greater oxidation of aniline to polyaniline during synthesis. This is unique to this solvent system and was not seen in the other systems. This is illustrated by the oxidation peak for aniline at 0.6-0.7 Volts.

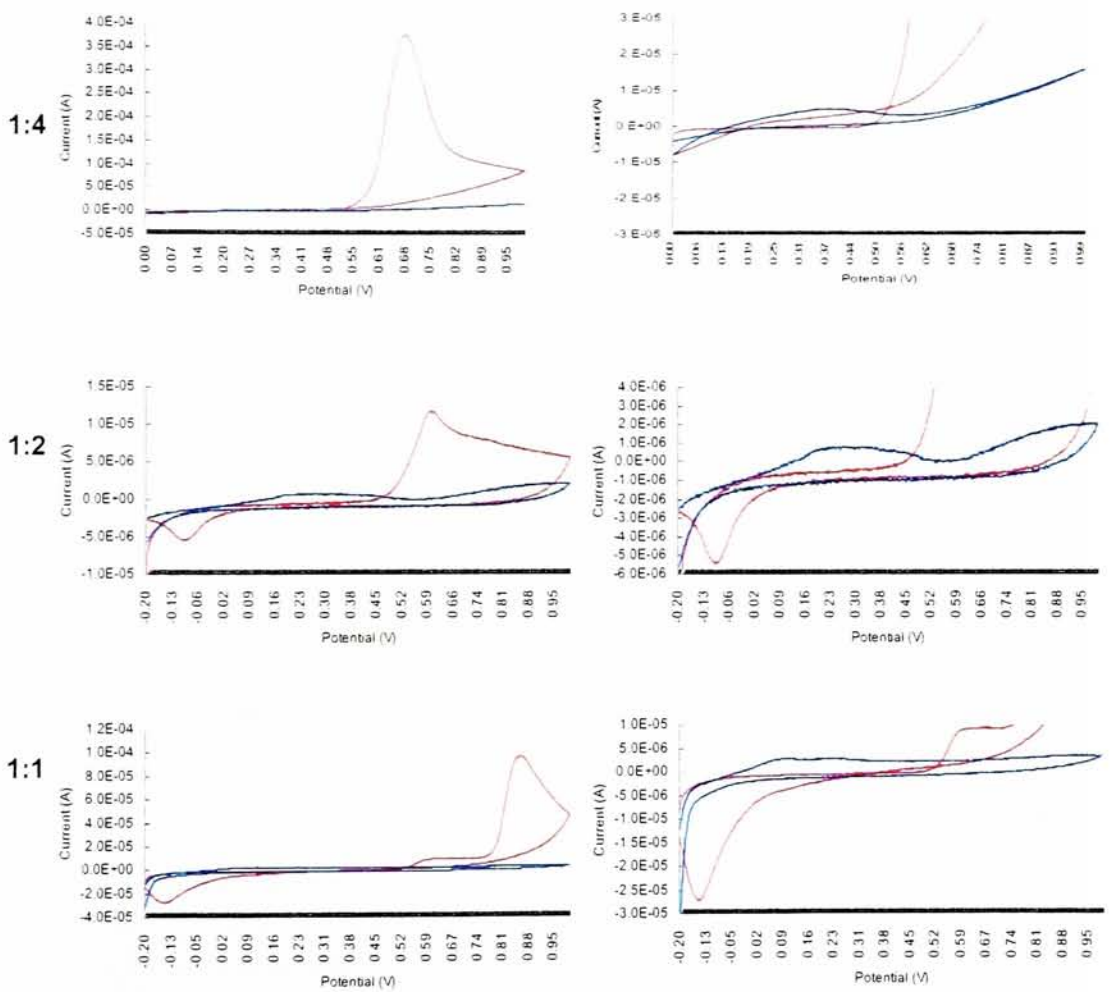

Figure 4.2 Nanotube Polymerization Voltammograms Using Different Mole Ratios of Aniline to Dopant in H_3PO_4 (aniline/dopant)

The blown up CV scans in Figure 4.2 show the cathodic peaks for polyaniline nanotubes at 0.250-0.450 mV which were taken during synthesis. The absence of a

reduction peak in these scans shows that the tube formation may be dependent upon the pernigraniline state of the polymer (different states of polyaniline will be discussed in section 5.9).

Table 4.1 shows the data for the nanotube synthesis in phosphoric acid medium. In this data set, the nanotube films on the Pt wire electrode were analyzed. These data show the typical cathodic (0.4 Volts) and anodic (0.5 and 0.35 Volts) peaks for polyaniline as well as a new cathodic peak around 0.8 V indicating that the synthesis is not a neat one but, that both conventional polymer and nanotubes are dispersed within

Surfactant Concentration (M) and β-NSA/Aniline Ratio	Aniline Oxidation E(mV)	I(μA)	Oxidation Peak #1 E(mV)	I(μA)	Oxidation Peak #2,3 E(mV)	I(μA)	Reduction Peak #1,2,3 E(mV)	I(μA)
0.4 M Surfactant 8/1 Dopant/Aniline	650	17.4	450	2.3	870	2	480	-1.2
					490	1.2	375	-0.7
							190	-1.5
0.2 M Surfactant 4/1 Dopant/Aniline	**658**	**385**	**387**	**3.4**	**802**	**2.5**	**500**	**-3.58**
					620	**1.3**	**344**	**-2.23**
							144	**-1.1**
0.1 M Surfactant 2/1 Dopant/Aniline	619	11.4	431	4.75	869	2.1	450	-1.45
					604	1.1	351	-3.2
							105	-1.25
0.05 M Surfactant 1/1 Dopant/Aniline	**623**	**6.55**	**481**	**2.05**	**877**	**1.25**	**503**	**-0.8**
					519	**1.37**	**375**	**-1.93**
							147	**-1.2**

Table 4.1 Peak Currents Obtained For Different Dopant Concentrations in Polyaniline Nanotube Synthesis in H_3PO_4

each other [59]. These data are shown in relative peak height for the three mole ratios of dopant/aniline used.

Optical microscopy in Figure 4.3 shows the various products produced from the three different reaction media and for sulfuric acid in which no surfactant was used. As can be seen from the micrographs, the polyaniline nanotubes produced in HCl are longer and with narrower diameter than the others. Phosphoric acid gives much shorter tubes with higher density. Sulfuric acid seems to give tubes which are longer than those produced in H_3PO_4 but shorter and larger in diameter than those produced in HCl.

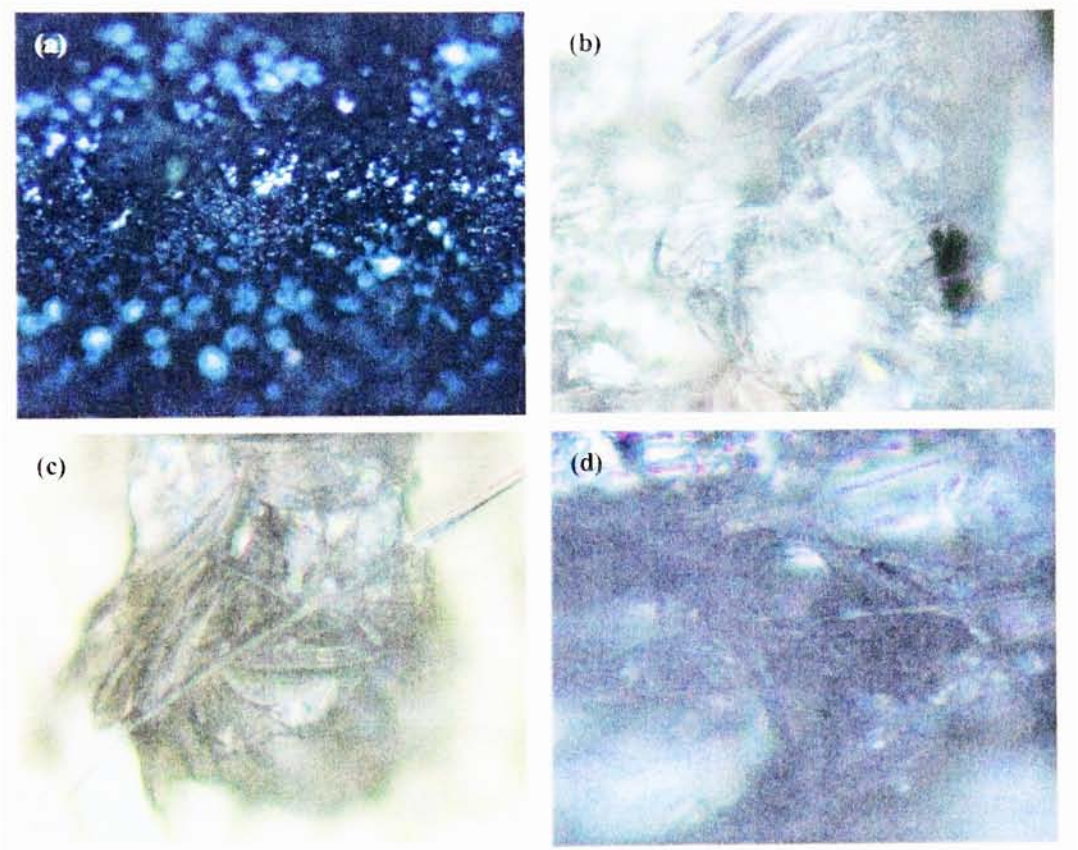

Figure 4.3 (a)Polyaniline formed in H_2SO_4 without β-NSA. (b)Polyaniline nanotubes formed in H_3PO_4. (c)Polyaniline nanotubes formed in HCl. (d)Polyaniline nanotubes formed in H_2SO_4. All micrographs were taken at 500 times magnification under reflective light.

4.2 Interfacial Polymerization of Polyaniline

The electrochemical synthesis method opens up many opportunities for electronic applications where a high degree of selectivity and purity are required. However,

β-NSA is required in the polymerization and post-synthetic treatments are needed to remove it. Furthermore, the throughput of the electrochemical process is relatively low because the amount of product is limited by the size of the electrode. Recently, a template-free interfacial polymerization route was reported, which synthesized polyaniline nanofibers with a very simple process [60]. This method has been adopted to make sufficient quantities of polyaniline for our ink formulations.

Experimental synthesis starts by dissolving aniline in chloroform. Other organic solvents such as hexane, benzene, toluene, xylene, diethyl ether, carbon disulfide, carbon tetrachloride, *o*-dichlorobenzene, methylene chloride, etc. can also be used. Ammonium peroxydisulfate is dissolved in 1M hydrochloric acid solution which is carefully layered onto the organic solvent to form an aqueous/organic interface. Generally the aqueous layer has the same volume as the organic and the acid serves as the dopant. Different dopants can be achieved by using a series of acids. Within a short period of time, depending on the acid used, emeraldine polyaniline appears at the interface, which then disperses through the aqueous phase. The whole process lasts overnight and the entire aqueous layer is filled with polyaniline nanofibers. The excess acid is removed by dialysis with distilled water and the product can be collected by filtration or centrifugation. It can then be mixed with dodecyl benzene sulphonic acid (DBSA) to form an organic based soluble ink [61], or mixed with resins to form a nanofiber based ink. Figure 4.4 shows the reaction process of the interfacial polymerization [60] and the product structure is shown in figure 4.5. Nanofibers with

diameters around 50 nm can clearly be seen.

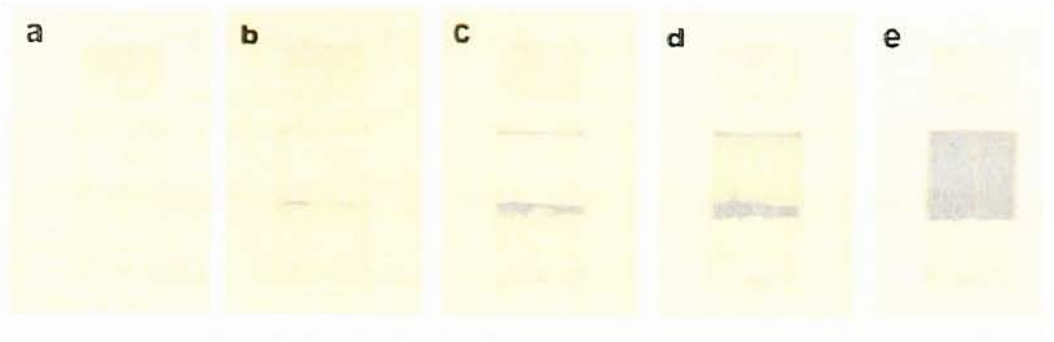

Figure 4.4 Interfacial Polymerization of Aniline in a Water/Chloroform System. (From a to e, the reaction times are 0, 1.5, 2.5, 4, and 10min, respectively.) [60]

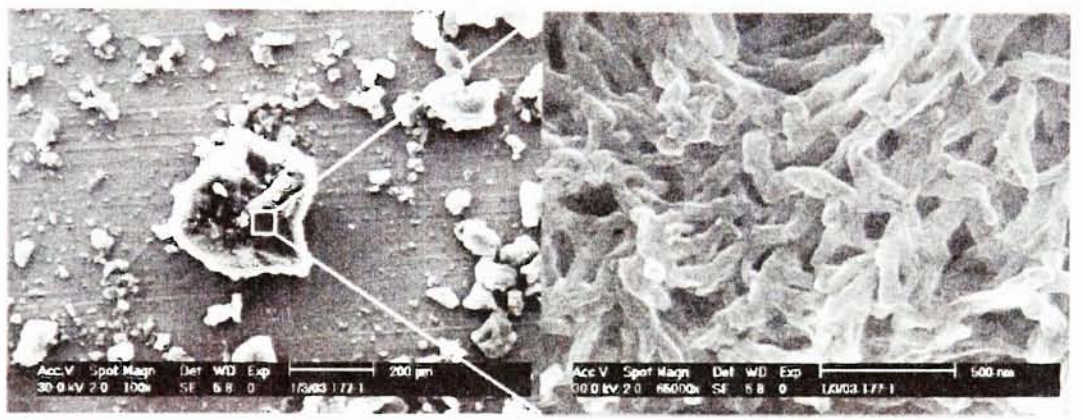

Figure 4.5 Polyaniline Powders Obtained after Filtration. Scanning electron microscopy images show that the powders (left; low magnification, ×100) are agglomerations of nanofibers (right; high magnification, ×65000). [60]

Chapter Five: All-printed Humidity and Gas Vapor Sensor

A two layer polyaniline (PANI) gas sensor has been fabricated by flexographic printing. This method offers advantages of low cost, high volume, and easy production. The resistance change with humidity has been investigated and compared with a commercial humidity sensor. The sensors response to acids, bases and volatile organic compounds (VOCs) have also been investigated. The sensor has been used for applications such as natural gas detection and food quality determination.

5.1 Introduction

Most popular gas sensors currently used are the Taguchi-type which is based on tin oxide (SnO_2) as the gas-sensitive element. They have good performance, but the high-temperature (typically between 300 and 400 °C) operation environment, bulk structure, and relatively high cost limit their applications [62]. Polyaniline is a promising material for gas sensing. It is able to switch between the insulating state (emeraldine base) and the conducting state (emeraldine salt) by reacting with protonating or deprotonating agents, as shown in (1). The conductivity depends on the ability of charge carriers to transport along the polymer backbone as well as to hop between the polymer chains.

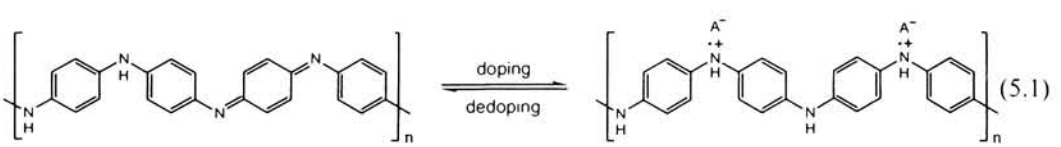

Emeraldine Base　　Emeraldine Salt　　(5.1)

To make a resistive sensor, thin film polyaniline structures can be easily prepared from solution [49] and deposited onto electrodes such as interdigitated [63-66] or coplanar [66,67] gold electrodes. When the sensor contacts certain gas vapors, the vapor molecules can diffuse through the surface and cause physical structure changes or chemical reactions to take place, which result in conductivity changes. A major advantage of a polyaniline sensor is its sensitivity at room temperature [64].

The research in this area mostly focuses on the improvement of sensitivity and selectivity of PANI. One of its common applications is sensing ammonia gas [64, 68-70], since the conductivity of polyaniline can change dramatically in the presence of ammonia. This is due to the deprotonation reaction [64] as well as the swelling of the polymers [70], which will be discussed specifically in the next section. The reported detection limitation can be as low as 20-50 ppm [70], and the relationship between the resistance and ammonia concentration was shown by Kuala et al. [64]:

$$R = R_0 \exp\left[(\alpha N)^{1/2}\right] \tag{5.2}$$

Where R0 is the initial resistance, N is the concentration of NH3, and α is the dimensional coefficient (= 5.65×10^{-3} ppm^{-1}, if N is in ppm).

The response of a PANI sensor to humidity has also been widely studied by several groups [71-73]. Water vapor with relative humidity between 6.4% and 97.3% has been sensed with a quick response and good repeatability [73]. Additionally, a series of organic and inorganic gas vapors have been studied using polyaniline sensors as well:

Athawale and Kulkarni have studied the difference in response to various alcohol vapors caused by substituents on aniline ring [74]. Agbor et al. have measured the sensitivity of PANI prepared by different deposition techniques to NO_x, H_2S, SO_2, CO, CH_4 diluted in N2, etc. [63], Xie et al. have studied the influence of thickness to the sensitivity and response time of NO_2 [75]. Meijerink et al. reported a special route for selective sensing [65]. They treated PANI sensors with vapors of methanol, ethanol, acetone and water, respectively, and assembled them as an array. Thus a good separation of different gas responses can be obtained.

Another way to increase the selectivity and the response time of the sensor is using a PANI blend as the sensing layer. Hosseini and Entezami reported the use of PANI blends with polyvinyl acetate, polystyrene and polyvinyl chloride for high quality gas sensing [76]. Cataldo et al. discussed the choice of PANI composition for selective gas detection [77]. Other applications include CO_2 sensors using PANI/polyvinyl alcohol [78, 79], ammonia sensors based on PANI/polystyrene (PS) or PANI/polymethylmethacrylate (PMMA) [79], chloroform sensor using PANI/copper nanoblends [81] and aliphatic alcohols sensor using PANI/PS [82], etc. A gas sensitive field effect transistor based on PANI has also been reported [83-85] which increased the signal to noise ratio [84] and avoided the drift problems in resistive sensors [85].

Recently, Weiller et al. reported a resistive gas sensor based on PANI nanofibers [86]. They compared the sensor's response to hydrochloric acid, ammonia, hydrazine,

chloroform and methanol with conventional PANI sensors and observed a considerable improvement in sensitivity and response time, which apparently due to the increased surface area of PANI nanofiber layer.

In all of this work, the most common methods to deposit PANI onto the substrate are spin-coating, electrochemical deposition, dip-coating and drop-coating. Other methods include thermal evaporation [63], Langmuir-Blodgett (LB) [63, 75] and self-assembly techniques [68, 75]. Most of these methods have limitations such as dopant, substrate and environment, etc. Most importantly, all of these methods need a relatively long production period and batch production is difficult or impassible to achieve. This may be why no commercial PANI sensor are available currently. Compared to those techniques, printing offers advantages such as the capability to fabricate sensors over large areas and on arbitrary surfaces at low cost and high volume. A patent application by Makela et al. claimed printing conductive PANI layers and using them as a sensor [87]. They printed the PANI onto the substrate directly without using highly conductive electrodes, which might result in low sensitivity and poor stability. In this chapter we report the use of commercial flexographic printing technology to make polyaniline sensors. In our investigation, a two layer sensor structure was fabricated by printing a silver interdigitated electrode (IDE) layer and a polyaniline layer on top of it. The whole device was printed on coated paper or the transparent plastic film (PET) substrates.

Flexographic printing is a traditional roll to roll printing process. It uses a raised rubber or photopolymer plate with a rubber fountain roller and an engraved chrome or ceramic anilox roller to carry the ink to the plate. Then the ink is transferred to the printing substrate in contact with the impression cylinder. The printing quality depends upon the viscosity of the ink, the pressure applied to the substrate, the printing speed as well as other factors [14]. It is a high-speed printing process which can print continuous patterns on many types of absorbent and non-absorbent materials. The typical printing speed for flexographic printing is 300 ft./min., which is much greater than any traditional sensor fabrication technique. After fabricating single layer commercially used RFID tags [15], we have now made two layer electronic devices.

5.2 Conductivity Dependence (General Sensing Mechanism) of PANI

The overall conductivity of polyaniline depends upon electron transport both within polymer chains (intrachain transport) and between polymer chains (interchain transport). A variety of factors can influence either or both of these types of transport, and thereby change the overall conductivity (resistance) of the sensor.

Intrachain transport is governed by a number of factors. The doping level of polyaniline dramatically affects the conductivity. The maximum conductivity is achieved when there is one dopant for every two aniline monomers [88]. The intrachain conductivity also depends upon the molecular conformation of the polyaniline chains. Charge conduction along the chain depends upon effective π

overlap between adjacent rings. In order to have optimal π overlap, the rings on adjacent chains need to be coplanar with each other.

In order to achieve high conductivity, a charge exchange process has been proposed. In this process, inter- or intra-chain proton exchange accompanies electron transport [89]. This proton exchange is facilitated by the presence of water, or other protic solvents.

Interchain transport depends largely upon how to close together adjacent polymer chains are to each other. Since charge needs to hop from chain to chain, anything that brings the chains closer together will improve the conductivity.

Exposure to chemical vapors, can affect the conductivity of polyaniline by influencing any of the factors described above. One of the things that make polyaniline such a good sensor material is the relationship of its electrical conductivity to so many different chemical effects.

The doping level of polyaniline can be changed upon exposure to acids and bases. Acids increase the doping of polyaniline, which usually results in an increase in conductivity. Doping of polyaniline with strong acids also makes the polymer unstable at high humidity [72]. Conversely, bases de-dope the polyainile, reducing the conductivity. Since these processes are chemical (acid-base) reactions, their effect on the conductivity of polyaniline is usually retained upon removal of the gaseous sensing

species. In order to reverse the effect of a doping agent, polyaniline can be treated with a de-doping agent.

More subtle chemical factors can also affect conductivity. Some vapors cause the polymer film to swell. This physical process moves the polymer chains further apart from each other, which impairs the interchain transport, reducing the conductivity. This process is generally reversible. When the vapor which induces the swelling is removed, the polymer chains contract again. Since most compounds which induce swelling of the polymer are only physisorbed, they can usually be removed upon purging with nitrogen or other inert gas.

Many analytes, can affect the conductivity of polyaniline by several different process. Ammonia, as we discussed before, has been shown to reduce the conductivity of polyaniline by both de-doping, and inducing swelling of the polymer chains [64, 70]. This may account for the great sensitivity of polyaniline to ammonia.

Molecular conformation plays an important role in determining the conductivity of polyaniline, and is sensitive to they presence of a variety of chemical species. One of the first examples of this was shown by MacDiarmid, et al., who described this as the "secondary dopant" effect [90]. A "secondary dopant" is an apparently "inert" substance which, when applied to a primary-doped polymer, induces still further changes in the above properties including a further increase in conductivity. It differs

from a primary dopant in that the newly enhanced properties may persist even upon complete removal of the secondary dopant [90]. Secondary doping changes the molecular confirmation from a compact to an expanded coil, as evidenced by spectroscopic evidence [54]. This coil expansion increases the electrical conductivity by both inter and intra molecular processes. The expanded molecular conformation acts to reduce π-conjugation defects in the polymer backbone due to ring twisting. This reduction of π-defects increases that component of the bulk conductivity due to *intra*-molecular effects. The opening-up of the coil tends to promote the linear conformation necessary for crystallization, thus increasing the crystallinity of the polymer with enhancement of the *inter*-molecular component of the bulk conductivity.

The phenomenon of secondary doping has been further elucidated by Ikkala et al. [91-94], who describe it as "molecular recognition" between polyaniline and certain solvents. Particularly, the conductivity of polyaniline that is doped with camphor sulfonic acid (CSA) is greatly increased upon exposure to m-cresol (either vapor or liquid). They describe a cyclicly associated species where the hydroxyl group of the m-cresol forms a hydrogen bond with the carbonyl group of CSA, while the phenyl rings in PANI and m-cresol mutually interact through van der Waals forces. The result of this is that the rings are twisted into a more planar conformation during the packing in crystalline domains, thereby increasing the conductivity.

A variety of chemical factors can influence the molecular conformation of polyaniline.

In solution, the polymer conformation depends upon the relationship of both the polymer solvent, and the polymer-polymer interactions. In a poor solvent, the polymer-polymer interactions dominate, and result in a coiled (low conductivity) conformation. In a good solvent, the polymer-solvent interactions dominate, and the polymer chains open up, improving the conductivity.

Since doped polyaniline is a charged polymer (polyelectrolyte), electrostatic interactions are also very important in determining the chain conformation. The polymer chain contains cationic nitrogen atoms, which repel each other, when they are not shielded by interactions with anionic dopants. This repulsion both flattens the chains (increasing intramolecular transport) and facilitates intermolecular transport between neighboring polymer chains.

Solvation of the dopant anions affects the degree to which they are electrostatically shielded from the polyaniline chain (cations). The better the solvation of the dopant anions, the larger their effective ionic radius, and the further they are from the polyaniline chain. This effect was initially shown for metallic dopants by Andre et al. in 1983 [95]. Thus, solvation of the dopant anions pulls away from the polymer chain, inducing the chain to expand and improving the electrical conductivity. In the presence of too many anions, the effect can be reversed, and the excess anions between cationic sites can screen cations from each other, decreasing the repulsion between them, and compacting the polymer. Excess anions may also effectively attract cationic sites to

each other.

5.3 Experimental

The silver ink used for electrodes is CLO-101A, obtained from Precisia, Inc. Polyaniline was synthesized, doped and formulated into an ink. The flexographic printing plate was designed in PostScript, and was produced on DuPont Cyrel by Adflex Corporation. The printing equipment used was IGT F1 and IGT AIC 2-5, provided by Globis Incorporated. The later one has a separate inking process achieved by IGT high speed inking unit, provided by the same company.

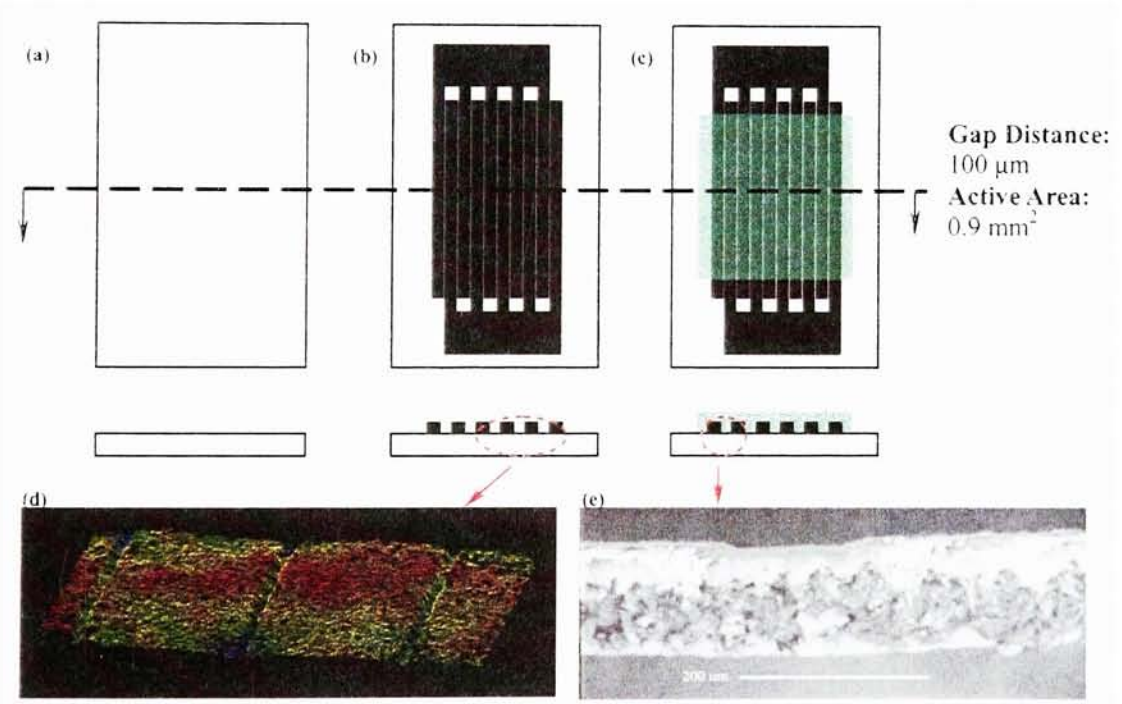

Figure 5.1 Sketch of Fabrication Process **(a)**substrate **(b)**first layer **(c)**second layer **(d)**IDE optical profilometry image **(e)**SEM image of cross section

The two layer sensor was assembled by printing polyaniline ink on top of silver interdigitated electrodes, which were directly patterned on the substrate using the same process. Figure 5.1 shows a sketch of the fabrication process. Each electrode has five

fingers interdigitated with each other. The pattern was designed at 300 dpi and the gaps between the electrodes are around 100 μm after printing. They can help increase the size of the current measured and the signal-to-noise ratio as well. A flat surface with sharp gaps can be seen from the optical profilometry image of the electrodes shown in figure 5.1(d). A thin layer of polyaniline on top serves as the sensing material. From the cross section image of the sensor (Figure 5.1(e)), the paper substrate, the silver layer with a gap of around 100 μm, and a thin polyaniline layer coated on the whole surface can be seen. Since this is a resistance sensor, the only functional area is the part between the electrodes, so the total active area of the sensor is ~0.9 mm^2 The sheet resistance of the silver electrode is ~1Ω/□ (tested by four probe technique), while the polyaniline active layer has a sheet resistance ~1MΩ/□. Therefore, the resistance of the electrodes does not significantly influence the performance of the sensor.

The original color of the printed polyaniline layer is green, since it is in the emeraldine salt form. The IR and Visible spectrum of printed polyaniline are shown in Figure 5.2, from which we can see the main characteristic bands and its green color. Stretches due to both quinoid rings (~1600cm^{-1}) and benzenoid rings (~1570cm^{-1}) are observed, indicating partial doping in the polyaniline used [96]. Further discussion of polyaniline spectra will be found in section 5.9.

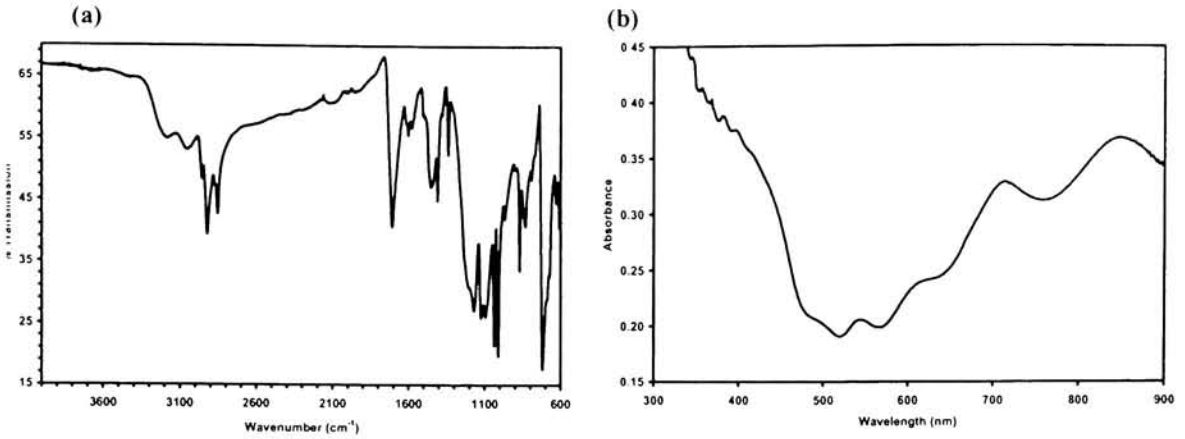

Figure 5.2 Spectra of printed polyaniline **(a)** Inferred **(b)**Visible

The performance of a polyaniline sensor can be improved by 1) Decreasing the distance between the electrodes to shorten the electron transfer time. 2) Decreasing the thickness of the active layer to make diffusion easier. 3) Using nanostructured polyaniline to expand the effective surface area. The sensor demonstrated in this paper has an inter-electrode distance about 100 μm and active layer thickness less than 5 μm, so good response is expected. The initial resistance can be made as low as a few hundreds ohms, which is considerably lower than the traditional PANI sensors reported [68]. Batch production with uniform performance can be achieved using a printing process. No post treatment needs to be done after the device is fabricated.

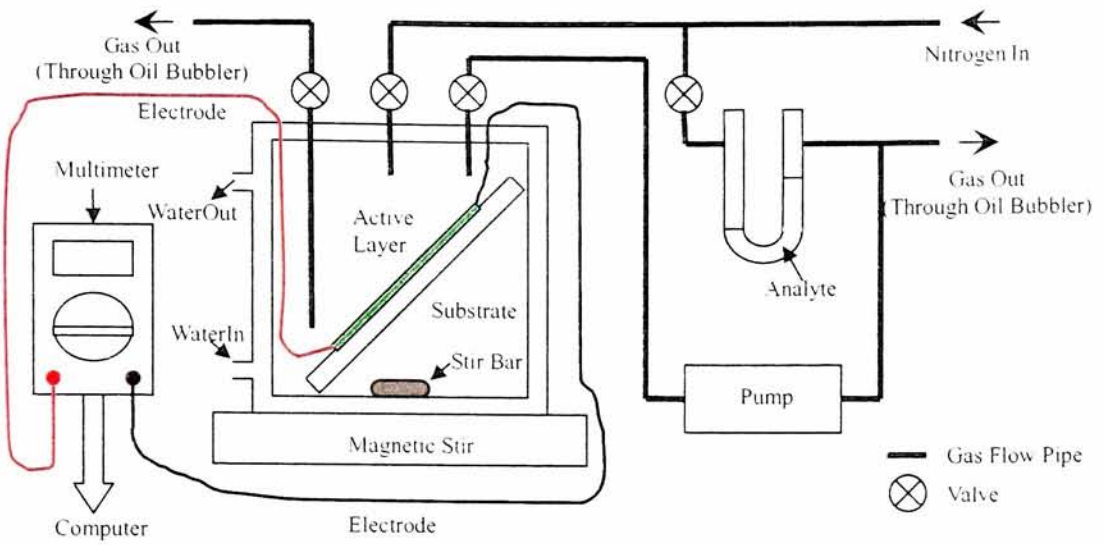

Figure 5.3 Sketch of Sensor Testing Equipment

The response of the printed polyaniline sensor to vapors and gases was tested using the system shown in figure 5.3. The sensor was placed in a sealed chamber with two electrodes connected to a Fluke 189 data logging multimeter. The temperature was controlled with a water jacket connected to a HAAKE D8 controller. Nitrogen gas was introduced into the chamber to create the initial environment. The analyte was put in a sealed U-tube. With nitrogen gas flowing through the U-tube and the solution bubbling, different kinds of saturated gas vapors could be obtained from the outlet of the U-tube. A Cole-parmer 10608 series peristaltic pump was used to continuously pump the vapor into the chamber. The flow rate was typically 40 ml/min. An airtight syringe could also be used to inject saturated gas vapors into the cell. Mixing was improved by using a magnetic stir bar. Nitrogen was introduced into the chamber to drive out the analyte vapor and by doing so the sensor recovery process could be studied. The effluent passed through an oil bubbler to prevent from the air from getting in. For humidity sensing, a Honeywell HIH-3610 humidity sensor was placed inside the chamber for

relative humidity calibration and performance comparison. For volatile organic compounds, the concentration was calculated from volume and partial pressure. The resistance change was recorded with the Fluke 189 data logging multimeter and logged with a computer. The volume of the chamber is about 300 ml.

IR spectra were measured using an Excalibur FTS 3000. UV-visible spectra were measured with a Cary 100 Spectrophotometer, SEM images were taken with a Cambridge Stereoscan 200, and the optical profilometry was done with a Zygo NewView Optical Profilometer.

5.4 Humidity Sensing

Humidity response was tested using three polyaniline sensors with different initial resistances. The initial environment was nitrogen gas and a very low relative humidity was measured. Water vapor was introduced and the relative humidity was measured by the Honeywell HIH-3610 humidity sensor. Simultaneously, resistance change of the printed sensors was recorded, as shown in figure 5.4.

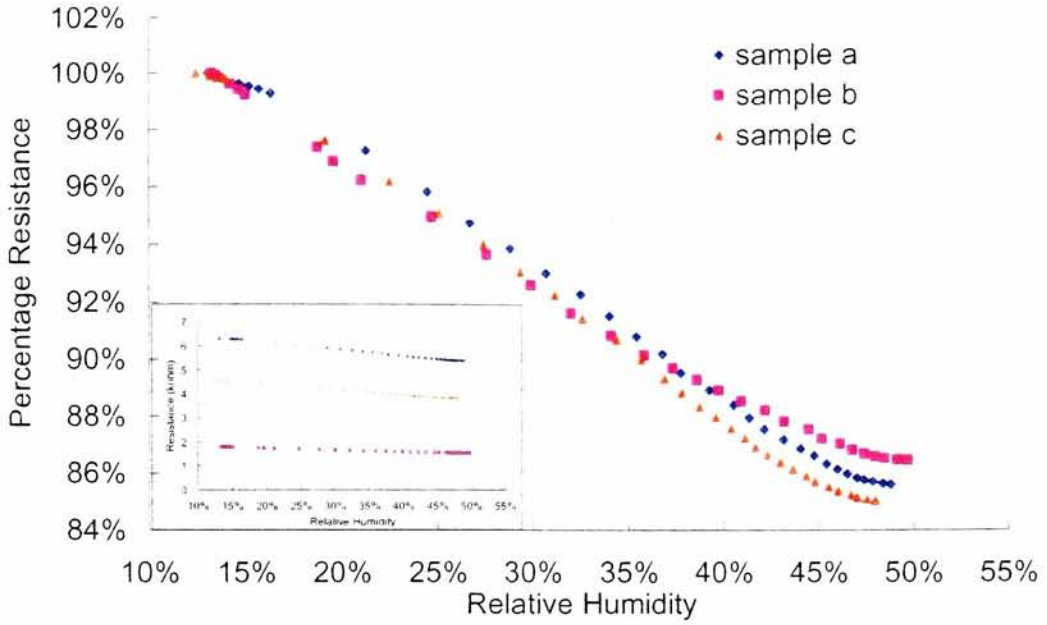

Figure 5.4 Humidity Response on Coated Paper

As can be seen from figure 5.4, although samples a, b and c have different initial resistances (inset curve), they all decreased in resistance as the level of relative humidity (%RH) increased. They experience almost same relative resistance change, which is a general definition of percentage sensitivity:

$$S = \left| \frac{RH_2 - RH_1}{RH_1} \right| \times 100 \tag{5.3}$$

Where RH_2 is the resistance of the sensor at humidity level 2, and RH_1 is the initial resistance of the sensor. The performance of the printed sensors was found to be quite uniform, and the percentage change with relative humidity was linear, around 0.42%/RH%. The sensitivity and sensing range is relatively low compared to the reported one [72], but the initial resistance is also much lower, which make the detection be more accurate.

HCl treatment after the sensor has been printed was found to help decrease its initial resistance. The humidity response of the sensor post HCl treatment has been studied and compared with the original response. As shown in figure 5.5, although the initial resistance of the sensor decreased after the treatment (inset curve), the range of the resistance change decreased as well. The resistance decreased only 7% for the HCl post-doped sensor while the original one changed more than 15% under the same conditions.

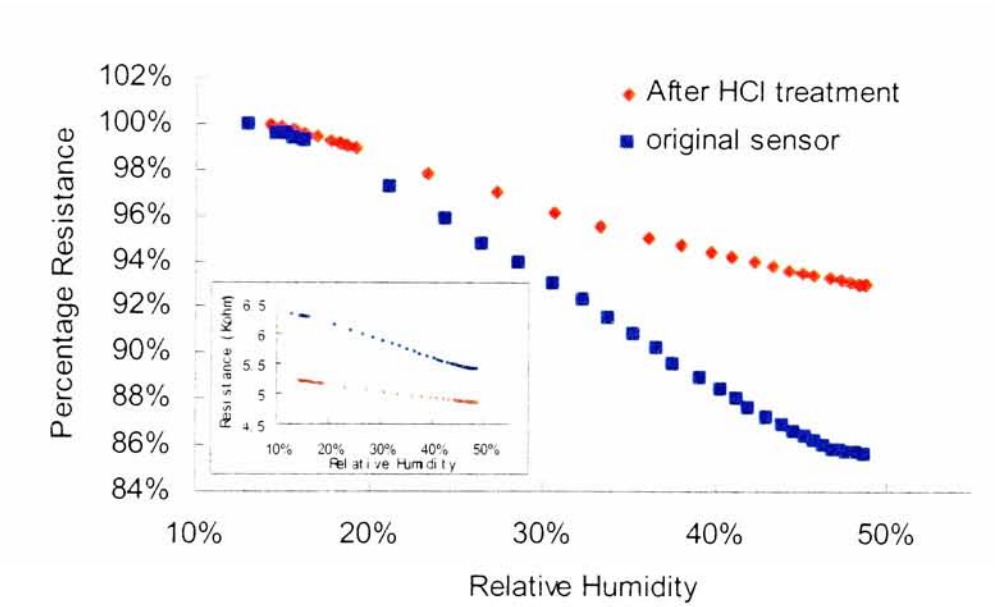

Figure 5.5 Performance Comparison of the Sensor with/without HCl Treatment

The same sensor structure has also been printed on a plastic (PET) substrate. The corresponding resistance change is shown in figure 5.6. The sensitivity increased tremendously compared to the sensor printed on coated paper. The resistance change was near 90% for the plastic substrate compared with about 15% on coated paper. However, the percentage sensitivity change for the PET sensor doesn't exhibit a linear relationship with relative humidity as the sensors printed on coated paper did.

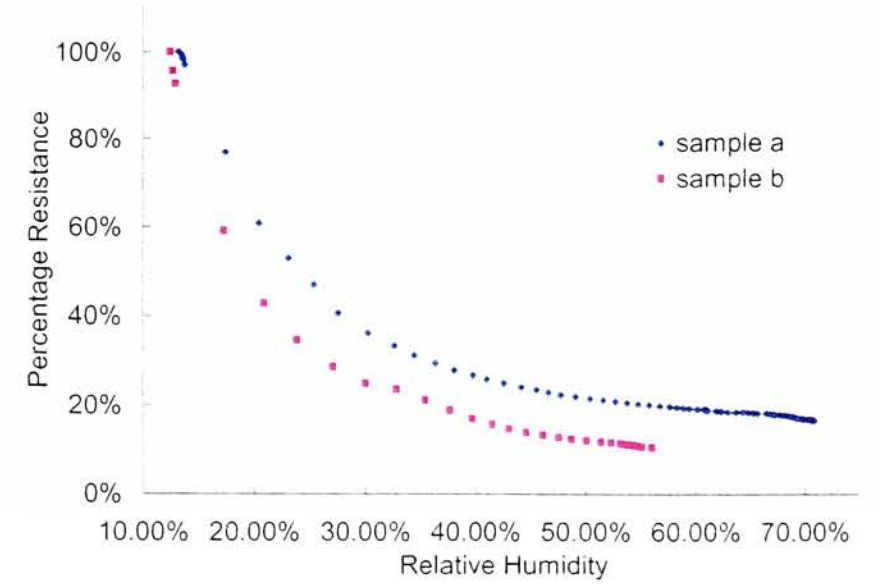

Figure 5.6 Humidity Response on Plastic Film

The recovery and repeatability of the printed humidity sensor was studied by exposing the sensor alternately to saturated water vapor and nitrogen gas. The sensor's resistance change is shown in figure 5.7. As can be seen from the curve, the sensor's response is repeatable and reproducible. In each cycle, after the resistance decreased

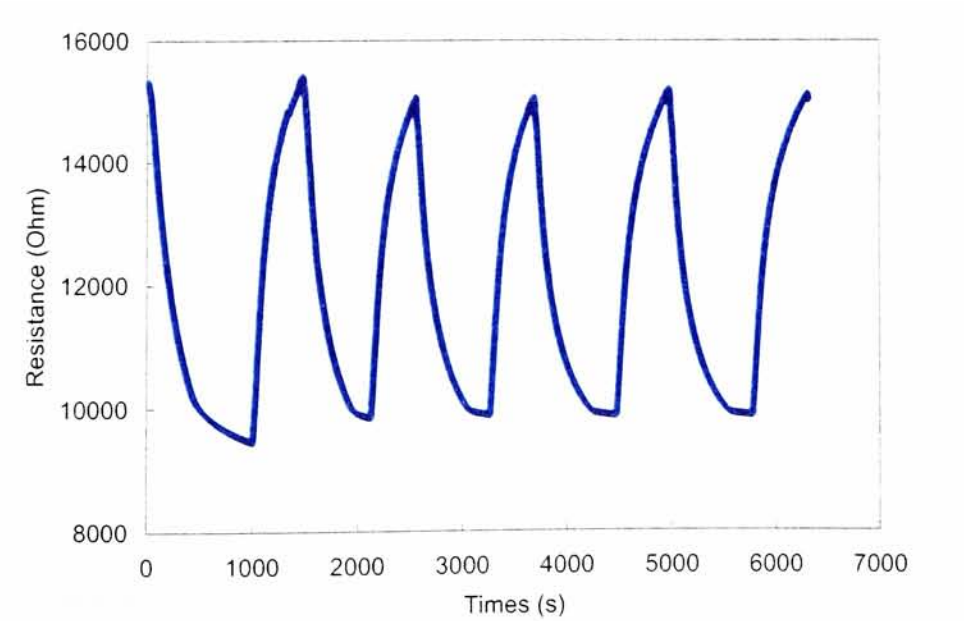

Figure 5.7 Humidity Cycling Response

from exposure to water vapor, introduction of nitrogen helped the sensor return to the original resistance in a short period of time. The percentage sensitivity change with time was almost the same in each cycle, which shows good repeatablility of the printed sensor.

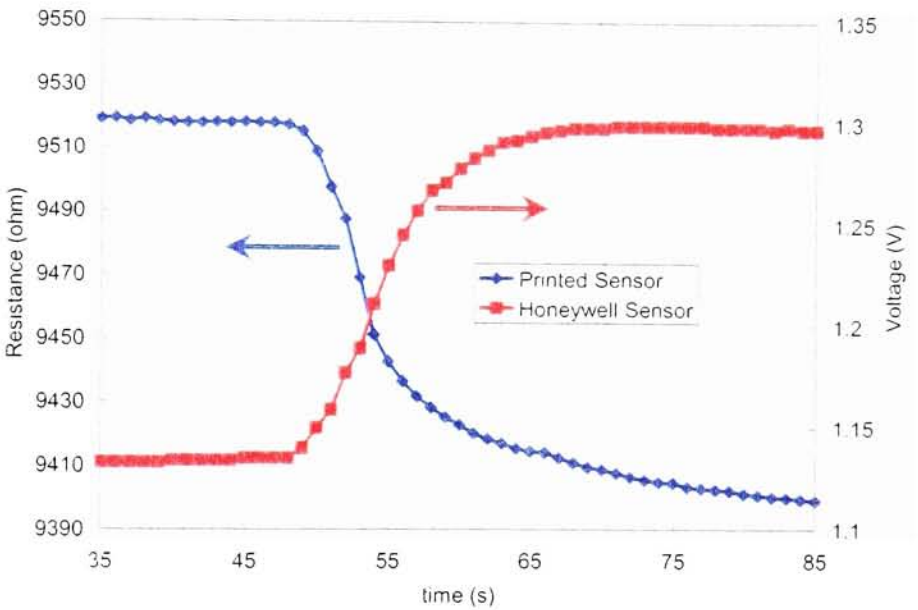

Figure 5.8 Sensor Response Comparison

The sensor's response to water vapor was compared with a Honeywell HIH 3610 humidity sensor. The initial relative humidity was around 10 RH%. A syringe was used to inject 30 ml of saturated water vapor into the chamber, and the response is shown in figure 5.8. HIH 3610 is a linear voltage based sensor whose voltage increases with humidity and can be measured using a voltmeter. The printed sensor showed a signal change of more than 80% of the total change within 10 seconds after injection. The temporal response of the two sensors was roughly equivalent, dominated by the mixing time in the chamber volume (~300ml). The time at which both sensors started to

respond was also almost same, proving that there was no lag time in the printed sensor. Although it showed a small continuous decrease in resistance afterward, the total response was still faster than the traditional spin coated sensors [68]. We suspect this is a result of the printing process enabling thin uniform active layers and a short inter-electrode distance. In the equilibrium state without air flow, the resistance variation of the printed sensor is less than 1%.

Generally, a resistance type sensor's sensitivity decreases as the active layer gets thicker. This is thought to be due to the carriers mostly passing and hoping through the polyaniline between the electrodes, while the upper layer doesn't have much contribution to the conductance. Too much polyaniline retards the environment vapor/gas diffusing through to the "active" material so its response is reduced [97].

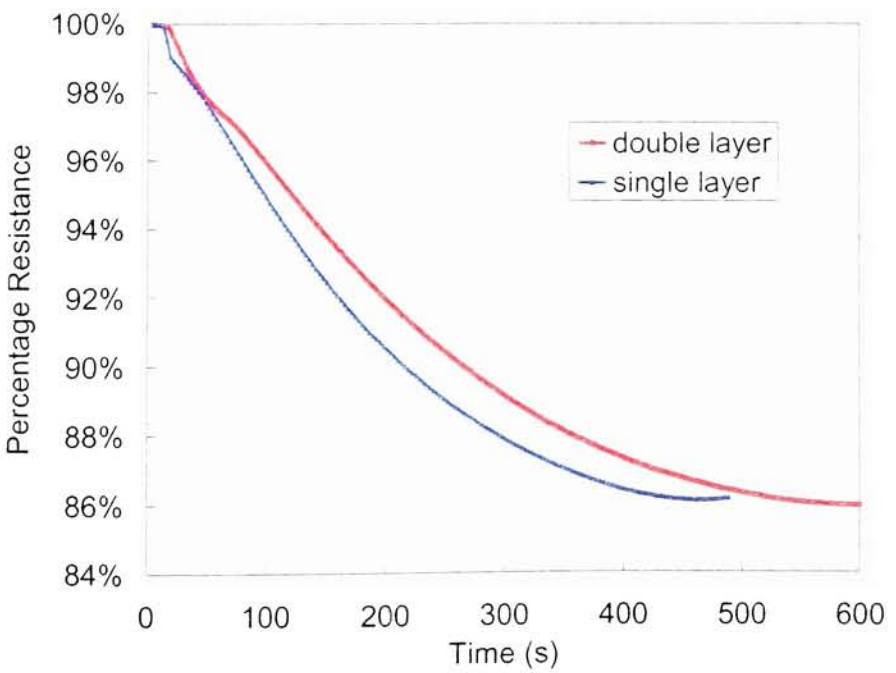

Figure 5.9 Performance Comparison of Single and Double Layer Printed Sensor

However, if the printed layer is too thin, carrier flow is limited and the initial resistance of the sensor might be very high, which will also influence its sensitivity. We compared the humidity sensing performance of the printed sensor with single and double impression of polyaniline layer. The latter one was fabricated by printing a same size second layer right over the original layer after it was totally dry. Both sensors were exposed to water vapor and the resistance changes were recorded in figure 5.9. As can been seen, both of them experienced a resistance decrease around 14%, but the signal response in the double impression polyaniline sensor had a small delay, and the resistance leveled off about 100 seconds later compared to the single impression one. From this we can conclude that the single layer flexographic printed sensor is better for vapor/gas sensing.

Stability of the printed sensor has been examined by keeping nitrogen gas flowing through the chamber for more than 70 hours, and the percentage resistance change is less than 0.1% per hour. We conclude that the all printed polyaniline sensor can be used for humidity sensing. The response and recovery performance are quick, stable and repeatable.

5.5 Acid and Base Sensing

There are many applications where detecting and measuring acid and base content are important. The printed sensor's responses to acids and bases were tested using hydrochloric acid and ammonia. The chamber was originally filled with nitrogen. For

each cycle 5ml of HCl/H_2O vapor was transferred into the chamber using an airtight syringe. After the response stabilized, nitrogen was introduced to study the sensor recovery. The process was repeated five times with HCl, and then the same procedure was done using ammonia. The resistance changes are shown in figures 5.10a and b, respectively. In the same figure the sensors responses to injections without recovery were also demonstrated for comparison.

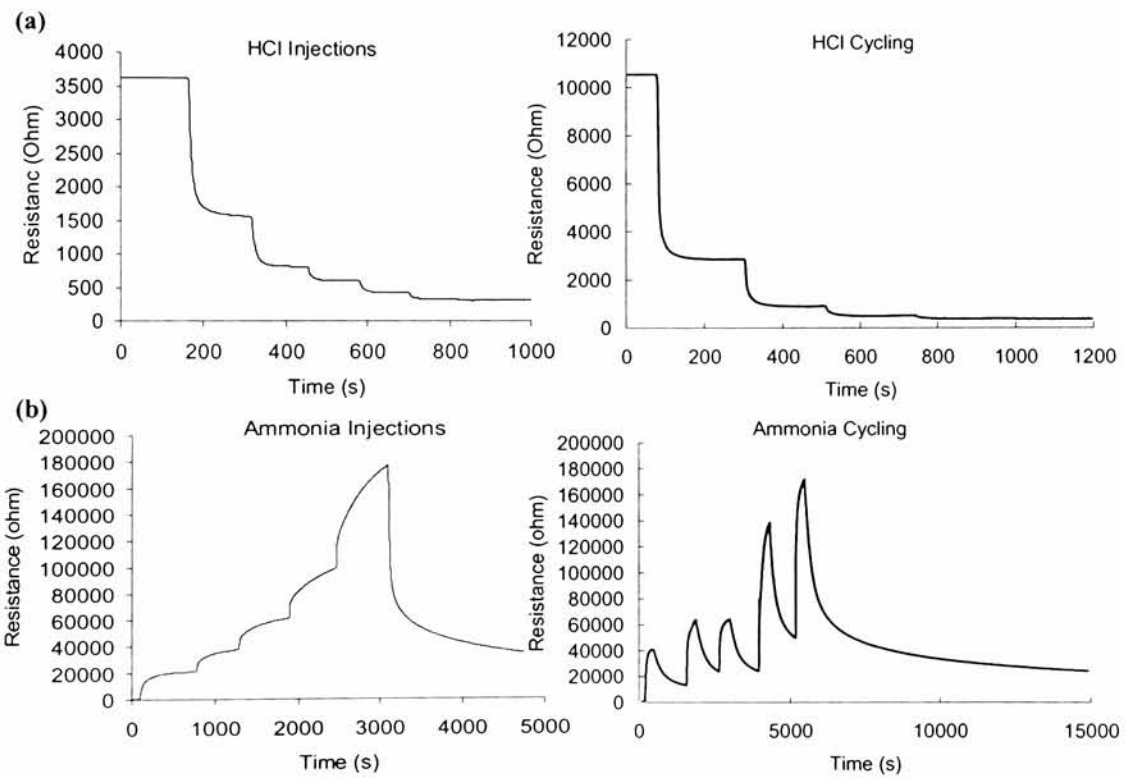

Figure 5.10 Sensor Response to Acid (a) and Base (b)

As shown in figure 5.10a, the sensor experienced a rapid drop in resistance in the presence of HCl. During this process, the polyaniline was doped by the protonation of the imine nitrogens by HCl (as shown in formula 1), with the generation of positive charge along the polymer backbone. The polarons (radical cations) created can travel along the backbone and thus increase the conductivity [49]. The reaction was fast and

efficient. Within a short period of time the curve leveled off. At this time all the HCl had been involved in the reaction and no more carriers could be created. Introducing nitrogen gas didn't induce any resistance recovery, which implies a chemical reaction with HCl that could not be reversed by nitrogen. After several cycles, the drop in resistance upon exposure became negligible. This could imply that all the imine nitrogens in the backbone (half the total nitrogens in the polymer) had been protonated and the polymer had reached its fully doped state.

The printed sensor's response to ammonia (Figure 5.10b) was opposite that of HCl. Upon exposure to NH_3/H_2O, there was a sharp increase in resistance at first, followed by much slower increase in resistance which lasted for hours, as shown in figure 5.11. This curve is actually an expanded plot from the resistance increase part of the fifth cycle in figure 5.10b. The resistance never leveled off like HCl did. Furthermore, when nitrogen was introduced, the resistance of the sensor decreased, although total recovery would require an extremely long period of time. Such result is similar to that reported for other polyaniline sensors [70].

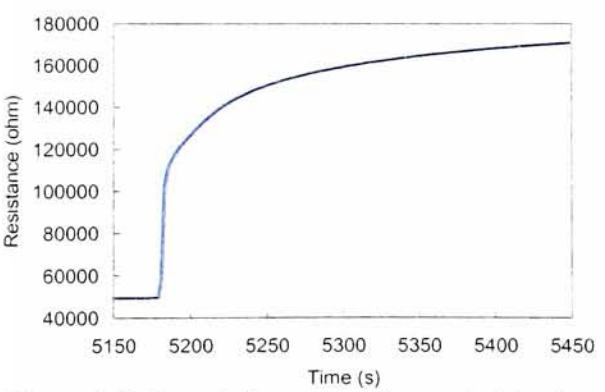

Figure 5.11 Sensor's Response to Ammonia Injection

The presense of ammonia causes a large increase in polyaniline resistance. This is likely due to two processes, where the ammonia de-dopes the polymer (increasing the intramolecular resistance), as well as

causing it to swell (which increases the intermolecular resistance) [64, 70]. This may explain the two stages of resistance increase shown in figure 5.11. Presumably, the first of these processes is irreversible, whereas the second is reversible. When the ammonia vapor is removed (for example, by purging with an inert gas), the resistance recovers (increases) slowly, but never completely regains its original resistance. Presumably, this is caused by the slow purging of the adsorbed nitrogen, which causes the chains to contract. The de-deoping effect can not be reversed by simply purging with nitrogen gas, but rather requires redoping with an acidic compound.

5.6 Volatile Organic Compounds (VOC's)

Several organic gas vapors were pumped (40 ml/min) or injected (5ml each time) into

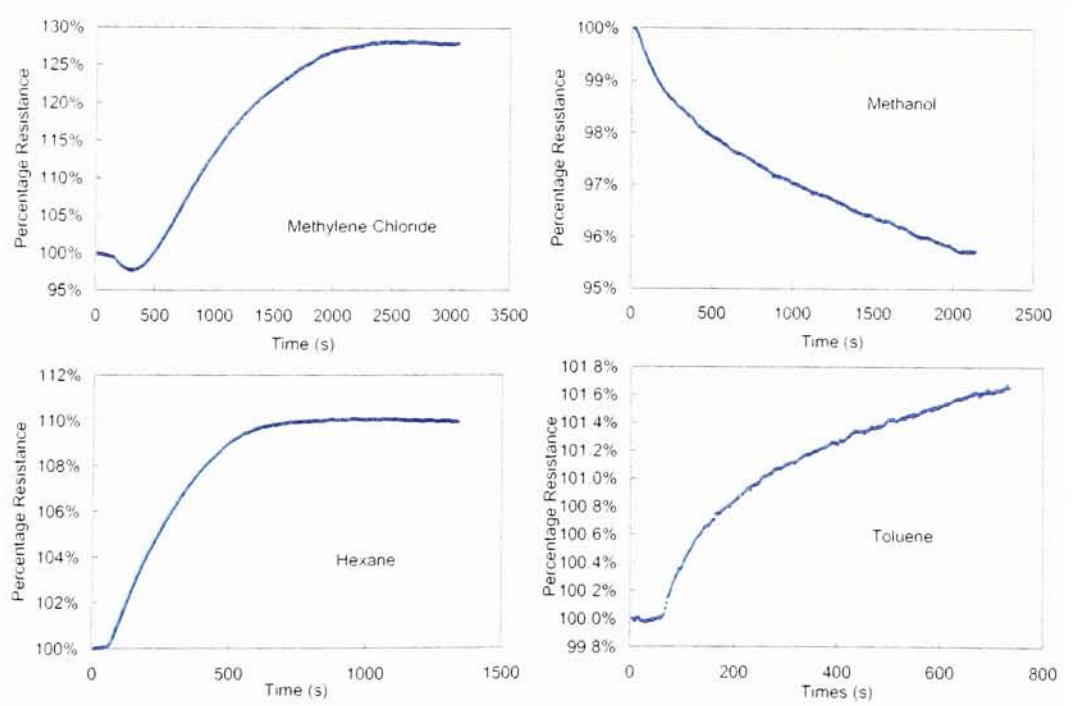

Figure 5.12 Sensor's Response to Volatile Organic Compounds Flow

the chamber and the corresponding resistance changes are shown in figure 5.12 and

5.13. All of these changes can be reversed with nitrogen.

For most volatile organic compounds, the resistance change was far less than that of acids and bases. As can be seen from table 5.1, the volatile organic acid (acetic acid) has a much larger sensitivity than the other organic compounds. This suggests that there is no chemical reaction taking place when the sensor is exposed to the non acidic volatile organic compounds, and the change in resistance is due to the physical structure change in the polymer chains, as has been described in section 5.2.

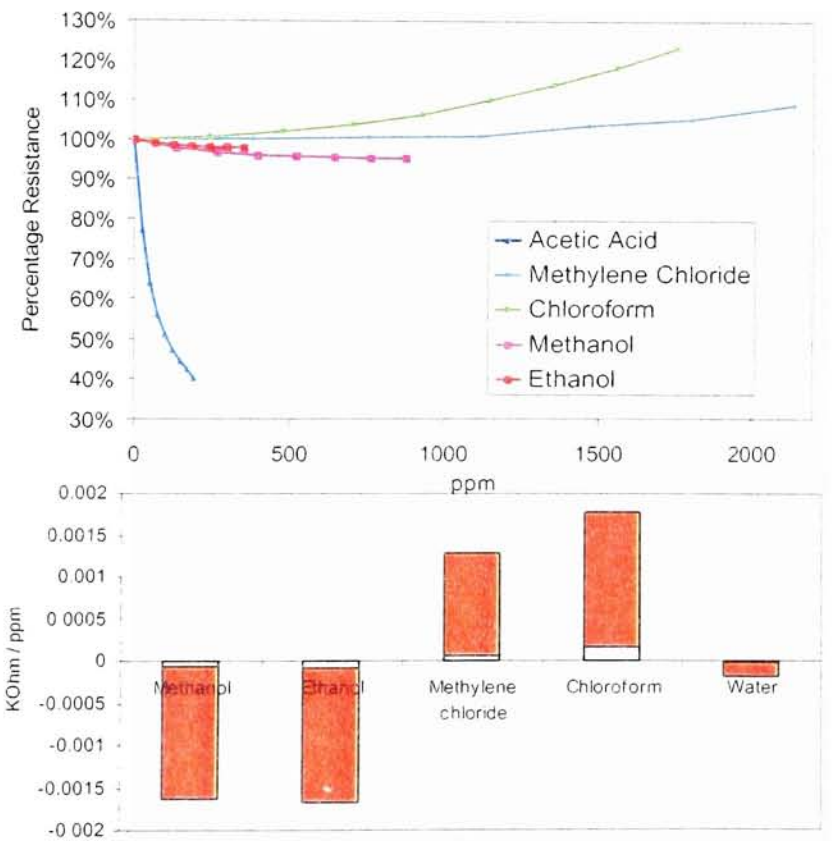

Figure 5.13 Sensor's Response to Volatile Organic Compounds Injection

	Acetic acid	Methanol	Ethanol	Methylene Chloride	Chloroform	Toluene	Hexane
Sensitivity (R/Ro/ppm)	-8.46E-05	-2.18E-07	-1.62E-06	6.18E-07	3.93E-06	4.26E-07	5.42E-07
Detection Limitation (ppm)	11.82	1085.13	617.28	513.72	254.45	2347.42	1692.37

Table 5.1 Volatile Organic Compounds Sensitivity and Detection Limitation

In our work, the behavior of chemical species can be summarized as follows: Strong acids increase conductivity, and strong bases decrease conductivity. Compounds which are not either strong acids or bases can also affect the conductivity. Relatively non-polar compounds like toluene or chlorinated solvents increase the conductivity, whereas polar protic compounds (strongly hydrogen bonding donors) like water, methanol and ethanol increase the conductivity. Most likely, this conductivity increase is due to the improved solvation of the dopant anions, inducing an expansion of the polymer chains.

The concentration of the gas vapor was calculated from the pumped volume (related to the time) and partial pressure. The sensitivity was obtained for each gas and is listed in table 5.1. Under constantly stirred conditions, the resistance variation was <10Ω even when the device is in equilibrium. However since the original resistance of the sensor used in this test is about 10 kΩ, a resistance change larger than 1‰ can be recognized as a change in response. Based on this, the detection limits have been calculated and are listed in table 5.1.

5.7 Natural Gas Sensor

Natural gas is a combustible, gaseous mixture composed almost entirely of methane (CH_4), but also contains small amounts of other gases, including ethane, propane, butane and pentane. Approximately 23 percent of the energy consumption of the U.S. comes from natural gas [98]. It is also used as a raw material to produce petrochemicals, plastics, paints, and a wide variety of other products. Natural gas leaks can cause fires or explosions, so its detection is important. An inexpensive small natural gas sensor could be helpful for industry and domestic natural gas leak detection.

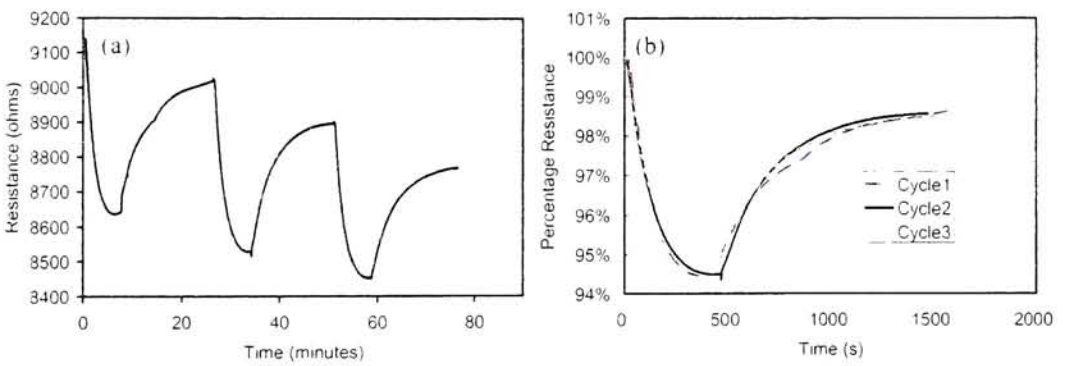

Figure 5.14 Sensor Response to Natural Gas (a) Total Change (b) R R_0 within Each Cycle

The response of the printed sensor to natural gas is shown in figure 4.19. In each cycle natural gas was pumped in until the resistance leveled off. After this, nitrogen was added to purge the natural gas. Three cycles were done to study its repeatability. As can been seen from figure 5.14, the resistance decreased when the sensor was exposed to natural gas. The decrease lasted about 8 minutes and then it reached equilibrium. The resistance recovered upon purging with nitrogen. After about 15 minutes the recovery process slowed, and it was difficult to return back to the original resistance. When

treated with natural gas again the resistance decreased at almost same rate, but the equilibrium resistance was lower than the first time. The recovery process was similar to the first recovery also. Comparing the relative resistance change in these three cycles (shown in figure 5.14b), the sensor exhibited almost the same relative rate and amount of change every cycle. The sensor's resistance changed about 5% in response to natural gas, and the nitrogen purge helped it recover up to 98.5% of the original resistance

5.8 Fish Preservation Sensor

Food preservation is an important issue for product quality and human health. Most kinds of meat and fish smell when they go bad. Their tissues contain an odorless chemical known as trimethylamine oxide. When the blood stops flowing and the tissues are exposed to air, the bacteria inside the meat or fish break down this chemical into two new chemicals, which are derivatives of ammonia (amines) and smell bad [99]. Fish tissue contains much more trimethylamine oxide, so during decay it smells much stronger than meat. Commercially fish is often packed in shrink wrap, so you cannot smell the contents. Given the high sensitivity of these sensors to ammonia, the use of printed sensors on the package to detect the fish quality could be an interesting potential application.

To detect the sensitivity to fish decomposition, a 0.47 lb catfish fillet was placed into a 1 gallon Ziploc bag with a printed sensor inserted. One sample was monitored at room

temperature (20.2 C), and another catfish fillet having almost same weight (0.51 lb) was tested in the refrigerator, with the temperature around 3 C. The sensors resistance change with time is shown in figure 5.15.

At room temperature, there was a slight decrease in resistance for the first hour, which could be caused by the increase of humidity in the bag. At just over an hour the resistance quickly increased about 3 times, presumably as a result of the formation of amines. This process only lasted for about 30 minutes. After that, the resistance was relatively stable for more than 13 hours. Later on the resistance increased sharply again.

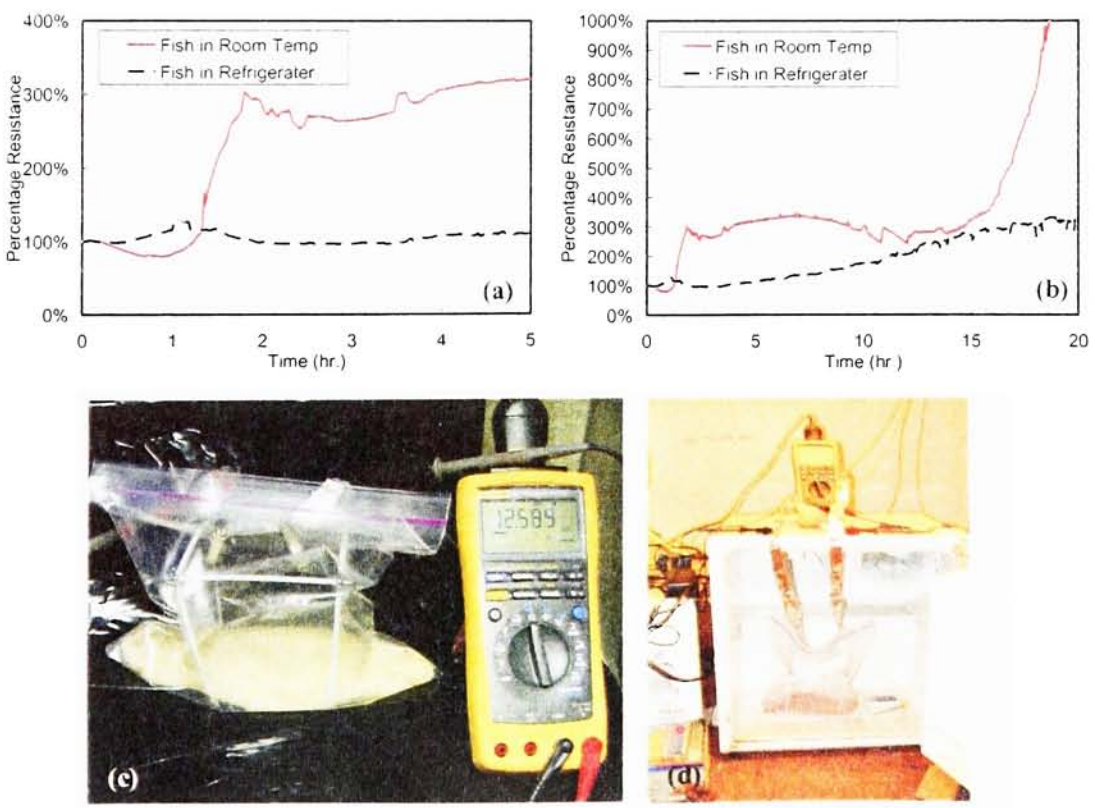

Figure 5.15 Bad Fish Detecting (a) in 5 Hours (b) in 20 Hours (c) (d) Experiment Set Image

From the resistance profile, refrigeration considerably slowed the fish deterioration. In the first 5 hours minimal change in resistance was observed, followed by a gradual increase lasting for more than 15 hours. The increase in resistance can be easily detected, and the printing process assures the low cost of the sensor. This technology could be amenable to printing sensors on packaging.

5.9 Polyaniline Degradation

When the fish preservation experiment was done, the polyaniline layer of the printed sensor was found to change its color. It was compared to the original one in figure 5.16. The plus and minus sign shown in figure 5.16 (b) were connected to the positive and negative electrode of the multimeter, respectively. As can been seen from the image, the color of the PANI layer coated on the negative electrode remained green, while the one coated on the positive electrode turned dark blue. This might due to an electrochemical reduction reaction occurring in the sensitive layer.

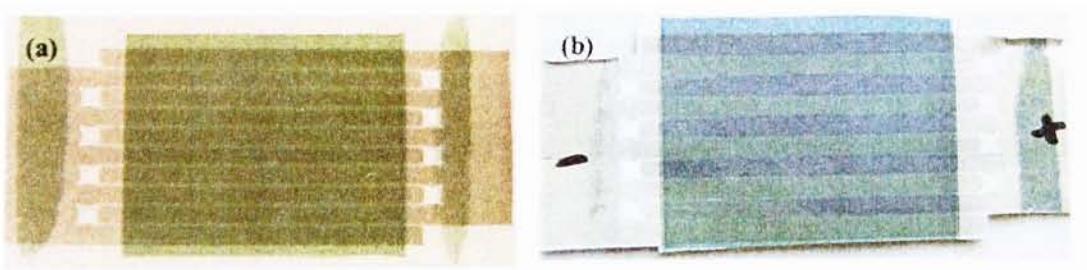

Figure 5.16 Photo Image of the Sensor (a) before fish testing (b) after fish testing

Further research [54] shows that the protonated polyanline have two distinct redox processes as shown in figure 5.17. Since the sensor was connect to the multimeter to test the resistance change, the potential of the multimeter made the interdigitated

1electrodes act like the working and counter electrodes in an electrochemical reaction. When the sensor was exposed to the amines generated by the bad fish, either protonation or reduction reactions may have taken place, both of which result in increase in resistance because the polyemeradine salt is the only conductive state. Influenced by the potential between the electrodes, the reduction products (polypernigraniline state) were only generated around the working electrode. That may explain the dark blue stripes on the polyaniline layer shown in figure 5.16 (b).

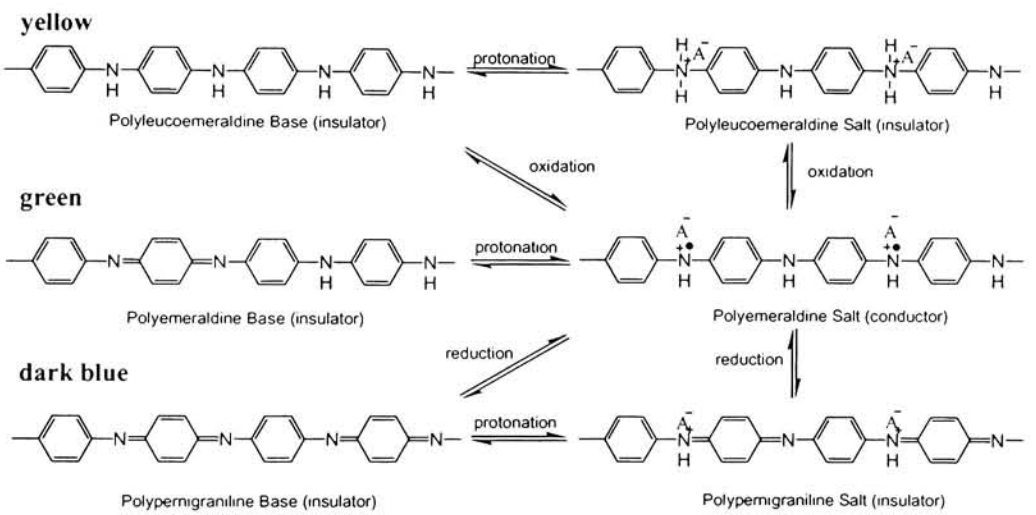

Figure 5.17 Protonation and Redox Reaction Between the Various Forms of Polyaniline

After the fish preservation test, diffuse reflectance fourier-transform infrared spectra was obtained to compare the different color strips on the polyaniline coated layer (shown in figure 5.18). Since the sensor was printed on paper, the substrate influenced the spectra of polyaniline especially in the range of 1300 cm^{-1}— 1500 cm^{-1} However, a band at around 1135 cm^{-1} can be found in the green strips which disappeared when the color turned blue. It is a characteristic band for conductive PANI and is due to the charge delocalization on the polymer backbone [96]. Moreover, the band shift from

1578 cm^{-1} to 1592 cm^{-1} indicating that the quinoid ring was generated again. Although overlapped by the paper spectrum, low intensity bands can still be found at wave number 1304 cm^{-1} for the green strips and 1315 cm^{-1} for the dark blue strips, which refer to the characteristic band of emeraldine salt form and pernigraniline, respectively [100].

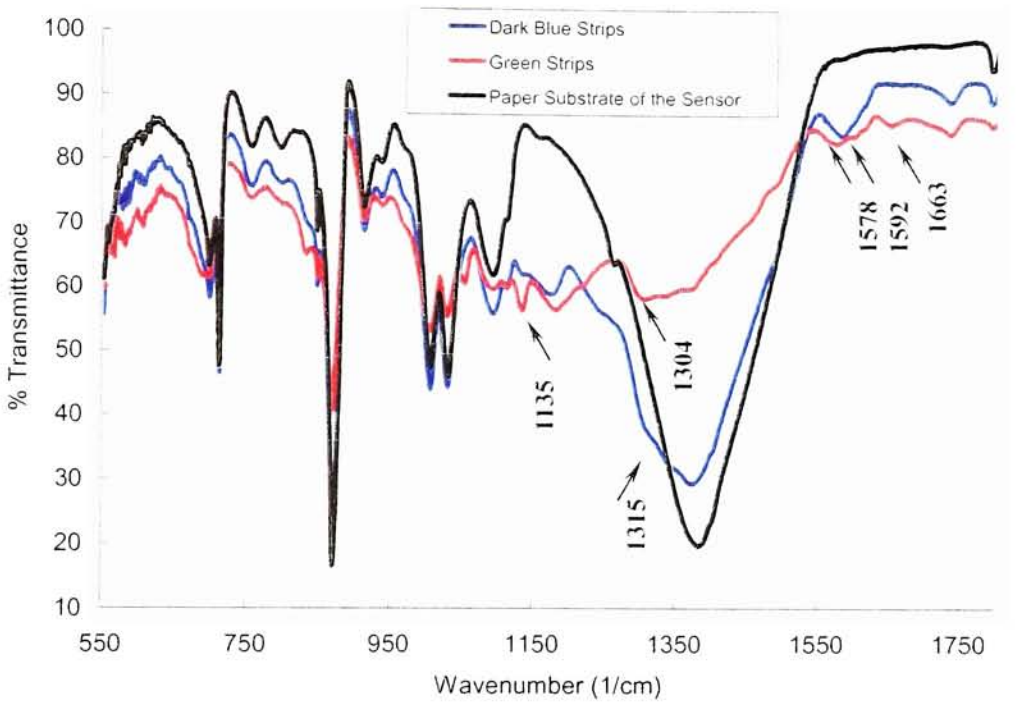

Figure 5.18 Diffuse Reflectance Fourier-Transform Infrared Spectra of Polyaniline Sensor

Figure 5.19 is the UV/visable spectra of the different colors, which also shows a peak shifted from around 500 nm to 480 nm. This information supports explain the presence of an electrochemical reaction taking place when the sensor was exposed to amines with a potential difference between the electrodes. To prevent this process a resistor with large resistance can be put in series with the sensor during testing. In this way most of the potential will be shared by the extra resistor and the current on the sensor will decrease. The degraded sensor can still be re-oxidized and re-protonated by

post-treatment with strong acids.

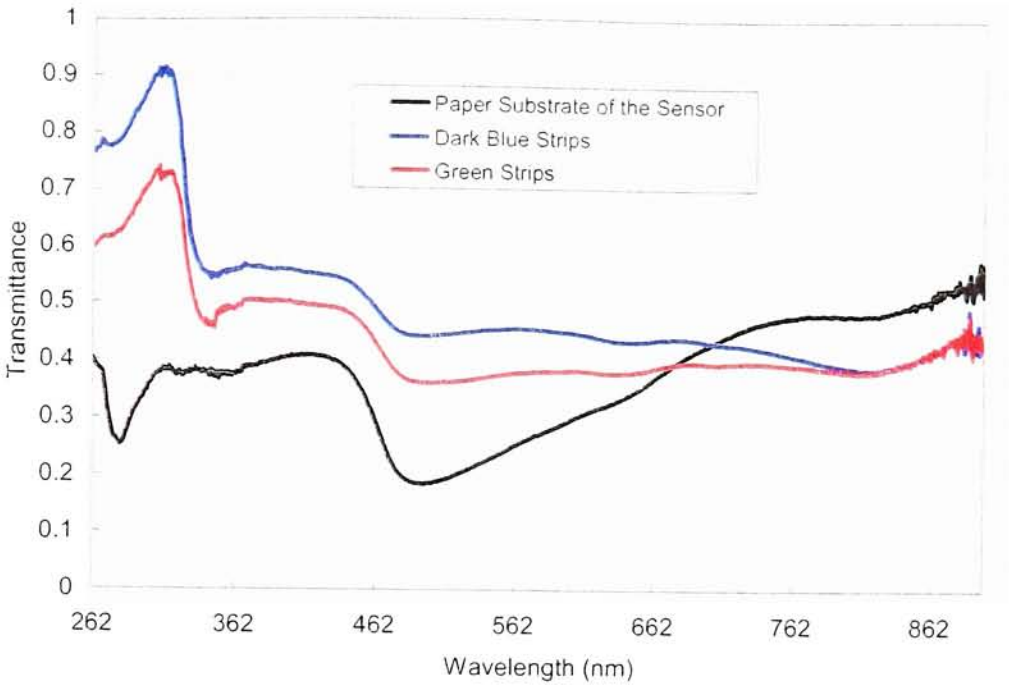

Figure 5.19 UV/Visable Spectra of Polyaniline Sensor

5.10 Conclusions

An all-printed chemical vapor sensor was fabricated by printing a polyaniline layer on silver interdigitated electrodes using flexographic printing.

The sensor's response to water vapors were tested, calibrated and compared with a commercial humidity sensor. Different substrates were used to study the performance. The sensor's response to different chemical vapors (hydrochloric acid, ammonia, acetic acid, chloroform, methylene chloride, ethanol, methanol, hexane, and toluene) was also tested and corresponding sensitivities were calculated. Two sensing prototypes usable in natural gas leakage and fish preservation were also demonstrated.

The printed polyaniline sensor can be easily fabricated on flexible arbitrary surfaces for very low cost. With the relatively low resistance and good sensitivity, they could prove useful in a variety of areas such as smart packaging, etc.

Chapter Six: Pattern Electronic Devices Using MicroPen

Patterning organic conductive materials with great precision is a necessity for printable electronics. The MicroPen can provide efficient use of polymeric electronic materials allowing for a timely assessment. In our investitation, Poly (3,4-ethylenedioxythiophene) poly (styrenesulfonate) (PEDOT:PSS) was patterned on a glass substrate with different line parameters. A thin film transistor structure was also fabricated by drawing two parallel conductive lines on highly doped silicon wafer with a silicon dioxide layer on the surface, and then filling the gap between electrodes with air stable polythiophene (PQT). The surface structures were evaluated through atomic force microscopy (AFM) and optical profilometry, and the electrical properties were tested as well.

6.1 MicroPen Directing Writing System

The MicroPen direct writing system, shown in figures 2.16, is a unique fabrication tool that deposits materials under high pressure through a fine conical capillary tip. The tool can work with fluids having viscosities ranging from water-like liquids to tar-like pastes. The capillary tip rides on the bead of material being dispensed but has substantial vertical travel and is

viscosities ranging from water-like to tar-like
pen tip can accommodate up to 1 mm of vertical topology
substrate moves on precision X-Y table with 5 μm resolution
writing process is computer controlled and CAD based
writing speeds up to 30 inches per second
100 nL minimum dispensable fluid with 0.3 nL resolution
deposit linewidths as small as 10 μm

Table 6.1 Performance Characteristics of the MicroPen

highly tolerant of substrate topology. The pen tip is fixed in x-y; while the substrate is translated by a high precision two axis table. The tool is driven by an integrated CAD layout program and requires no lithographic masking of any kind. The MicroPen is particularly suited for rapid prototyping, expensive materials, deposition of thick films, and use on substrate surfaces with extreme topology or non-standard geometries such as broken wafers, wafer die, and packaged die. Under highly optimized conditions, line widths as narrow as 10 um have been observed. Table 6.1 summarizes some of the important performance characteristics of the MicroPen.

6.2 PEDOT:PSS Conductive Lines

The transparent PEDOT:PSS was provided by H. C. Starck company (Baytron P). The chemical structure of PEDOT:PSS can be found in figure 2.7. Baytron P is normally found as aqueous dispersion (H2O; $[\text{-}C_6H_4O_2S\text{-}]_x^{0.33+}$ / $[\text{-}CH_2CH(C_6H_4SO_3)\text{-}]^-_{0.33x}$) which can be mixed with solvent and varnish, etc. to formulate the Baytron-based conductive coatings. The pattern (shown in figure 6.1) was designed to have groups of parallel lines with varying parameters such as length, width, and gap distance between them. During operation, the

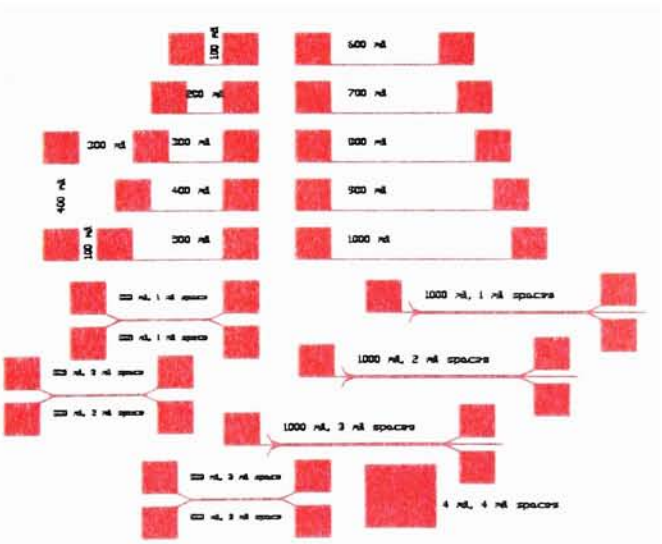

Figure 6.1 Conductive Line Testing Plate

movement of the MicroPen tip was precisely controlled by this CAD design. Two different MicroPen tip sizes, 6-4 mil and 4-3 mil (outside-inside diameter in mils) were used to write the pattern onto the substrates.

A roughness analysis was produced using an Atomic Force Microscope in tapping mode. An area of 40×40 μm was scanned from a single patterned line as well as the surface of the glass. To reduce any instrument errors or noise from the environment, each sample was scanned vertically and horizontally to acquire two images of the same area. Statistics of the surface roughness characteristics were obtained as shown in figure 6.2-6.3 and table 6.2. Results show higher uniformity on the patterned surface

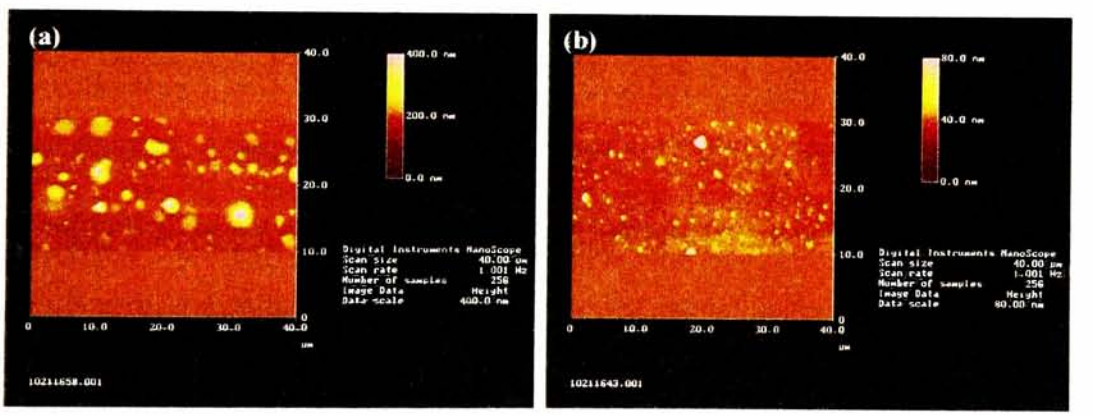

Figure 6.2 AFM Image of the Conductive Line (a) 6-4 tip (b) 4-3 tip

Roughness Analysis (unit nm)				
	4-3 Line	6-4 Line	4-3 Glass	6-4 Glass
MAX				
Z range	188.23	214.01	523.85	319.08
Mean	0.075	0.055	0.05	0.063
Raw Mean	610.86	176.79	47.712	423.42
Rms (Rq)	5.048	9.799	30.267	16.914
Mean Roughness	1.129	3.78	10.608	6.138
MIN				
Z range	17.11	54.124	47.594	37.287
Mean	-1.462	-3.477	-13.422	-5.527
Raw Mean	650.83	259.46	51.686	418.08
Rms (Rq)	1.488	3.727	4.961	5.961
Mean Roughness	1.117	2.755	3.467	2.893

Table 6.2 Roughness Analysis Data

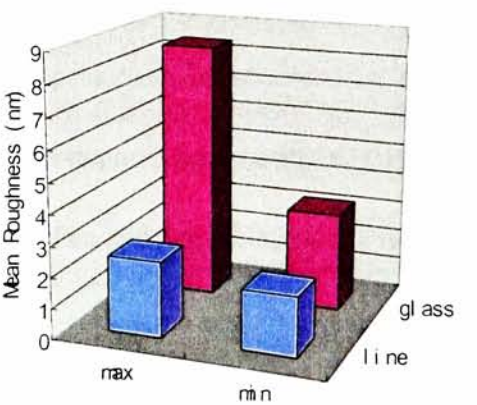

Figure 6.3 Roughnesses of Line and Substrate

(roughness 2-3 nm) compared to the glass surface (roughness 3-9 nm). The scanned 3-dimensional image of the glass substrate displays a higher irregularity of peaks and valleys as well as a higher value for the mean average roughness.

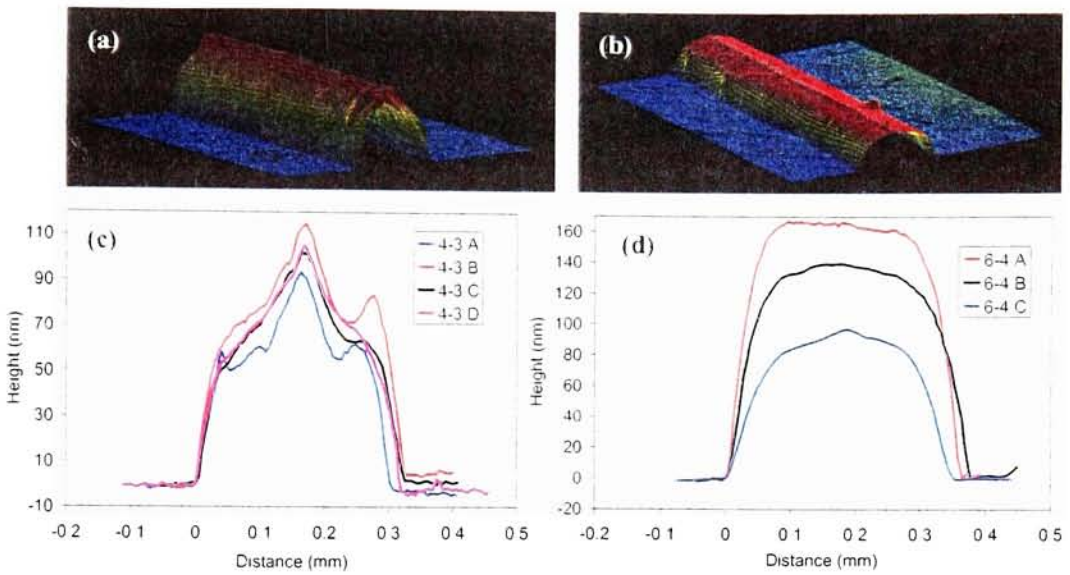

Figure 6.4 Profilometry Image of the Conductive Lines (a) 4-3 tip line 3-D image (b) 6-4 tip line 3-D image (c) 4-3 tip line cross section (d) 6-4 tip line cross section

The structure of the lines drawn by 4-3 tip and 6-4 tip were compared using optical profilometry. As shown figure 6.4, both of the tips managed to draw straight lines with nearly vertical sides and smooth surfaces. However, the 4-3 tip tends to write lines with a peak-shape cross section, while the 6-4 tip has a plateau-shape cross section. Moreover, both the height and width of the line patterned with the 4-3 tip are smaller than the ones patterned by the 6-4 tip. Some sharp peaks can be observed on the surface of patterned lines, which might be attributed to impurities in the PEDOT:PSS dispersion, or particles attached to the end of the MicroPen and depositing on the lines during the patterning process.

The sheet resistance along the 100 mil line was determined to be around 4 MΩ/□. The high resistance was attributed to the thinness of the lines (~100 nm). Surface uniformity and edge sharpness and are two other important characteristics to assess the conductive line. A smooth and uniform surface without spikes prevents the trap and field emission of the electronics, thus increasing the carrier flow rate. For multilayer electronic device fabrication it can be used as high quality bottom-electrode. The shape of the edge limits the resolution of the system and it can be adjusted according to the surface energy of the ink and the substrate. Our lines have almost rectangular shaped cross section which makes it possible to draw parallel lines with very narrow gap

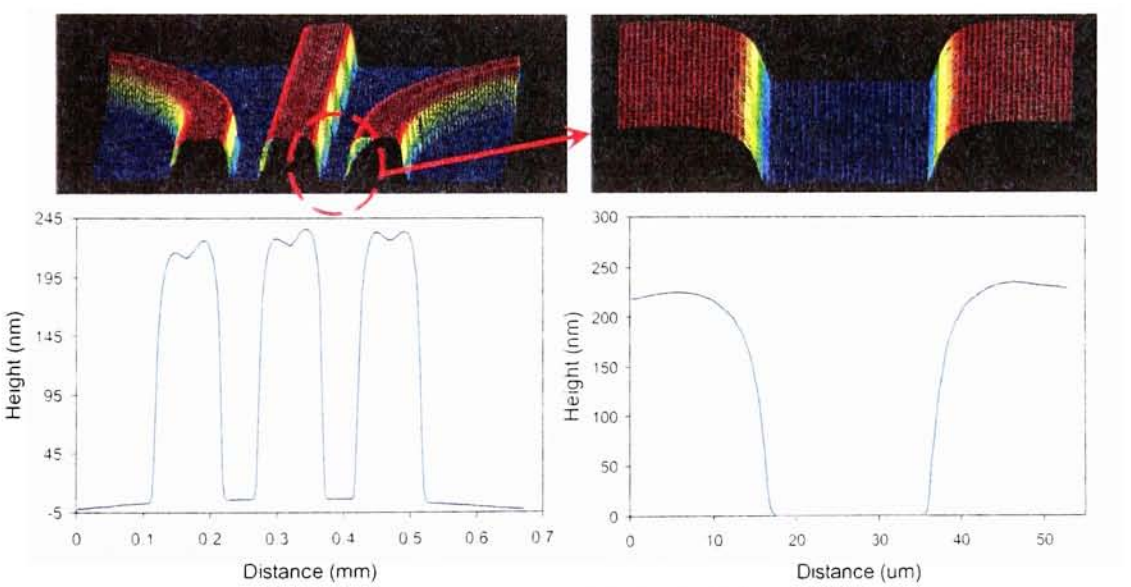

Figure 6.5 Profilometry Image of the Parallel Lines and Gaps

distance. Figure 6.5 shows three conductive lines connected to separate electrodes which approached and became parallel to each other. The gap distance is around 20 μm and the edge of the lines only dispersed less than 5 μm. The result of this work suggests that the MicroPen may be capable of writing transistors and other delicate electronic devices.

6.3 Organic Thin Film Transistor and Polythiophene

Thin film transistors (TFTs) based on hydrogenated amorphous silicon (a-Si:H) and polysilicon (poly-Si) have already been used in a variety of applications including liquid crystal displays (LCDs), sensors, imagers, and consumer electronics [101-103]. Meanwhile, the potential for being fabricated on flexible substrates using low-cost processing methods makes organic thin film transistor (OTFTs) in the forefront of scientific and technical research [104-111]. OTFTs can be used as backplane drivers for organic light emitting diodes (OLEDs) to form active matrix displays. They can also form the basic electronic units like complementary transistors, inverters, ring oscillators, etc. and by combining them together, large area electronic circuits can be achieved.

Figure 6.6 demonstrates the cross section of four variations of lateral OTFT structures. All of them use gate insulator, organic semiconductor as well as gate, soure and drain

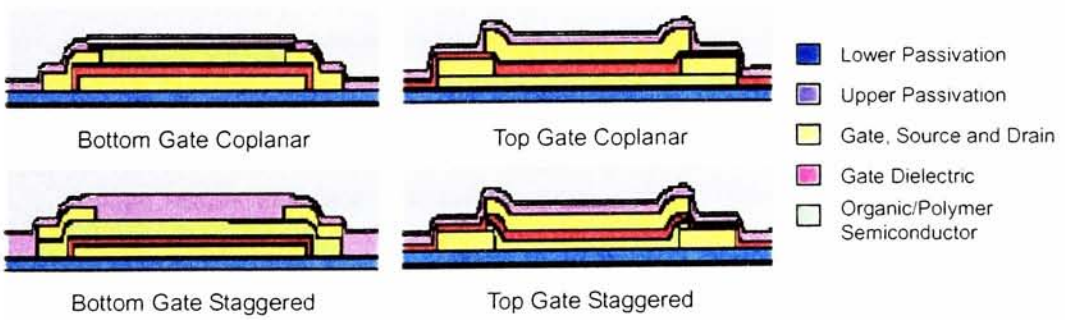

Figure 6.6 Device Cross Section of OTFTs [112]

electrodes. Different stack structures may influence the performance of the transistor, but they have the same working mechanism. It shows the similar device performance

compared to the traditional field effect transistors (FETs) but it operates as accumulation mode devices while the FETs is generally depletion or inversion mode devices. For example, a p-channel organic TFT has abundant positive carriers provided by the semiconductor material. During operation a negative voltage is applied to the gate and drain (compared to source). As a result the positive carriers are injected from the source into the active layer. The injected carriers are accumulated at the gate insulator/active layer interface by the surface potential, which contributes first to filling trap states in the energy gap between the relevant carrier conduction levels. As the gate-source voltage reaches a threshold voltage, the carrier injection fills all the trap states in the energy gap and thus makes a thin active layer close to the gate insulator interface, has its Fermi level near the mobility edge so the carrier is ready to flow. Above threshold voltage, the drain current (output current) first experiences a linear increase with the source-drain voltage, and then it levels off and quickly becomes uniform. At this region the gate insulator field is reduced to zero at the drain end of the device, which makes the channel at the drain side nearly pinched off and saturates the drain current. Therefore the drain current is independent to source-drain voltage, but only determined by the gate voltage. A small change in the gate-source voltage results in a large increase in drain current. Figure 6.7 shows some typical characteristic curves for a p-type organic TFT. Other than the lateral structure, some solution-processed vertical insulated gate OTFTs [113] and vacuum processed vertical static induction OTFTs [114] have also been investigated.

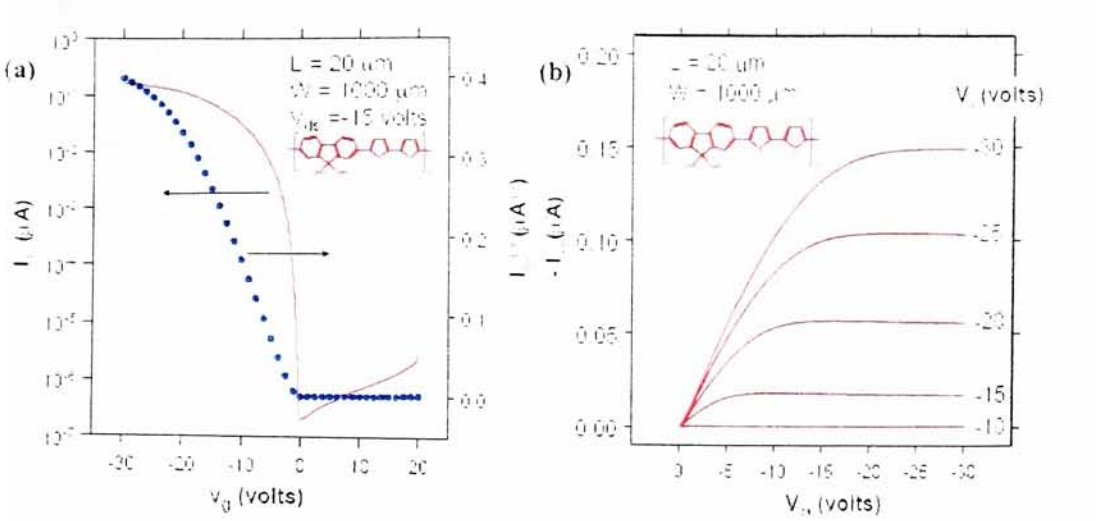

Figure 6.7 Characteristic Curves of an OTFT Based on F8T2 [112] (a) Source-drain current vs. gate voltage. (b) Source-drain current vs. source-drain voltage with various gate voltages.

The behavior of the devices is determined by a series of macroscopic quantities such as field effect mobility, threshold voltage, on/off current ratio, contact resistance, leakage current, etc. Among them the field effect mobility is the merit factor which is strongly dependent on the structural order of the semiconductor materials used. Recently several p-type ([n]-acenes, oligophenylene, oligo- and poly- thiophene, etc.) and n-type (perylene derivatives, phthalocyanines, etc.) organic semiconductors have been developed with good electrical transport properties [115-117]. Some of their chemical structures as well as their mobility and on/off current ratios were shown in figure 1.1 before. The common feature of all these structures is the presence of π-conjugated bonds, which facilitates the carrier injection by decreasing the ionization potential or the electron affinity. Moreover, the charge placed on a conjugated molecule is rapidly delocalized over the π-orbital system, which also contributes to the potential electrical performance.

Among all the p-type conductive organic materials the best electronic performance was

found in pentacene whose carrier mobility is larger than $3cm^2/V \cdot s$ with on/off current ratio 10^5 [116]. Unfortunately, pentacene has a very high melting point and is virtually insoluble, which means high temperature thermal deposition process or soluble precursor molecule must be introduced in device fabrication. Moreover, the environmental instability also limits the application of pentacene. On the other hand, regioregular poly(3-substituted thiophene)s are soluble in common organic solvents and have been satisfactorily solution-processed into OFET semiconductor layers [118]. Figure 6.8 shows some of their chemical structures. The presense of the 3-substituent dramatically increases the solubility and processability of the material, while the regioregular head-to-tail structure improves the micro-structural ordering and crystallinity in the solid state, thus decreasing the band gaps between the highest occupied molecular level (HOMO) and the lowest unoccupied molecular level (LUMO), and substantially improves its electrical conductivities [118].

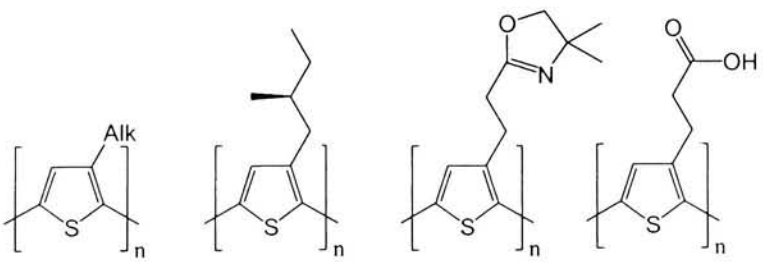

Figure 6.8 Regioregular Isomers of Poly(3-substituted thiophene)s

Nonetheless, environment instability remains an issue for these solution-processable polythiophenes. For example, TFTs fabricated in air with the most well studied regioregular head-to-tail poly(3-hexylthiophene) (HT-P3HT) generally exhibited much lower performance characteristics[119] than those fabricated in an inert atmosphere [120], This was primarily due to the sensitivity of HT-P3HT to

atmospheric oxygen. The relatively air-stable copolymer poly(9,9'-dioctyl-fluorene-co-bithiophene) (F8T2, chemical structure shown in figure 1.1) requires very high annealing temperature [121]. They are still not suitable to be used as ink for the regular printing process.

For our MicroPen device fabrication, a new class of solution-processable high performance regioregular polythiophene, poly(3,3''-dialkylquaterthiophene) (PQT) (chemical structure shown in figure 6.9a) was provided by Xerox. Its mobility was reported to be up to 0.1-0.2 $cm^2/V \cdot s$ [122]. Properly conditioned thin films of PQT showed the lamellar structure consisting of both the π-π and the interlayer stacking of backbones, with an additional ordering from side chain interdigitation (Figure 6.9b).

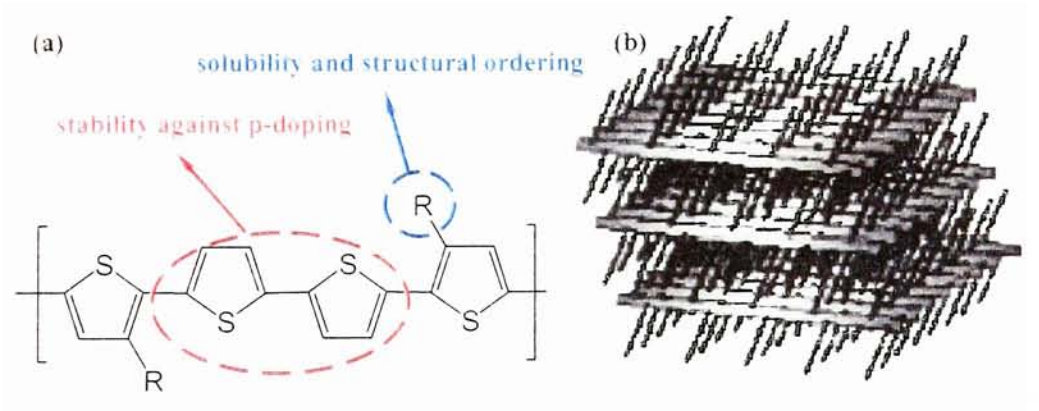

Figure 6.9 (a) Molecular structure of PQT (b) 3D packing of PQT molecules [122]

The appropriately long alkyl side-chains in this polythiophene help increase the solution processability and self-assemble of the material, while the proper control of extended π-conjugation may achieve a delicate balance between transistor functionality and oxidative doping stability. Compared to other regioregular polythiophenes such as P3HT, PQT possesses higher air stability, which enables its

fabrication into a high-mobility semiconductor layer using printing techniques under ambient conditions [122].

A major advantage of our work is that we are actually pattering the semiconductor material. In most other organic transistors, the semiconductor is made by spin coating or thermal deposition [123]. Even for those printed transistors discussed in chapter 2 [10, 15, 17, 31], generally they just use printing techniques to make the source and drain electrodes, while the semiconductor layer is made by traditional methods. However, organic semiconductor is the most expensive material of the device, if we can pattern it at the exact place we want without any waste, the cost of such a device could be much lower.

6.4 Fabricating Thin Film Transistor Using MicroPen

The fabrication process is shown as figure 6.10. The substrate is a highly doped silicon wafer (used as gate electrode) with 3500 Å silicon dioxide on its surface. A series of square patterns were drawn at first using silver ink, which work as contact electrodes. Then silver source and drain electrodes were drawn parallel to each other and connected to different contact electrodes. Finally the semiconductor channel was formed by drawing PQT in between the source and drain. In the designed pattern (figure 6.10a), each row has a different channel width, from 150 μm to 25 μm. Figure 6.11 and 6.12 shows several optical microscopy and optical profilometry images of the TFT structure.

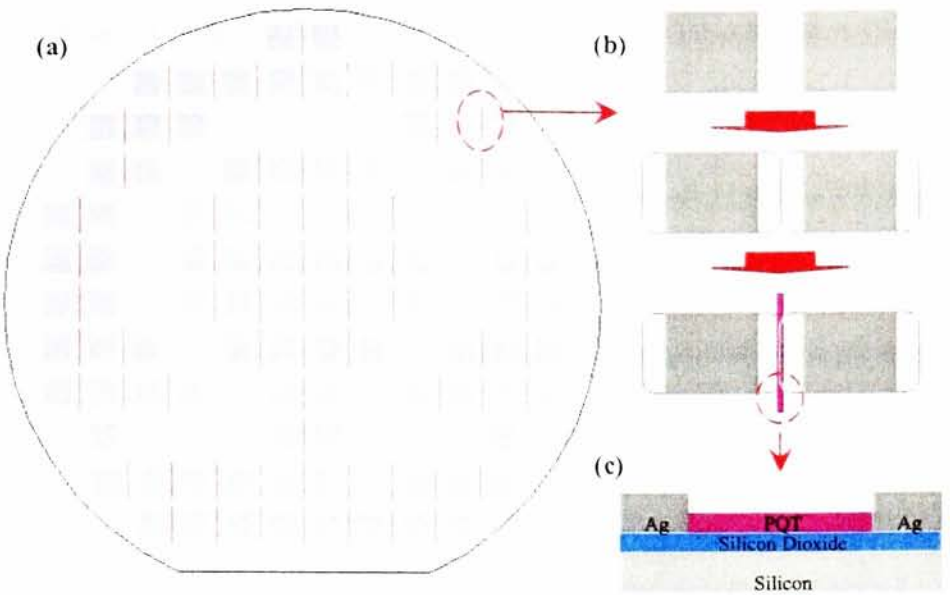

Figure 6.10 Thin Film Transistor Fabrication (a) Pattern design on the silicon wafer (b) Fabrication process of a single transistor (c) Cross section of a single transistor

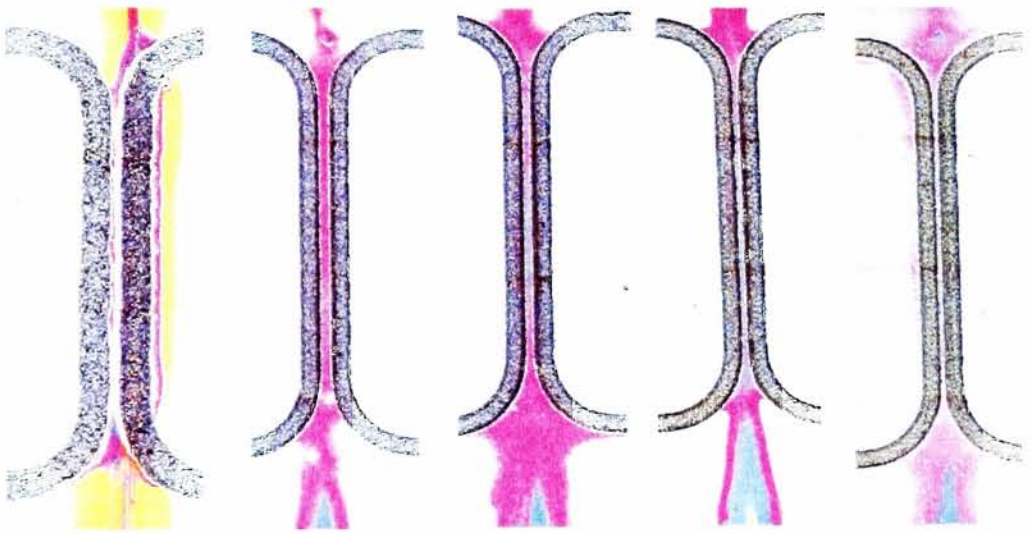

Figure 6.11 Optical Microscopy Images of TFTs with Different Channel Lengthes

Two types of silver ink (CMI 114-31 Ag conductor, typical sheet resistance 40-50 mΩ/□, cured at 125 °C and Metech 9695, typical sheet resistance 5 mΩ/□, cured at 850 °C) have been used to print the electrodes. In figure 6.11, rough edges can be observed from the lines drawn by the CMI ink, which result in short circuits when the channel

width decreases. Compared to the CMI ink, the Metech ink created very smooth channel even when the width of the channel decreased to 25 μm. However, Metech ink needs to be cured at 850 °C. At such a high temperature the silver diffused through the silicon dioxide layer and caused shorts between the source/drain and the gate electrode. Silicon nitride was also used as dielectric layer with this ink but the same phenomenon was observed. Moreover, as can been seen from figure 6.12, the organic semiconductor layer deposited between source and drain electrode is very thin (several nanometers), which will restrict the current flow.

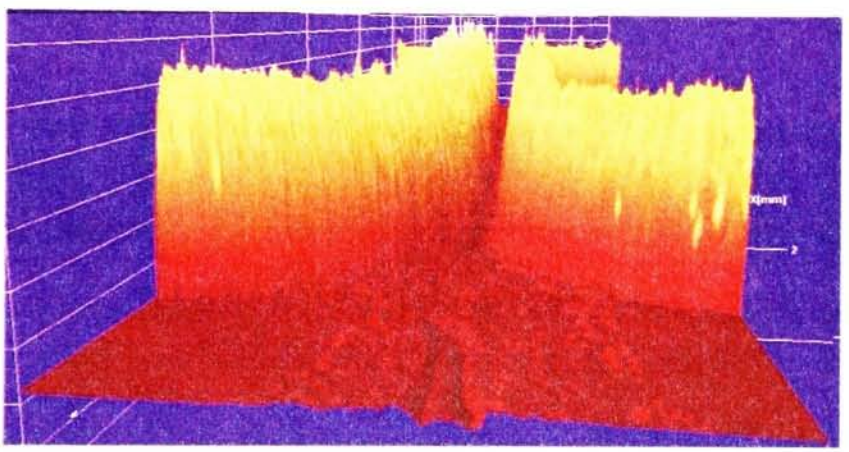

Figure 6.12 Optical Profilometry Image of TFT (Metech 25μm)

Another type of silver ink provided by Parelec (RIA 101, sheet resistance 0.1Ω/□) with lower curing temperature (150 °C) has been used, and a thicker layer of PQT has been drawn as well. The thickness is around 2000 Å, measured by stylus profilometry. The characteristic family of curves has been observed by Keithley 4200 semiconductor characterization system, as shown in figure 6.13. It is similar to the typical output curves shown in figure 6.7b.

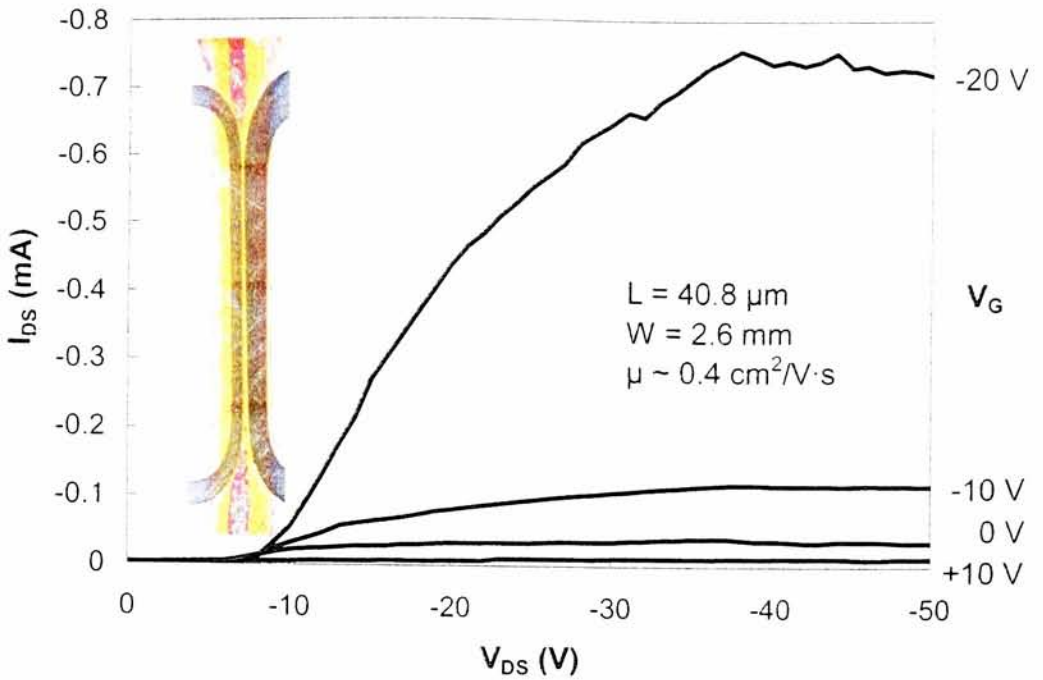

Figure 6.13 Output Family Curves of the OTFT Fabricated by Micropen

The actual channel length of the transistor was measured to be 40.8 μm, and the channel width was 2.6 mm. The mobility can be found using the standard "linear regime" equation [124]:

$$I_D = \frac{W}{L} C_{ox} \mu \left[(V_G - V_T) V_D - \frac{V_D^2}{2} \right] \qquad (6.1)$$

where C_{ox} is the capacitance of the insulator (3500 Å silicon dioxide) per unit area, typically reported in nF/cm^2 Assuming that the threshold gate voltage V_T is equal to 10, we calculated the mobility μ of our organic thin film transistor to be around 0.4 cm^2/V·s. This result is in the same scale as the reported PQT transistor [122].

However, most of the TFTs tested were not stable. When the source/drain voltage was held and the gate voltage swept several times, the output current was different each time. This indicates the existence of traps and other energy barriers, causing the

carriers to accumulate slowly. In some of the TFT samples, current has been observed under positive gate voltage and the current didn't saturate even when the positive bias was increased up to 50 V. Moreover, relatively high negative bias (more than -20V) caused a decrease in output current rather than an increase. The source-drain voltage required to drive the transistor is somewhere around -5V rather than 0V. Another problem with this transistor is we cannot get a good I_{ds}-V_{gs} curve. Figure 6.14 shows a typical I_{ds}-V_{gs} curve. Instead of showing a threshold voltage around 0V (refer to figure 6.7), the current kept decreasing with decreasing gate voltage utill around 0V and then leveled off. After that, the current quickly decreased to 0A at around -20V. This may explain why the device didn't work when the gate bias was higher than -20V. The reason causing this strange current-voltage relationship is still unclear.

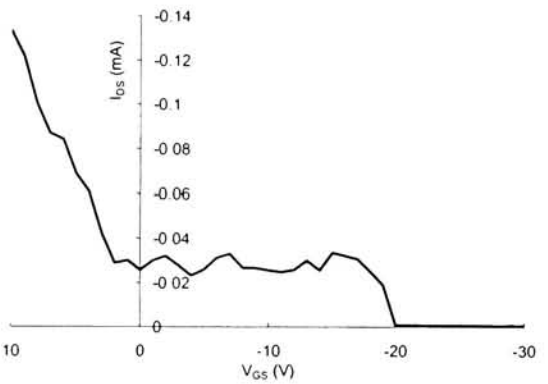

Figure 6.14 I_{ds}-V_{gs} curve at V_{ds} = -10V

The transistor was then heated to ~140 °C in vacuum oven, transferred to a dessicator, and allowed to cool to room temperature. The structural parameters didn't appear to change when observed under optical microscopy. The electrical performance was studied as well, as shown in figure 6.15. Compared to the devices before annealing, the current is more stable and repeatable. A good output current curve was observed until the gate bias reached -40V and then the curve saturated. However, the source-drain voltage required to drive the transistor shifted to -10V, and the calculated mobility

decreased to about 0.1 $cm^2/V \cdot s$. Still, we were unable to obtain a reasonable I_{ds}-V_{gs} curve.

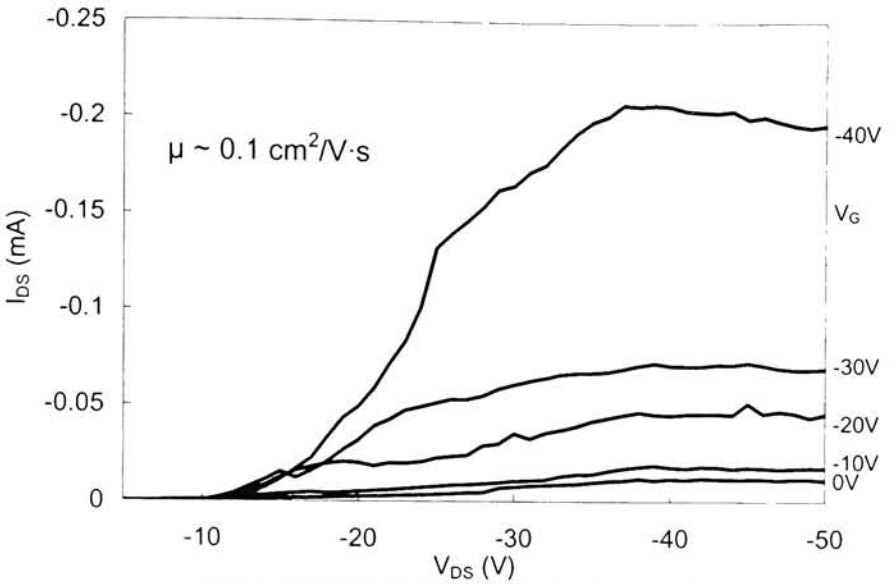

Figure 6.15 Output Family Curves after annealing

6.5 Conclusion

A variety of materials (PEDOT:PSS, Ag, PT) have been written using MicroPen direct writing system on different substrates such as Glass, SiO_2, Si_3N_4, etc. Smooth surfaces and sharp edges have been observed in the printed patterns. A thin film transistor (TFT) structure was fabricated by drawing two parallel conductive lines on highly doped silicon wafer with a dielectric layer on the surface, and then filling the gap between electrodes with air stable polythiophene (PQT). Three types of silver inks have been used for conductive electrodes. The channel lengths of the TFT can be as small as ~20 μm and for a transistor with 40.8 μm channel length and 2.6 mm channel width, the mobility was calculated to be around 0.4 $cm^2/V \cdot s$ before annealing and 0.1 $cm^2/V \cdot s$ after that.

Chapter Seven: Future Research

Solution processible fabrication is one of the most interesting topics in electronic device research. Only by this process can low cost manufacture of the devices over large areas on flexible substrates be realized. From the summary and the printed devices discussed in this thesis, one can see the great potential of using traditional or moderated printing techniques to fabricate various electronic devices. However, there remain large challenges both in the ink formulation and in the printing process itself.

Conductive ink containing metal particles have already been commercially developed by several companies. But there need to be a lot of work done on organic, especially organic semiconductor ink. The performance of the devices is strongly dependant on the macro-structure of the functional layer. The printed layer should have sharp sides and smooth surface, which is influenced by the material properties, the additives added to the ink, and the surface energy of the ink and the substrate. Further work can be done to formulate the ink which can form the "best shape" of the printed layer.

The micro-structure of the printed ink is another interesting aspect to study. The response of the electronic devices is also influenced by factors like the material crystallization, the organic chain order, etc. We need to understand film formation from the liquid phase and how this affects the electrical transport. How to decrease the impurities introduced by the solvent, surfactant, etc. should also be considered about.

As has been summarized in the second chapter, every printing process has its own advantages and disadvantages. Improving their properties and finding the most suitable process for a certain application is another task for the researcher. Moreover, how do the pre-treat of the substrate and the post-curing of the ink influences the device performances should also be take into concern.

Finally, based on all the single devices people have patterned, we can start thinking about printing the "smart device circuit", which combine the detector, processor and feedback unit all together. Promising examples are the combination of the printed transistor and antenna to form a RFID tag, the printed circuit includes a sensor, a cell and an alarm, etc. Such devices must be very competitive and make great contributions to our lives.

References:

[1] Moore, *Scientific American*, Jun, 2002

[2] A. Pochettino, *Acad. Lincei Rendic.*, **15**, 355 (1906)

[3] J. Koenigsberger, K. Schilling, *Annalen der Physik*, **32**, 179 (1910)

[4] R. G. Kepler, P. E. Bierstedt, R. E. Merrifield, *Phys. Rev. Lett.*, **5**, 503 (1960)

[5] L. B. Coleman, M. J. Cohen, D. J. Sandman, F. G. Yamagishi, A. F. Garito, and A. J. Heeger, *Solid State Communications*, **12**, 1125 (1973)

[6] M. Pope, H. P. Kallmann, and P. Magnante, *J. of Chem. Phys.*, **38**, 2042 (1963)

[7] W. Helfrich and W. G. Schneider, *Phys. Rev. Lett.*, **14**, 299 (1965)

[8] M. Pope and C. E. Swenberg: *Electronic Processes in Organic Crystal and Polymers, 2nd ed.*, Oxford University Press, 1998

[9] C. K. Chiang. C. R. Fincher, Y. W. Park, A. J. Heeger, H. Shirakawa, E. J. Louis, S. C. Gau, and A. G. MacDiarmid, *Phys. Rev. Lett.*, **29**, 1098 (1977)

[10] H. Sirringhaus, *Science*, **290**, 2123 (2000)

[11] Burns, et. al., *MRS Bull.*, Nov. 2003

[12] J. Rogers, *Proc. Natl. Acad. Sci. (US)*, **98(9)**, 4835 (2001)

[13] B. Michel, et. al., *IBM J. Res. Dev.*, **45(5)**, 697 (2001)

[14] H. Kipphan, *Handbook of Print Media*, Springer Press, 2001

[15] R. Sangoi, C. G. Smith, M. D. Seymour, J. N. Venkataraman, D. M. Clark, M. L. Kleper, B. E. Kahn, *Journal of Dispersion and Science Technology*, **25(4)**,513 (2004)

[16] J. Kaverman, *Introduction to Pad Printing*, http://www.padprinting.net

[17] Knobloch (PolyIC Company), *IMAPS/TAGA 3rd Advanced Technology Workshop on Printing an Intelligent Future*, Sep, 2004

[18] T. Hu, X-E. Zhang, Z-P. Zhang, *Biotechnology Techniques*, **13(6)**, 359 (1999)

[19] C. Xu, L. Liu, S. E. Legenski, D. Ning, and M. Taya, *J. Mater. Res.*, **19(7)**, 2072, (2004)

[20] Shimoda, et. al., *MRS Bull.*, Nov. 2003

[21] G. Blanchet, et. al., *MRS Symp. Proc.*, 736 (2003)

[22] Y. Xia, and G. Whitesides, *Angewandte Chemie*, **37**, 550 (1998)

[23] J. Xu, *Synthetic Metals*, **155**, 1, (2000)

[24] X. Zhao, Y. Xia, and G. Whitesides, *J. of Mat. Chem.*, **7**, 1069 (1997)

[25] D. Qin, Y. Xia, J. Rogers, R. Jackman, X. Zhao, and G. Whitesides, *Topics in Current Chemistry*, **194**, 1 (1998)

[26] W. Childs, and R. Nuzzo, *J. Amer. Chem. Soc.*, **124**, 13583, (2002)

[27] R. G. H. Lammerlink, M. Peter, M. A. Hempenius, G. J. Vancso, *Poly. Mat. Sci. and Eng.*, 86, 101 (2002)

[28] A. Bernard, E. Delamarche, H. Schmid, B. Michel, H. Bosshard, and H. Biebuyck, *Langmuir*, **14**, 2225 (1998)

[29] R. G. Nuzzo, L. G. Dubois, *Annu. Rev. Phys. Chem.*, **43**, 437 (1992)

[30] B. Michel, et. al., *IBM J. Res. Dev.*, **45(5)**, 697 (2001)

[31] J. Rogers, *Proc. Natl. Acad. Sci. (US)*, **98(9)**, 4835 (2001)

[32] J. Rogers, *MRS Bull.*, **26**, 530 (2001)

[33] B. Comiskey, J. D. Albert, H. Yoshizawa, J. Jacobson, *Nature*, **394**, 253 (1998)

[34] Y.-L. Loo, Robert L. Willett, Kirk W Baldwin, and John A. Rogers, *J. Amer. Chem. Soc.*, **124**, 7654, (2002)

[35] Yu Xia, Anupama Karwa, Franz Sigg, Daniel M. Clark, and Bruce E. Kahn, *ACS Northeast Regional Meeting*, **239**, Nov. 2, 2004, Rochester, NY

[36] P. Calvert; *Chem. Mater.*, **13**, 3299, (2001)

[37] B. J. Ramsey, P. S. A. Evans, D. Harrison, *Journal of Electronics Manufacturing*, **7**, 63, (1997)

[38]D. Lochun, M. Kilitziraki, *IEEE/CPMT Int'l Electronics Manufacturing Technology* Symposium, (1999)

[39] P. M. Harrey, B. J. Ramsey, etc., *Sensor and Actuators B*, **87**, 226, (2002)

[40] P. R. Shepherd, P. S. A. Evans, B. J. Ramsey, D. J. Harrison, *Electronics Letters*, **33(6)**, 483 (1997)

[41] P. S. A. Evans, P. M. Harrey, B. J. Ramsey, D. J. Harrison, *Electronics Letters*, **35(19)**, 1634 (1999)

[42] T. Rieko, *Cutting Method for Lithographic Printing Plate Material and Manufacturing Method for Lithographic Printing Plate*, Patent JP 2004058189 (2004)

[43] E. Akihiro, T. Toshitaka, *Lithographic Print Master Plates with Excellent Storage Ability, Resolution, and wear resistance for CTP*, Patent JP 2005084304 (2005)

[44] Stivers, R. Alan. Tejnil, Edita, *Dependence of mask-defect printability and printability criteria on lithography process resolution.* Proceedings of SPIE-The International Society for Optical Engineering, **4562** (Pt. 1, 21st Annual BACUS Symposium on Photomask Technology, 2001), 122 (2002)

[45] Ibaraki, Kazuhiko, Yoshida, Akio, *Platemaking of lithographic printing plates for high-resolution images.* Patent JP 11208136 (1999)

[46] A. Nakajima, N. Suzuki, H. Tomiyasu, A. Kasakura, *Developing solution comprising organic solvents and surfactants for waterless lithographic plate materials.* Patent JP 02166458 (1999)

[47] P. M. Harrey, P. S. A. Evans, etc., *Journal of Electronics Manufacturing*, **10**, 69 (2001)

[48] A. G. MacDiarmid, J. C. Chiang, A. F. Richter, N. L. D. Somasiri, and A. J. Epstein, in *Conducting Polymers*, L. Alcacer, Ed., Reidel, Dordrecht, 105, (1985)

[49] W.-S. Huang, B. D. Humphrey, A. G. MacDiarmid, *J. Chem. Soc., Faraday trans.*, **82**, 2385 (1986)

[50] M. Angelopoulos, A. Ray, A. G. MacDiarmid, and A. J. Epstein, *Synth. Met.*, **21**, 21 (1987)

[51] M. Angelopoulos, G. E. Asturias, S. P. Ermer, A. Ray, E. M. Scherr, and A. G. MacDiarmid, *Mol. Cryst. Liq. Cryst.*, **160**, 151 (1988)

[52] L. W. Shacklette and C. C. Han, *Mater. Res. Soc. Symp. Proc.*, **328**, 157 (1994)

[53] Y. Cao, P. Smith and A. J. Heeger, *Synth. Met.*, **48**, 91 (1992)

[54] G. G. Wallace, G. M. Spinks, P. R. Teasdale, *Conductive Electroactive Polymers second edition*, Technomic Press, (1997)

[55] P. J. Kinlen, J. Liu, Y. Ding, C. R. Graham, E. E. Remsen, *Macromolecules*, **31**, 1735 (1998)

[56] Z. X. Wei, Z. M. Zhang, M. X. Wan, *Langmuir*, **18**, 917 (2002)

[57] Z. X. Wei, M. X. Wan, *J. Appl. Polym. Sci.*, **87**, 1297 (2003)

[58] J. J. Langer, G. Framski, R. Joachimiak, *Synth. Met.*, **121**, 1281 (2001)

[59] R. Mazeikiene, G. Niaura, A. Malinauskas, *Synth. Met.*, **139**, 89 (2003)

[60] J. Huang, R. B. Kaner, *J. Amer. Chem. Soc.*, 126, 851 (2004)

[61] O. T. Ikkala, T. M. Lindholm, H. Ruohonen, M. Seläntaus, and K. Väkiparta, *Synth. Met.*, **69**, 135 (1995)

[62] K. Ihokura and J. Watson, *The Stannic Oxide Gas Sensor*, CRC Pr., Boca Raton., (1994)

[63] N.E. Agbor, M.C. Petty, A.P. Monkman, *Sens. Actuators B*, **28**, 173 (1995)

[64] A.L. Kukla, Yu.M. Shirshov, S.A. Piletsky, *Sens. Actuators B*, **37**, 135 (1996)

[65] M.G.H. Meijerink, D.J. Strike, N.F. de Rooij, M. Koudelka-Hep, *Sens. Actuators B*, **68**, 331 (2000)

[66] P. Ingleby, J.W. Gardner, P.N. Bartlett, Sens. Actuators B, 57, 17 (1999)

[67] S. Takeda, *Thin Solid Films*, **313**, 343 (1999)

[68] D. Li, Y. Jiang, Z. Wu, X. Chen, Y. Li, *Sens. Actuators B*, **66**, 125 (2000)

[69] V.V. Chabukswar, S. Pethkar, A.A. Athawale, *Sens. Actuators B*, **77**, 657 (2001)

[70] F. Hajdu, *IEEE Polytronic 2002 Conference*, **2002**

[71] G.E. Collins, L.J. Buckley, *Synth. Met.*, **78**, 93 (1996)

[72] S. Jain, S. Chakane, etc., *Sens. Actuators B*, **96**, 124 (2003)

[73] M. V. Kulkarni, A. A. Athawale, Journal of Applied Polymer Science, **81**, 1382 (2001)

[74] A.A. Athawale, M.V. Kulkarni, *Sens. Actuators B*, **67**, 173 (2000)

[75] D. Xie, Y. Jiang, W. Pan, D. Li, Z. Wu, Y. Li, *Sens. Actuators B*, **81**, 158 (2002)

[76] S.H. Hosseini, A.A. Entezami, *Polym. Adv. Technol.*, **12 (8)**, 482 (2001)

[77] F. Cataldo, P. Maltese, *Polym. Adv. Technol.*, **12 (5)**, 293 (2001)

[78] K. Ogura, H. Shiigi, Electrochem. *Solid-State Lett.*, **2 (9)**, 478 (1999)

[79] K. Ogura, H. Shiigi, T. Oho, T. Tonosaki, *J. Electrochem. Soc.*, **147 (11)**, 4351 (2000)

[80] M. Matsuguchi, J. Io, G. Sugiyama, Y. Sakai, *Synth. Met.*, **128**, 15 (2002)

[81] S. Sharma, C. Nirkhe, S. Pethkar, A.A. Athawale, *Sens. Actuators B*, **85**, 131 (2002)

[82] E. Segal, R. Tchoudakov, M. Narkis, A. Siegmann, Y. Wei, *Sens. Actuators B*, **104**, 140 (2005)

[83] P.S. Barker, A.P. Monkman, M.C. Petty, R. Pride, *Synth. Met.*, **85**, 1365 (1997)

[84] M.G.H. Meijerink, M. Koudelka-Hep, N.F. de Rooij, D.J. Strike, J. Hendrikse, W. Olthuis, P. Bergveld, Electrochem. *Solid-State Lett.*, **2 (3)**, 138 (1999)

[85] M. Liess, D. Chinn, D. Petelenz, J. Janata, *Thin Solid Films*, **286**, 252 (1996)

[86] S. Virji, J. Huang, R. B. Kaner, and B. H. Weiller, *Nano letters*, **4**, 491 (2004)

[87] T. Makela, S. Jussila, M. Pietila, R. Korhonen, Layered Structure, Sensor and Method of Producing and Use of the Same, Patent US 2004/0099211 A1

[88] J. C. Chiang, A. G. MacDiarmid, *Synth. Met.*, **13**, 193 (1986)

[89] Y. Lu, J. Li and W. Wu, *Synth. Met.*, **30**, 87 (1989)

[90] A. G. MacDiarmid, A. J. Epstein, *Synth. Met.*, **65**, 103 (1994)

[91] O. T. Ikkala, L. O. Pietila, L. Ahjopalo, H. Osterholm, P. J. Passiniemi, *J. of Chem. Phys.*, **103 (22)**, 9855 (1995)

[92] T. Vikki, H. Isotalo, J. Ruokolainen, P. Passiniemi, O. Ikkala, *Synth. Met.*, **101**, 742 (1999)

[93] J. Tanner, O. T. Ikkala, P. Passiniemi, J. E. Oesterholm, *Synth. Met.*, **84**, 55 (1997)

[94] H. Kosonen, J. Ruokolainen, M. Knaapila, M. Torkkeli, R. Serimaa, W. Bras, A. P. Monkman, G. ten Brinke, O. Ikkala, *Synth. Met.*, **121**, 1277 (2001)

[95] J. J. Andre, N. Bernard, B. Francois, C. Mathis, *J. Phys.*, **44**, C3-199 (1983)

[96] Y. H. Kim, C. Foster, J. Chiang and A. J. Heeger, *Synth. Met.*, **26**, 49 (1988)

[97] N. Li, X. Li, W. Geng, T. Zhang, Y. Zuo, S. Qiu, *J. Appl. Poly. Sci.*, **93**, 1597 (2004)

[98] M. J. Carson, *High Noon for Natural Gas*, Chelsea Green, (2004)

[99] M. Al-Waiz, R. Ayesh, S. C. Mitchell, J. R. Idle, R. L. Smith, *Trimethylaminuria (Fish-Odour Syndrome): An inborn error of metabolism*, Lancet, (1987)

[100] V. Luca and S. Thomson, *J. Mater. Chem.*, **10**, 2121 (2000)

[101] P. G. Le Comber, W. E. Spear, and A. Ghaith, *Electronic Letters*, **15**, 179 (1979)

[102] R. A. Street, *Hydrogenated Amorphous Silicon*, Cambridge Press (1991)

[103] Y. Kuo, *Poly-Si Thin Film Transistors*, Kluwer Publishing Company (2003)

[104] C. J. Drury, C. M. J. Mutsaers, C. M. Hart, M. Matters, and D. M. de Leeuw, *Appl. Phys. Lett.*, **73**, 108 (1998)

[105] H. Klauk, M. Halik, U. Zschieschang, G. Schmid, W. Radlik, R. Brederlow, S. Briole, C. Pacha, R. Thewes, and W. Weber, *2002 International Electron Devices Meeting Technical Digest*, 557 (2002)

[106] M. G. Kane, J. Campi, M. S. Hammond, F. P. Cuomo, B. Greening, C. D. Sheraw, J. A. Nichols, D. J. Gundlach, J. R. Huang, C. C. Kuo, L. Jia, H. Klauk, T. N. Jackson, *IEEE Electron Device Letters*, 21, 534 (2000)

[107] G. H. Gelinch, T. C. Genus, D. M. de leeuw, *Appl. Phys. Lett.*, **77**, 1487 (2000)

[108] W. Fix, A. Ullmann, J. Ficker, W. Clemens, *Appl. Phys. Lett.*, **81**, 1735 (2002)

[109] P. Mash, S. J. Rodriguez, R. Nortrup, P. Wiltzius, and J. A. Rogers, *Appl. Phys. Lett.*, **78**, 3592 (2001)

[110] C. D. Sheraw, L. S. Zhou, J. R. Huang, D. J. Gundlach, T. N. Jackson, M. G. Kane, I. G. Hill, J. Campi, and B. K. Greening, J. Francl, and J. West, *Appl. Phys. Lett.*, **80**, 1088 (2002)

[111] H. Edzer, A. Huitema, G. H. Gelinck, J. Bas, P. H. van der Putten, K. E. Kuijk, K. M. Hart, E. Cantatore, and D. M. de Leeuw, *Advanced Materials*, **14**, 1201 (2002)

[112] Paul Townsend, et al. (Dow Company), *Polymer Semiconductor Development for Thin Film Transistors*, presentation in RIT, Oct. 2003

[113] F. Garnier, R. Hajlaoui, and M. El Kassmi, *Appl. Phys. Lett.*, **73**, 1721 (1998)

[114] K. Kudo, K. Shimada, K. Marugami, M. Iizuka, S. Kuniyoshi, and K. Tanaka, *Synth. Met.*, **102**, 900 (1999)

[115] D. J. Gundlach, C. C. Kuo, S. F. Nelson, T. N. Jackson, *57th Device Research Conference Digest*, 164 (1999)

[116] H. Klauk, M. Halik, U. Zshienschang, G. Schmid, W. Radlik, and W. Weber, *J. Appl. Phys.*, **92**, 5259 (2002)

[117] C. R. Newman, C. D. Frisbie, D. A. da Silva Filho, J. L. Bredas, P. C. Ewbank, and K. R. Mann, *Chem, Mater.*, **16**, 4436 (2004)

[118] A. Pron, P. Rannou, *Prog. Polym. Sci.*, **27**, 135 (2002)

[119] Z. Bao, A. Dodabalapur, A. Lovinger, *J. Appl. Phys. Lett.*, **69**, 4108 (1996)

[120] H. Sirringhaus, N. Tessler, R. H. Friend, *Science*, **280**, 1741 (1998)

[121] H. Sirringhaus, R. J. Wilson, R. H. Friend, M. Inbasekaran, W. Wu, E. P. Woo, M. Grell, D. D. C. Bradley, *Appl. Phys. Lett.*, **77**, 406 (2000)

[122] B. Ong, Y. L. Wu, P. Liu, S. Garden, *J. Am. Chem. Soc.*, **126**, 3378 (2004)

[123] C. R. Kagan, P. Andry, Thin Film Transistor, Marcel Dekker (2004)

[124] D. A. Neamen, Ed. *Semiconductor Physics and Devices: Basic Principles*, 2nd ed.; Irwin: Chicago (1996)